

INFORMATION TO USERS

This manuscript has been reproduced from the microfilm master. UMI films the text directly from the original or copy submitted. Thus, some thesis and dissertation copies are in typewriter face, while others may be from any type of computer printer.

The quality of this reproduction is dependent upon the quality of the copy submitted. Broken or indistinct print, colored or poor quality illustrations and photographs, print bleedthrough, substandard margins, and improper alignment can adversely affect reproduction.

In the unlikely event that the author did not send UMI a complete manuscript and there are missing pages, these will be noted. Also, if unauthorized copyright material had to be removed, a note will indicate the deletion.

Oversize materials (e.g., maps, drawings, charts) are reproduced by sectioning the original, beginning at the upper left-hand corner and continuing from left to right in equal sections with small overlaps.

Photographs included in the original manuscript have been reproduced xerographically in this copy. Higher quality 6" x 9" black and white photographic prints are available for any photographs or illustrations appearing in this copy for an additional charge. Contact UMI directly to order.

Bell & Howell Information and Learning
300 North Zeeb Road, Ann Arbor, MI 48106-1346 USA

UMI[®]
800-521-0600

UNIVERSITY OF OKLAHOMA
GRADUATE COLLEGE

A 2-D MODEL FOR THE O'CONNELL EFFECT IN
W URSAE MAJORIS SYSTEMS

A Dissertation

SUBMITTED TO THE GRADUATE FACULTY

In Partial Fulfillment of the Requirements for the Degree of

Doctor of Philosophy

By

SCOTT A. MCCARTNEY

Norman, Oklahoma

1999

UMI Number: 9949702

UMI[®]

UMI Microform 9949702

Copyright 2000 by Bell & Howell Information and Learning Company.

All rights reserved. This microform edition is protected against
unauthorized copying under Title 17, United States Code.

Bell & Howell Information and Learning Company
300 North Zeeb Road
P.O. Box 1346
Ann Arbor, MI 48106-1346

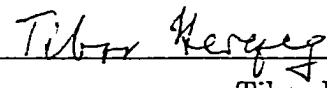
© Copyright by SCOTT A. MCCARTNEY 1999

All Rights Reserved.

A 2-D MODEL FOR THE O'CONNELL EFFECT IN W URSAE MAJORIS SYSTEMS

A Dissertation APPROVED FOR THE
DEPARTMENT OF PHYSICS AND ASTRONOMY

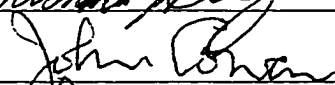
BY



Tibor Herczeg (Chair)



Richard Henry



John Cowan



Edward Baron



Brian Fiedler

Acknowledgments

It is a great pleasure to thank my advisor, Dr. Tibor J. Herczeg for his guidance and patience which makes this work possible. Our many discussions over the years, both astronomical and non-astronomical, were interesting and enjoyable. I thank my committee members, Dr. John Cowan, Dr. Edward Baron, Dr. Richard Henry and Dr. Brian Fiedler for helping answer my innumerable questions during these past nine years. I also wish to recognize Dr. Kam-Ching Leung of the University of Nebraska-Lincoln, for his long term assistance with my work. His guidance and support for the past fourteen years have proved invaluable. Thanks goes to the Department of Physics and Astronomy at Oklahoma for their many years of financial support during my pursuit of this degree.

I would like to acknowledge Olen Boydston and Adam Fisher, with whom I had many long, useful talks about computing and physics over the years. My gratitude also goes to Grettie Bondy for her considerable assistance with helping me through the graduate program rules and regulations, particularly these past two years. Additional thanks go to Paul Schleck and Kim Hannagan, who helped proofread the final manuscript.

I wish to pay tribute to the many friends I made at OU, all of which helped make my graduate years memorable. I can't close without recognizing the assistance of my good friend, Bill Marriner, who has helped me through many tough times.

Finally, I wish to thank my parents, Kent and Willa McCartney, for their continued support and guidance.

Contents

1	Introduction	1
1.1	The W Ursae Majoris Class	1
1.2	W Ursae Majoris Modeling	5
1.3	The O'Connell Effect	6
1.3.1	Photometrically Derived Spot Models	8
1.3.2	Spectroscopically Derived Spot Models	9
1.4	Database-Theory Comparisons	10
2	Contact Binary Modeling Theory	11
2.1	Early Attempts	11
2.2	The Roche Model	13
2.3	Using The Roche Model To Fit The Light Curves	19
2.4	Problems With W Ursae Majoris Light Curves	21
2.5	Irradiation Theory	25
2.6	Flow Dynamics	31
2.7	Energy Transfer Dissipation In Contact Binaries	34
2.8	Inherent Existence Of Circumfluence	36
2.9	The Coriolis Force	40
3	Modeling Code	43
3.1	The Irradiated Model	43
3.1.1	Calculation Of The Irradiated Temperature Profile	44
3.1.2	The Flow Velocity	45
3.1.3	Application Of The Coriolis Force	47
3.1.4	Luminosity Calculation	52
3.2	The Contact Model	52
3.2.1	Tassoul's Coordinate System	53
3.2.2	The Contact Flow Velocity	56
3.2.3	Application Of The Coriolis Force	56
3.2.4	Transferred Luminosity Calculation	56
3.3	Grid Sweeping	57

4	The W Ursae Majoris database	59
4.1	Database Details	59
4.1.1	Derivation Of Physical Properties	60
4.1.2	Relationships Of Non- <i>OER</i> Parameters	61
4.2	Determination Of The O'Connell Effect Ratio	66
4.3	Determination Of The Light Curve Asymmetry	70
5	Model Results	76
5.1	Results For The Irradiated Model	76
5.1.1	Observational Fits	84
5.2	Results For The Contact Model	90
5.2.1	Observational Fits	101
5.3	Conclusions	108
	Bibliography	112
A	W Ursae Majoris Data Table	129
A.1	The Database	129
A.2	Column Descriptions	138
A.3	Table References	140
B	V401 Cygni: A Wilson-Devinney Model	143
B.1	Basic Data	143
B.2	Preliminary Photometric Solution	144
B.3	Spot Model Solution	146
B.4	Discussion	150

List of Tables

4.1	Long Term Measurements Of The O'Connell Effect	70
B.1	Final Values for Parameters	151
B.2	Final Spot Parameters	152

List of Figures

1.1	Examples of W UMa Light Curves	2
1.2	W UMa Schematic	4
1.3	O'Connell's Method	7
2.1	Potential On A Point	16
2.2	Roche Equipotentials	17
2.3	Overcontact System	18
2.4	Envelope Differences	20
2.5	Third Light Effect	23
2.6	Irradiation Model	27
2.7	Entire Irradiation Region	29
2.8	Partial Irradiation Region	30
2.9	Zhou and Leung Coordinate System	38
2.10	The Direction Function	39
3.1	Irradiation Effect	46
3.2	Flow In An Irradiated Star	49
3.3	Coriolis Effect On Temperature	51
4.1	Color-Period Diagram	62
4.2	Temperature-Density Diagram	63
4.3	Total Mass Diagram	64
4.4	Separation Of A Types	65
4.5	Binning Method Example	67
4.6	O'Connell Effect Comparison	69
4.7	Reflected Light Curve	72
4.8	Maximum Asymmetry Location	73
4.9	Low <i>OER</i> And High <i>LCA</i> In The Same System	74
4.10	<i>OER</i> vs <i>LCA</i>	75
5.1	Hertzsprung-Russell Diagram For Primaries	78
5.2	Irradiation Model And M_p	79
5.3	Irradiation Model And ΔT	80

5.4	Irradiation Model And WD $r_1 + r_2$	81
5.5	Irradiation Model And Period	82
5.6	OER vs Primary Mass	85
5.7	OER vs Theory, W Types	87
5.8	OER vs q	88
5.9	OER vs $q\Lambda$ for W types	89
5.10	OER vs Secondary Mass, W Types	91
5.11	OER vs Primary Density, W Types	92
5.12	OER vs Secondary Density, W Types	93
5.13	LCA Correlations For W Types	94
5.14	OER Correlation In V	95
5.15	OER Correlation In U	96
5.16	Contact Model and M_p	97
5.17	Contact Model and ΔT	98
5.18	Contact Model and $r_1 + r_2$	99
5.19	Contact Model and P	100
5.20	OER vs Theory, A Types	102
5.21	OER vs $q\Lambda$ for A Types	103
5.22	LCA Correlations For A Types	104
5.23	OER vs Primary Density, A Types	105
5.24	OER vs Secondary Density, A Types	106
5.25	OER Correlation For Secondary Mass, A Types	107
B.1	Σ vs q	145
B.2	V401 Cygni: Hot Solution	147
B.3	V401 Cygni: Cool Solution	148

Chapter 1

Introduction

Binary star formation, structure and evolution are important areas of research in modern astrophysics. These systems provide the best determination of stellar mass, the most fundamental of stellar parameters. Close and contact binaries offer severe tests for evolutionary models. W Ursae Majoris (hereafter W UMa) stars comprise one class of close binaries and they form the basis of this study.

1.1 The W Ursae Majoris Class

W UMa systems are eclipsing binaries with short periods (~ 0.4 d). Binnendijk (1970) noted the significant fact that there are two main types of W UMa light curves. These types have been classified as W and A. The difference between the two types is demonstrated by the difference in light curve (hereafter LC) shape during primary and secondary eclipse. W types have the primary eclipse as flat while A's have a flat secondary eclipse (see Figure 1.1). Similarly the W secondary eclipse is curved while the A type primary eclipse is curved.

The standard model to explain these differences is the direction of the temperature

W Ursae Majoris Light Curves

Examples of the A and W subclass

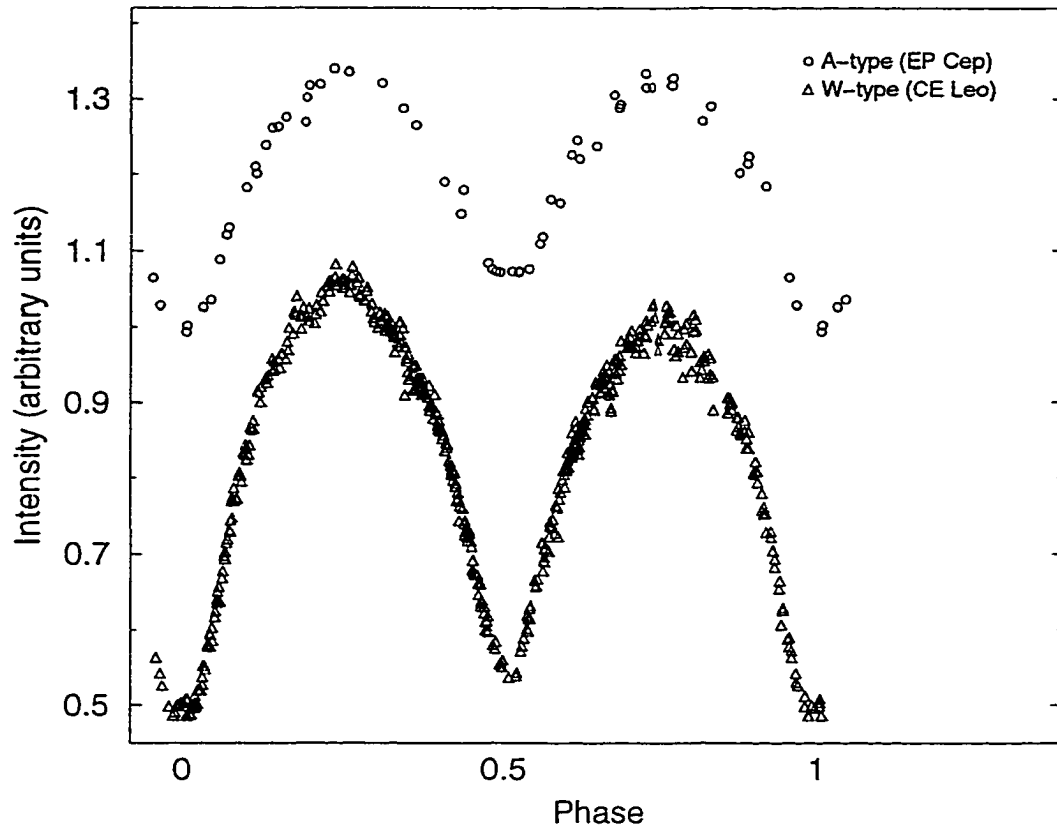


Figure 1.1: Light curves of W UMa stars of the A and W subclass. The distinguishing characteristics include the shape of the light curve at phase = 0.5. For EP Cep (the A type), the curve is flat near this region, meaning the smaller star is in front. For CE Leo (the W type), the curve is not flat near this phase. Rather it is flat near phase = 0.0. This is where the smaller star is in front for a W type. EP Cep data from Branly, *et al.* (1990), and for CE Leo the data is from Samec, *et al.* (1993).

difference between the two components. If we make the basic assumption that both components are on the main sequence, then the hotter star should be the bigger star. This would lead to an A type LC. If the components have their temperatures reversed a W type configuration results (see Figure 1.2).

Another difference between A and W types is the spectral classification of the members. A type W UMa's usually have spectral types in the A to early F region while W types are in the F to K region. This would tend to hint at possibly different underlying mechanisms for these two types of contact systems. However, a fraction of A types are much cooler than the norm—that is they have spectral types more like mid-G, in the typical W type region. It would then seem we might be dealing with two main types, the hot A types and the cool A/W types. Evidence for this hypothesis will be drawn from the database, which will show correlations between such parameters as period vs color. In addition, some other striking evidence is offered by those systems that have 'flipped' classification type. An example of this is TZ Boo, observed extensively by Hoffmann (1978). Based on observations taken between 1967 and 1976, Hoffmann classified TZ Boo as a W type. Later work (McLean and Hilditch, 1983) classified this system as an A type; indeed the light curve had changed to reflect this. The class A/W has been adopted for this system by Rovithis-Livaniou, et. al. (1992). It should be noted that TZ Boo is a cool system by A type standards. Also it has one of the lowest mass ratios among the W UMa class.

W UMa systems are usually described as being nearly zero-age. This would imply that both components are Zero-Age Main Sequence (ZAMS) stars. However the temperature difference between the components is much smaller than we would expect for detached stars of the same mass. This leads to the so called "Light Curve Paradox" for contact binaries. The secondaries are much hotter than they should be for a main sequence star. The paradox is even more extreme for the W type, where the secondary

Schematic of W Ursae Majoris Subclasses

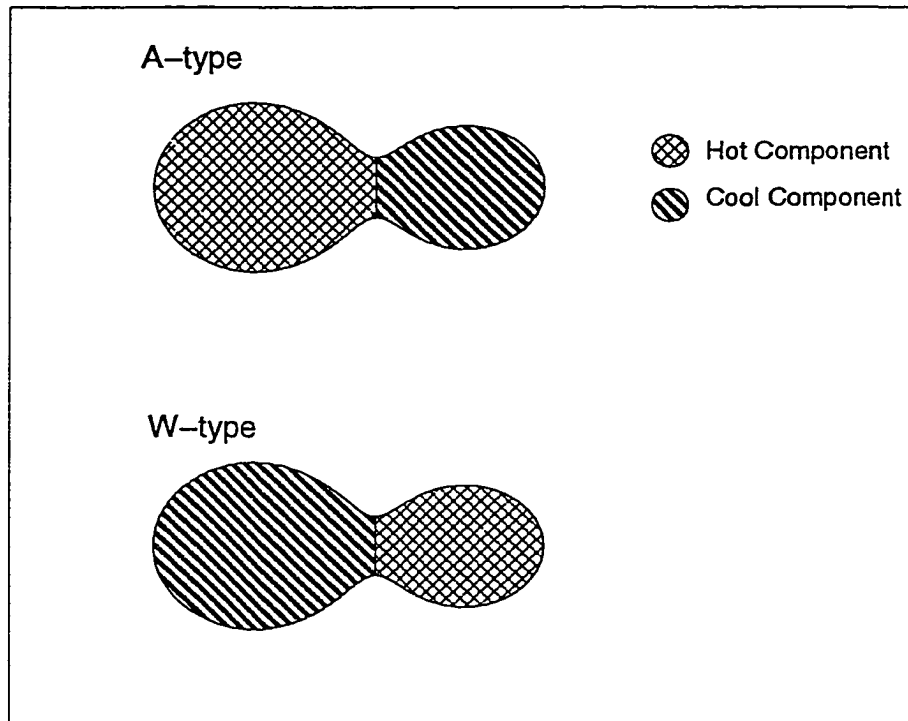


Figure 1.2: A representation of the two main subclasses of the W UMa class. The A types have the physically larger star as hotter and more massive. The W types have the physically larger star as cooler and more massive. Here, and in all later plots, the Roche lobe representation was created by the program of C.H. Kim.

is actually hotter than the primary. The usual explanation is the common envelope the two stars share allows this surplus temperature for the secondary.

Since the stars are so close, a common envelope which is primarily heated by the hotter primary dominates the luminosity from the secondary. This results in a much smaller temperature difference than would be expected for detached components of the same mass. This would adequately explain A types. In the case of the W types, the primary is actually slightly cooler than the secondary. However, the primary's larger size means that its overall luminosity is still higher than the secondary's. Again, envelope interactions are invoked. Hazlehurst's theory (see Section 2.7) tries to explain how this temperature inversion can develop.

1.2 W Ursae Majoris Modeling

In the past quarter century, static models of contact binaries have made great advances. The computational difficulty of the problem meant that good numerical models had to await the proliferation of fast computers. The differences between Lucy's early models (1967a and 1967b) and the current Wilson-Devinney code (hereafter WD) (1992) demonstrate this advance.

Most of the current advanced models are based on the Roche model, outlined extensively in Kopal's work (1958 and 1990). Its primary property is that the contact surface of the system is described by the so-called Roche equipotentials. Most of these current models are static. There are several reasons for this, foremost being the difficulty of doing 3-D non-spherical hydrodynamics. Chapter 2 extensively discusses Kopal's work and the history behind the early Roche based models, including the heavily used WD method.

1.3 The O'Connell Effect

The Wilson-Devinney code and its rivals do a very good job of fitting the light curve, with the exception of certain asymmetries. A static model is going to predict that a light curve is symmetric about the eclipses. However, observations of W UMa types show that for many systems there are significant asymmetries in the light curves. In many cases, these asymmetries are the difference in peak luminosity at the two out of eclipse phases (see Figure 1.3).

Observations of these light curve irregularities are nothing new. One of the earliest significant studies of these light curve asymmetries was done by O'Connell (1951). In his method he measured the peak magnitude asymmetry, later renamed the O'Connell effect (Milone, 1968). O'Connell calculated the magnitude difference as the difference between the second maximum and the first maximum:

$$\Delta m = m_{MaxII} - m_{MaxI}. \quad (1.1)$$

A positive Δm implies that Max I is brighter. O'Connell measured this asymmetry for many systems, both contact and non-contact systems. Later, a study of non-contact systems (Davidge and Milone (1984)) was completed, which compared the asymmetry amount with various parameters. Physical quantities such as the radii of the larger component, the relative radii of both components and so forth were analyzed in an attempt to find correlations with the asymmetries. Davidge and Milone mostly excluded contact systems from their study, since they felt a different mechanism might be responsible for asymmetries in the light curves of these systems.

In Chapter 4, two new methods of measuring light curve asymmetries will be explained. The O'Connell method, above, will be compared with these methods.

O'Connell's Method to Measure Light Curve Asymmetries

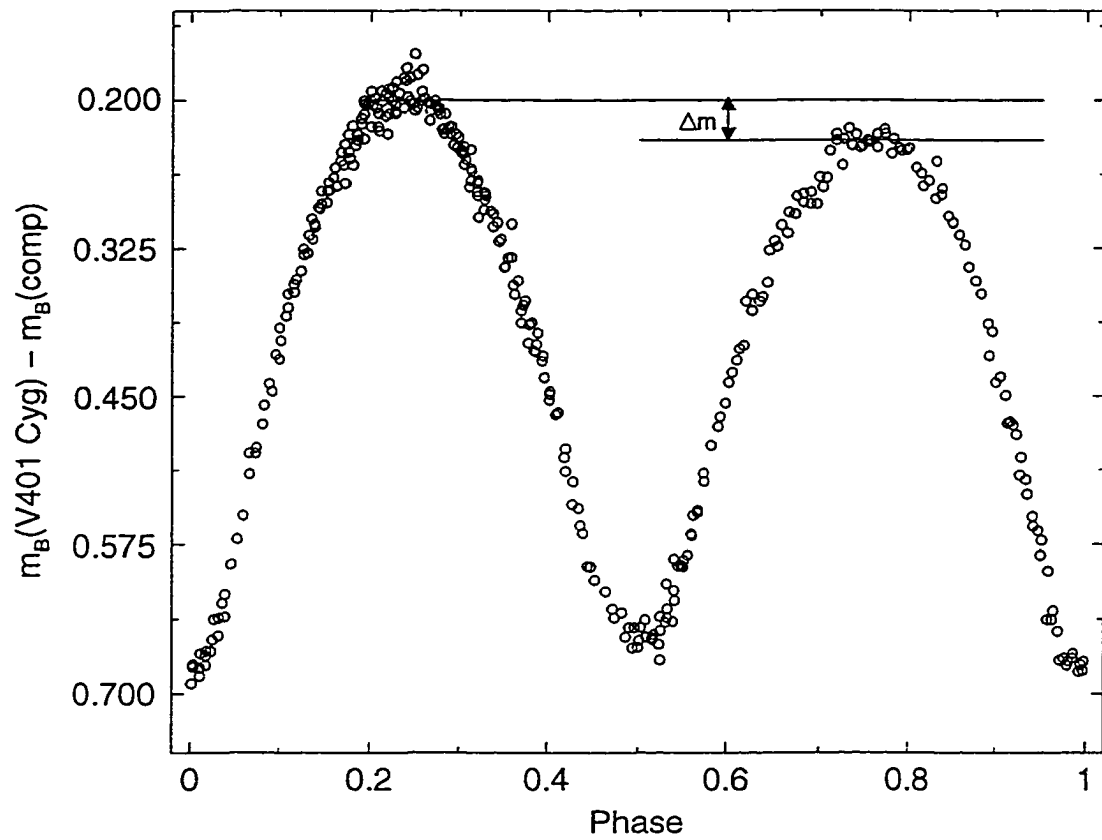


Figure 1.3: An example of the O'Connell method for measuring the peak asymmetry. Δm is the peak asymmetry difference in units of magnitude (see Equation 1.1). For this system (V401 Cygni) $\Delta m = 0.071$. Data from Purgathofer (1964).

1.3.1 Photometrically Derived Spot Models

For contact systems, the usual method to deal with such asymmetries is to state that they are of a magnetohydrodynamic (MHD) origin and place an ad hoc spot which adjusts the luminosity by the necessary amount, but in a non-physical manner. Therefore the modeled luminosity for the system is no longer kept constant (with a flux re-distribution), instead a net change is added to the overall value of the luminosity. This change can be positive or negative depending on whether a hot or cool spot is placed on the system. This method works very well for some subclasses of close binaries, particularly RS CVn systems. In these systems, the spots can be seen to “drift” over time, allowing a good determination of their latitude, longitude and size. Reducing these ambiguities greatly helps in refining the more fundamental parameters for the system.

Long-term monitoring of the spots’ movements are needed to accurately determine their physical parameters. Trying to model spots on a system without some independent determination of the spot parameters leads to a uniqueness problem. Maceroni and Van’t Veer (1993) show that just by including spots without good latitude, longitude and size values, solutions can vary by 20% to 30% in such critical parameters as inclination, mass ratio of the components and contact surface potential.

Unfortunately, the light curve asymmetries of W UMa systems seem to be quite different from their non-contact counterparts. With the exception of a few systems (most notably VW Cep), it has proven difficult to find a drift period for the spots in W UMa systems. Since the geometry of the situation is quite different compared to RS CVn class, this is not surprising. While circulating the star, the spots would enter the mass-interaction region between the two components. The effects of this turbulent region on spots is not understood, so a good independent determination of physical

parameters is extremely useful. This drift problem has led to much higher ambiguity into the nature of the spots on contact systems. Without some kind of drift it is hard to determine the fundamental spot parameters, meaning most of the WD models involving spots have a uniqueness problem. Difficulties in getting good fits with cool spots has led some authors (see e.g. Samec 1993) to attempt hot spot solutions, which cannot have conventional “sunspot like” explanations.

Another important distinction between the W UMa asymmetries and RS CVn asymmetries is longevity. Some W UMa systems, such as RW Com and AM Leo have complete light curves dating back 40 years or more. Small changes appear, but in general the peak asymmetry seems remarkably constant on these time frames. This has led to attempts to find non-MHD explanations for the mechanism.

1.3.2 Spectroscopically Derived Spot Models

Better determination of the spot’s longitude and latitude is necessary to develop more reliable models. One method that holds promise is Doppler imaging. Piskunov and Rice (1993) describe in detail the Doppler imaging technique for obtaining a surface temperature profile. An initial guess of the distribution of temperature over the star’s surface is used to calculate the local line profiles and local continuum intensity. This calculated residual intensity, R_{calc} (from line profiles), is then compared to R_{obs} obtained from actual observed line profiles. Adjustments to the initial temperature distribution are then made to minimize the difference between R_{Calc} and R_{obs} .

The primary drawback is that sufficient spectroscopic resolution is needed to get a detailed line profile. Observing constraints have slowed data collection in this area. W UMa types orbit quickly (~ 0.4 day) and since it is difficult to get high resolution spectra with a short integration time, high resolution W UMa spectra are uncommon. As stated by Maceroni (1994), the 1.5m ESO telescope in La Silla is limited to systems

with $m_v < 8$ and strong H_α lines - which have possible chromospheric contamination. Thus the current Doppler imaged sample is too small for a statistical survey at this time.

1.4 Database-Theory Comparisons

A database of around 100 W UMa systems has been compiled and is outlined in Chapter 4, along with some of the current observational problems associated with W UMa types. This database will be used to provide an observational comparison with the model.

For modeling the systems, one avenue being explored is using dynamical models to attempt to explain the light asymmetries by such mechanisms as the Coriolis effect (Zhou and Leung, 1990) and irradiation (Zhou and Leung, 1997a). This is a difficult problem because of the inherent non-spherical nature of the model. Rather than spherical harmonics, a different method developed by Tassoul (1992) involving Roche harmonics must be used. Zhou and Leung's method form the basis of the model described in Chapter 3, a simplified model which primarily hopes to understand the equatorial flow (where the Coriolis acceleration should be strongest) and provide motivation for more detailed and complicated 3-D calculations. This method incorporates Hazelhurst (1985, 1993, 1996 and 1999) as well as the Zhou and Leung models, thus the code represents a simplified dynamic model. The remaining two chapters are devoted to analyses of the code output in conjunction with the database. Finally an appendix details the actual database in a detailed tabular form.

Chapter 2

Contact Binary Modeling Theory

The Roche model as developed by Kopal is used to explain the non-spherical surfaces of W UMa systems. Lucy's work showed that W UMa systems exist as contact binaries, having a common convective envelope with the photosphere lying between the inner and outer zero-velocity Lagrangian surfaces. A discussion of the current theoretical work of Leung and Zhou as well as Hazelhurst is included.

2.1 Early Attempts

Wilson (1994) summarized in detail the historical background of the earliest light curve modeling. An overview of the important models from history is appropriate, since the models which came out of these early attempts and are still in use today will provide the focus of this chapter. The Russell Method (e.g. Russell (1912a, 1912b, 1948)) was the dominant model of the first half of the 20th century. Its intricate ellipsoidal configurations which used the "reflection effect" was usually the only model used to fit observations. This method was primarily a *geometric* one, since it made several incorrect assumptions about the local physics in order to have a tractable solution during the pre-

computer age. A central point was the process of “rectification”, whereby an observed light curve was modified to correspond to a binary system made up of spherical, limb-darkened components in a circular orbit. This rectified light curve could then be used to determine the geometric (i.e. orbital inclination, component radii) and photometric (i.e. surface temperature) properties of the two stars. These could then be related back to the real stars by the transformation formulas used to obtain rectification. However, as stated above, in order to make this a solvable solution, somewhat non-physical models had to be used. In the late 1960’s, computer programs based on these rectifiable models were developed (Jurkevich (1964) and Proctor and Linnell (1972)).

By this time, models were being developed based on the important work of Kopal. In particular, his *Close Binary Systems* (1959) provides an analytical model which incorporates Roche geometry, rather than the ellipsoidal geometry of the Russell model. Combining the Russell method for light curve analysis with the improved physical models of Kopal led to a burst of activity in modeling of contact binary systems. Around the same time, Lucy (1968a and 1968b) published two important papers on W UMa structure. These papers provide the first good models for W UMa systems and are still the fundamental basis for today’s work. Lucy’s important contribution was to provide a method to model contact systems as they really were – two stars with a common outer envelope, undergoing significant thermodynamic interactions in this envelope. Using the two separate sphere method of Russell would lead to serious systematic errors for systems with a common convective envelope. So instead, Lucy (1968b) used Kopal’s work to develop some simple power law relationships between such important quantities as the luminosity, radius and mass ratios of the components. Computerization of Lucy’s method required very finely spaced coordinate grid elements on the surface, otherwise numerical noise dominated the results. Despite these limitations this work was crucial as it allowed the light curves of distorted stars to be computed directly, by using real

physical parameters. This replaced the need for the process of rectification.

Many advanced computer models quickly developed. A list of these models needs to include the work of Hill (Hill and Hutchings (1970)), Wilson and Devinney (WD), Wood (1971), Nelson, Davis and Etzel (Nelson and Davis (1972)), Mochnacki and Doughty (1972) and Budding (1977). Several other models appeared, but are not used extensively except by their originators. The above models comprise around 75% of the solutions published during the 1987-1990 time period (IAU Comm 42 Bulletin (1991)). The WD method accounted for 44%. During the latter half of the 1990's, the WD percentage has risen even higher, to around 65%. An in depth discussion of the WD method is below, in Section 2.3.

2.2 The Roche Model

In Chapter 2 of his *Close Binaries* (1959), Kopal extensively analysed the Roche Model. A summary of his work will be used to understand the numerical models used.

The total potential, Ψ , acting on an arbitrary point $P(x, y, z)$ for a pair of close stars is:

$$\Psi = G\frac{m}{r} + G\frac{m'}{r'} + \frac{\omega^2}{2}\left\{\left(x - \frac{m'r}{m+m'}\right)^2 + y^2\right\}. \quad (2.1)$$

Here, m and m' are the mass of the two components, ω the angular rotation velocity (constant everywhere) and G is the gravitational constant. Furthermore,

$$r^2 = x^2 + y^2 + z^2, \quad (2.2)$$

and

$$r'^2 = (r - x)^2 + y^2 + z^2. \quad (2.3)$$

These values represent the squares of the distance of P from the center of gravity of the two components (see Figure 2.1). For very close systems, assuming the components are centrally condensed, we can assume the angular velocity is equal to the Keplerian angular velocity:

$$\omega^2 = G \frac{m + m'}{R^3}. \quad (2.4)$$

Next, we adopt the separation R of both components as the unit of length. Then, converting from cartesian to spherical coordinates:

$$x = r \cos \phi \sin \theta = r\lambda, \quad (2.5)$$

$$y = r \sin \phi \sin \theta = r\mu, \quad (2.6)$$

$$z = r \cos \theta = r\nu, \quad (2.7)$$

results in the common expression:

$$\Omega = \frac{1}{r} + q \left(\frac{1}{\sqrt{1 - 2\lambda r + r^2}} - \lambda r \right) + \frac{q + 1}{2} r^2 (1 - \nu^2), \quad (2.8)$$

where $\Omega = \frac{R\Psi}{Gm} - \frac{m'^2}{2m(m+m')}$, and using the standard definition for the mass ratio, $q = \frac{m'}{m}$. Here, and in all later cases, m is the mass of the more massive (also called primary) component. m' designates the less massive (also called secondary) component. This implies: $0 < q < 1$. Some authors prefer to define the primary as the hotter component

and the secondary as the cooler component. As we will find, the hotter component is not necessarily the more massive one. Thus, for these authors, it is possible for $q > 1$. In all work, a conversion of their temperature method to the mass method will be done.

Setting $\Omega = \text{constant}$ will generate a surface called the Roche Equipotential. For large Ω , the corresponding equipotentials consists of separate ovals (nearly circles) around the two mass points. As Ω decreases, the ovals become more elongated in the direction of the center of gravity. Eventually, for a value Ω_1 , the two ovals will touch. This dumbbell configuration (see Figure 2.2) is called the Roche Limit by Kopal. The contact point is known as the L_1 Lagrangian point. As Ω continues to decrease we get a common envelope configuration (see Figure 2.3). A useful quantity is the fillout, f . It is defined as:

$$f = \frac{\Omega_1 - \Omega_{\text{contact}}}{\Omega_1 - \Omega_2} \times 100\%, \quad (2.9)$$

where Ω_{contact} is the Roche equipotential value for the system in question and Ω_2 is the Roche equipotential value for contact with the L_2 Lagrangian point. The fillout gives us a simple way of estimating how overcontact a binary system is. If $f = 0\%$, this means the components just touch at the L_1 point. For $f = 100\%$, the envelope completely surrounds both components and is filled to the L_2 point. Any further decrease in Ω will not enlarge the envelope. Instead, mass loss through the L_2 point occurs. The β Lyrae types, which are similiar to W UMa types, have such a configuration.

For W UMa types, the fillout provides another parameter which distinguishes the W and A subclasses. From Maceroni and Van't Veer's (1996) sample, the average fillout for W's is 14% with a range from -9% to 41%, while for A's the average is 31% with a range from 2% to 87%. A typical W is then in lower thermal contact than a typical A. Since some W's have a f less than 0%, this implies that any energy transfer between

Potential on an Arbitrary Point

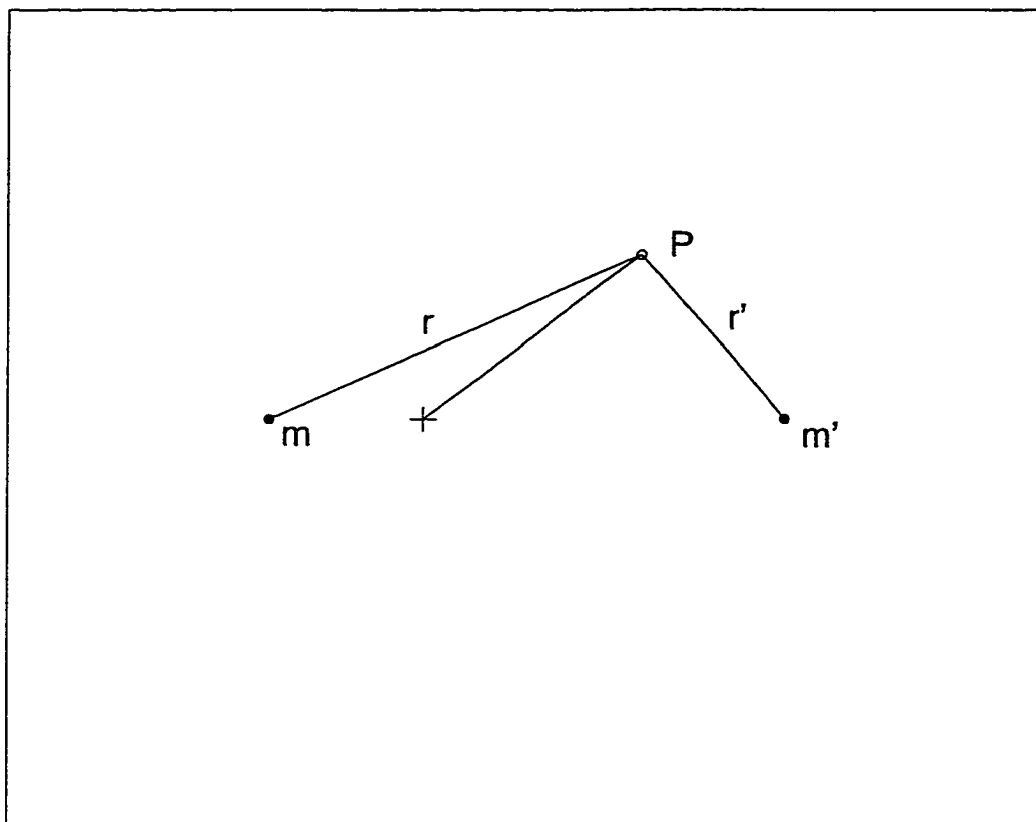


Figure 2.1: The point, P , has a potential Ψ acting upon it from masses m and m' as shown in Equation 2.1. The center of mass is marked with a '+'.

Roche Equipotentials, Ω

Detached Systems

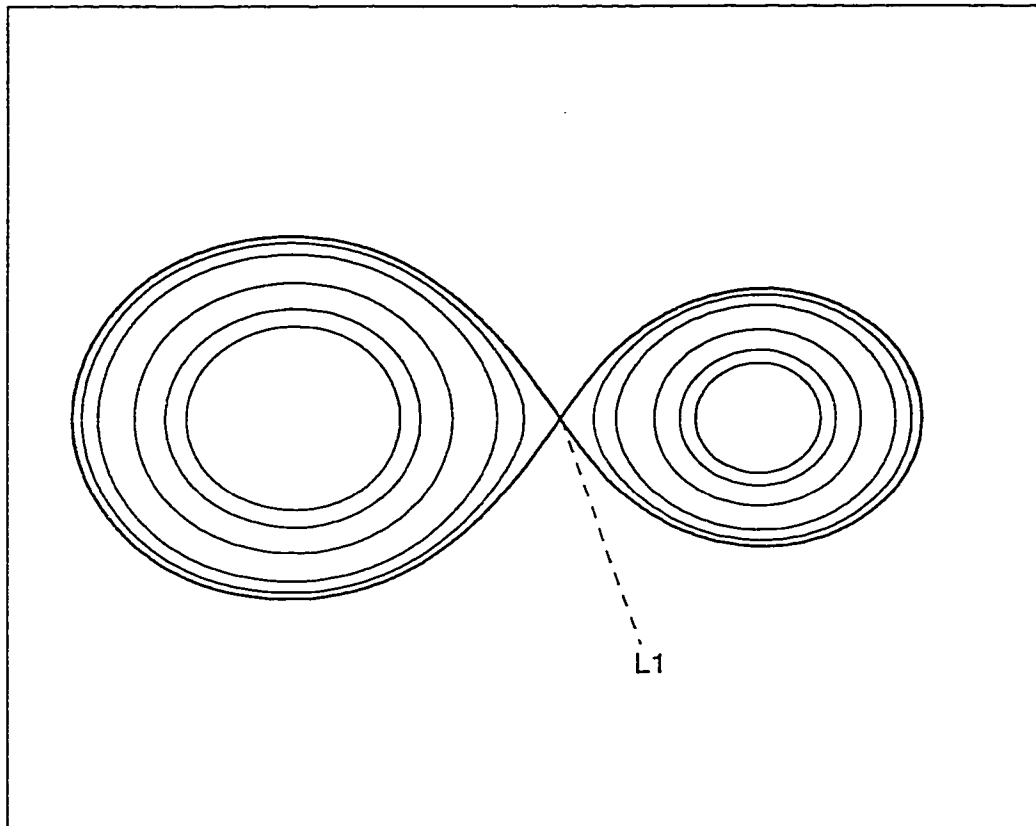


Figure 2.2: A plot of the Roche Equipotentials for the case where the components are detached. For this example, the mass ratio is 0.5. The smallest pair of ovals represent an Ω of 5.0, while the largest ovals are for $\Omega = 2.95$. The $\Omega_{contact}$ surface is 2.88 in this case. The inner contact Lagrangian point, L_1 is indicated.

Example of an Overcontact System

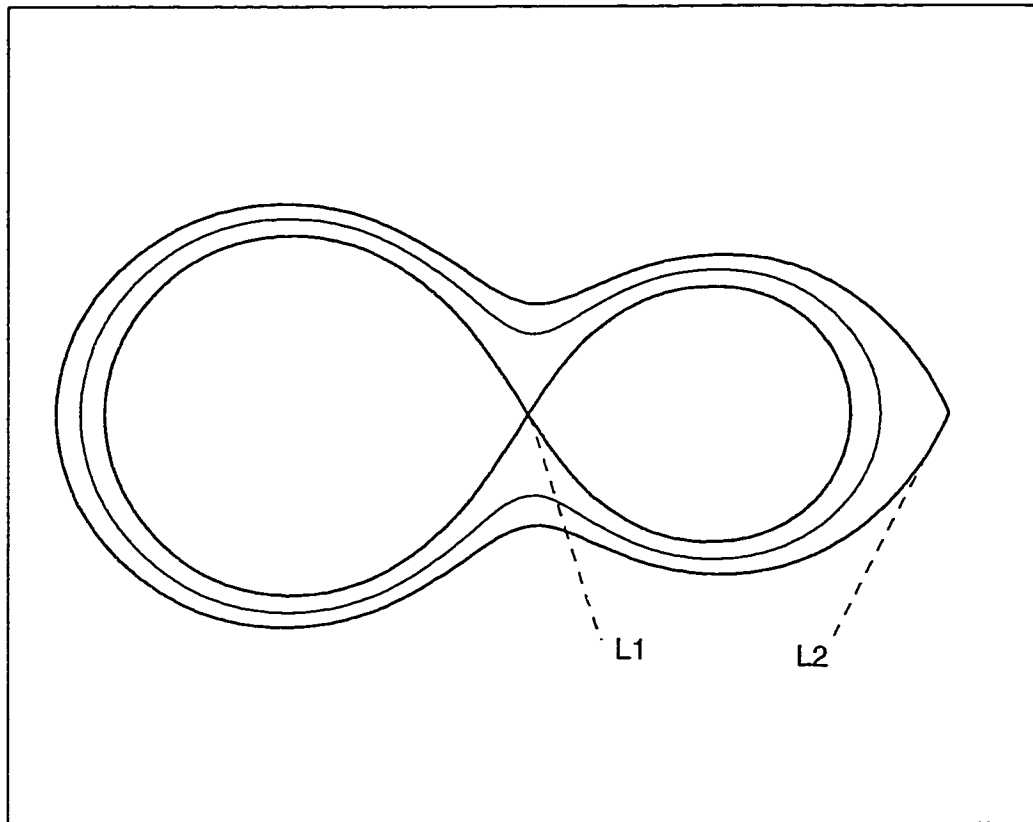


Figure 2.3: An example where one common surface exists. As with Figure 2.2 above, $q = 0.5$. The surface represented is for $\Omega = 2.70$. The inner contact Lagrangian point, L_1 and the outer contact Lagrangian point, L_2 are indicated. For the inner surface, $\Omega_1 = 2.88$ and for the outer, $\Omega_2 = 2.58$. This corresponds to an $f = 60\%$. See Figure 2.4 for an example of each subclass.

components is radiative rather than convective. Looking at an example of a low contact W-type vs a higher contact A-type (Figure 2.4), it would seem that a model must incorporate this radiative exchange for low contact systems. Later sections will deal with the theory behind these two methods. Section 2.5 will review the Zhou and Leung irradiation model for close and low contact binaries. Sections 2.6-2.8 will outline a flow model based on the work of Webbink, Zhou and Leung, and Hazlehurst.

2.3 Using The Roche Model To Fit The Light Curves

Among the models mentioned above, the Wilson-Devinney model is the most extensively used among solutions published in the literature. Since the bulk of calculated parameters printed in Appendix A are values obtained by the WD method, a summary of the pertinent points of this model are in order.

The WD method uses the physics of the Kopal and Lucy theoretical models. By analyzing a light curve of photometric observations, important parameters (e.g. the mass ratio of the components, the inclination of the system, the photospheric temperatures of the components and the Roche potential of the common surface) are calculated. The code contains two FORTRAN programs, LC (for generating light and radial velocity curves) and DC (to calculate differential corrections to the parameters). LC works by reading in a data file which contains photometric observations of a system (from one or more filters) and values for some 30-odd “significant” parameters. These parameters include such fundamental quantities as the rotation period of the system and the orbital inclination. Other parameters of secondary importance are also included, such as limb darkening.

Of course, when beginning, very few of these parameters are known. Most likely the period and color of the system are known. From there, educated guesses are made about

Roche Surface Potentials

Examples of W and A Subclass

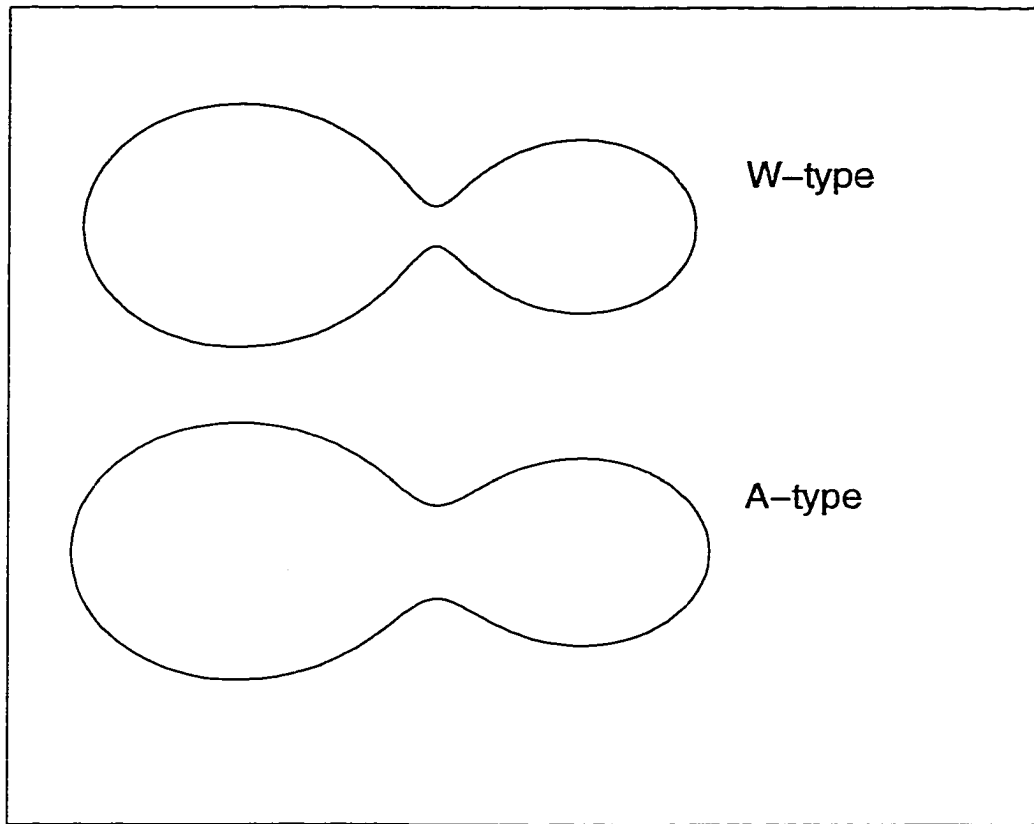


Figure 2.4: Examples of the potential surface for the envelope for typical W and A subclass members. In both cases, $q = 0.5$. $f_W = 14\%$ and $f_A = 40\%$, typical values from the Maceroni and Van't Veer (1996) data.

the other parameters. Once the parameters are given values, the LC code is used to get an eyeball fit of the these guesses with the observed light curve. Usually these first guesses are quite bad, but after some manipulation a reasonable visual fit will be made. Now, the latest set of parameter guesses are used as input for the DC program. This program calculates (via least squares fitting) how much a parameter should be adjusted, based upon the value given and the photometric data provided. Since we have a 30+ dimensional space in which to find the minimum solution in, simultaneously adjusting all the parameters is not possible. Instead the preferred method is to leave the secondary parameters fixed and only adjust the important parameters at first. Since varying q , the mass ratio, can lead to instabilities in the solution, q is usually kept fixed until a stable solution is found, then q is incremented and the process restarted. This will lead to solutions than can be plotted as Σ (the root mean square error) vs q . At the q value for minimum Σ , a solution is usually ran with the above primary parameters plus q as free parameters. This trick allows us to “fall” as close as possible to the final solution ahead of time, saving greatly on computation time. Some authors have tried just sweeping large grids of solutions and looking for the minimum in some n-dimensional space, but that solution proves woefully inefficient compared with the above method. Due to the difficulty in finding a stable solution, the WD method is not set up to self-iterate to a solution. It is possible to fall into a back and forth oscillation around the solution, without ever converging.

2.4 Problems With W Ursae Majoris Light Curves

The above scenario works well if the input light curve is “simple”; that is it contains no large scale asymmetries. However in the case of most W UMa systems this is unfortunately not the case. Two important problems exist with W UMa light curves:

- **Third Light.** The problem of third light is caused when the binary is part of a larger, multiple system. 44i Boo is an example of such a system. In some cases, the extra member (responsible for the “third light”) can be brighter than the components. This causes the light curve to show less net intensity change, since we have a constant background intensity which is part of the light curve (see Figure 2.5). An undesirable effect of making it harder to observe small-scale asymmetries in the light curve results, and the resulting model is less reliable.
- **Light Curve Asymmetries.** This includes all short-term and long-term variations in the light curve, grouping together a possibly heterogeneously derived set of effects. Included is the O’Connell effect and the spot method used to compensate for it. The O’Connell effect is sometimes called the Kwee effect, but the former is far more common.

The O’Connell effect led to a situation where two solutions were generally published, one where the brighter peak was well fit and another where the dimmer peak was well fit. The true solution was figured to lie somewhere in between. These two solutions became known as “hot” and “cold” solutions respectively, since the temperature of the secondary component varied wildly for these two solutions. The WD method reconciled this problem by allowing the user to add an ad hoc spot onto the stellar surface. These spots are generally placed on the surface as an after effect to make the light curve fit. Thus, if one favors the “hot” secondary solution, a cool spot would be placed on one of the stars which would depress the lower intensity half of the light curve, making a good fit. Conversely, if the “cool” secondary solution was picked, a hot spot would be placed on the secondary instead. Usually a hot spot is placed only on the cooler star, not the hotter star. The reasoning behind this is that stable hot spots on the hotter star are not thermodynamically possible. Possible brightening mechanisms such as flares, which

Effects of Third Light

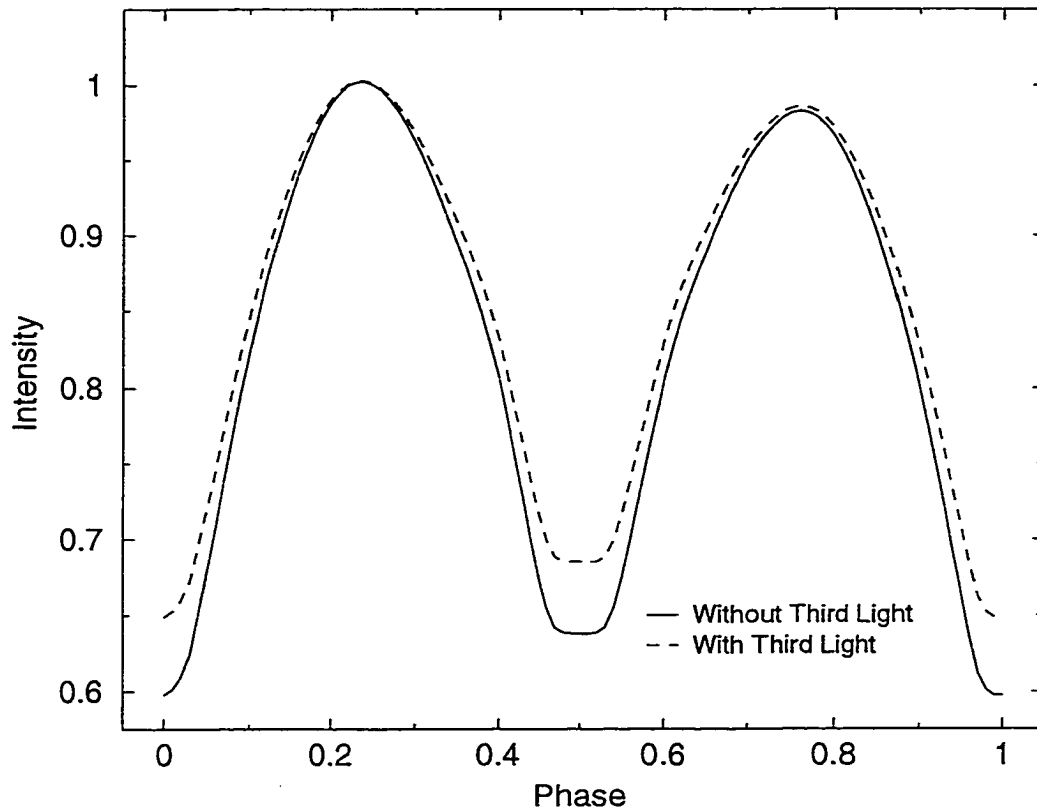


Figure 2.5: This plot shows the difference caused by third light. In both cases, $q = 0.27$, $\Omega = 2.32$, $f = 32\%$ and $\Delta T = 100\text{K}$. The third light is 10% of the total system intensity. The WD method was used to generate these and all later theoretical light curves.

could result in a hot spot on the hotter component, are too short term to explain the O'Connell effect.

Most of the early solutions with spots used the cool spot method. The reasoning behind this was that the spots must be similar to sunspots, which are cooler than the surrounding region. An even better comparison was to another class of binaries, the RS CVn systems. These are detached binaries where both components are spherical. For these systems variations in the light curve existed, which were very well modeled with spots. Over time, the asymmetries on the light curve would drift which would allow a good independent determination of the spot latitude and longitude. These spots are considered as being magnetohydrodynamic in origin. As described in recent work by Kallrath and Milone (1999), these could be the result of flares or coronal holes around the star. The primary problem is that most of these effects are short term, much shorter than the observed O'Connell effects time scale.

W UMa light curves show some variance from one period to the next. Small (compared to the peak asymmetry) 'dimples' and 'bumps' occur on the light curve with intensity changes on the order of a few tenths of a %. These changes, which are possibly explained by the above magnetohydrodynamic theory, are out of the scope for the current topic. Confusingly, these small scale short term effects are sometimes referred to as the O'Connell effect. As Kallrath and Milone state: "Unfortunately, it has become practice to use these names (*the O'Connell or Kwee effect*) as catch-all terms for a variety of physical effects." Many effects (with most likely different causes) have been inappropriately grouped together under the O'Connell effect classification.

For the W UMa class, the solution is much harder to come by. Many of the systems show remarkable stability in their asymmetry over a longer time period as compared to the RS CVn class, which in turn makes an independent determination of the latitude and longitude of the spot impossible. So, by adding spots to a contact binary model, we

add an additional four degrees of freedom (radius, longitude, latitude and temperature of the spot) per each spot, unless we have doppler imaging of the surface to provide some constraint. Since the system is already underdetermined, this makes getting a stable solution very difficult. Compounding this problem is the fact that the spot models commonly used are *non-physical*, that is, they aren't used as part of the overall flux equations, but are later add-ons to (or subtractions from) the net flux. In the 1993 analysis of Maceroni and Van't Veer, the uniqueness problem led to solutions where acceptable q 's varied between 0.408 and 0.681 - a very large range. Kallrath and Milone state, with regards to the current spot models: "One way to overcome this problem is to include spots in the light curve modeling, although in such cases spots serve only as an artifice to save the phenomena.....Therefore we cannot show in any conclusive way that the O'Connell effect is correctly modeled by spots; neither can we show that it was not." This summarizes the ad hoc nature of current spot modeling very well.

A sample solution using the WD method and requiring spots is shown for the system V401 Cygni in Appendix B.

2.5 Irradiation Theory

A good starting point for building a sophisticated model is to first simplify the problem before creating the more complex model. Before a discussion of a solution involving actual flow of material in a large, convective envelope is detailed, a simpler solution involving irradiation of each component by the other will be used. In the WD model, one parameter is the albedo of the system. This is merely a fractional measurement of how much of the radiation that one star receives from the other is reflected back out, also referred to as the reflection effect. From Wilson's (1990, 1993) theory, a value between 0.5 and 1.0 is typically chosen. This is a fractional amount that is between

50% and 100% of the radiation being reflected. Cooler systems tend toward the 50% value, while hotter ones (with radiative envelopes) are given values of 100%. Since W UMa stars are cool enough to fall in the convective envelope class, a value near 50% is usually used in modeling them. The rest of the radiation is absorbed by the star. Currently the WD model does not consider this absorption. Zhou and Leung (1997a) have outlined the theory dealing with this absorbed portion. Their analysis yields that the temperature variation on the surface of star 1, due to irradiation by star 2 is:

$$\left(\frac{\Delta T_1}{T_{10}}\right)^4 = s \left(\frac{T_{20}}{T_{10}}\right)^4 F(\theta), \quad (2.10)$$

where s is the absorption fraction and T_{x0} is the unperturbed surface temperature of star x . $F(\theta)$ is a function of the solid angle of star 2 visible at an angle θ on the surface of star 1 (Figure 2.6, a reproduction of Figure 2, pg 71 in Zhou and Leung (1997a)):

$$F(\theta) = \frac{1}{\pi} \int_{\Omega} \cos \delta \cdot d\omega, \quad (2.11)$$

where $\cos \delta = \vec{n} \cdot \vec{m}$, \vec{n} and \vec{m} being unit vectors. \vec{n} is the normal to the surface of the *irradiated* star at the point the irradiation is being measured. \vec{m} is the direction from this point to the point on the second star that the radiation is coming from, as shown in Figure 2.7. For simplicity, Leung and Zhou used spherical stars. To do a detailed model, the non-spherical nature of the stars must be incorporated. A discussion of how to transform coordinates from spherical geometry to Roche geometry will be included in Chapter 3. This will handle the distortion of the two components. We collect the formalism of Zhou and Leung below. The integral over the solid angle, Ω , is broken up into four regions:

1) **Entire Irradiation Region.** This is for the region $\theta < A$, where $\cos A = r_1 + r_2$. r_1 and r_2 are the relative radius of the primary and secondary, respectively. These values

Close Binary Model Used For Irradiation Theory

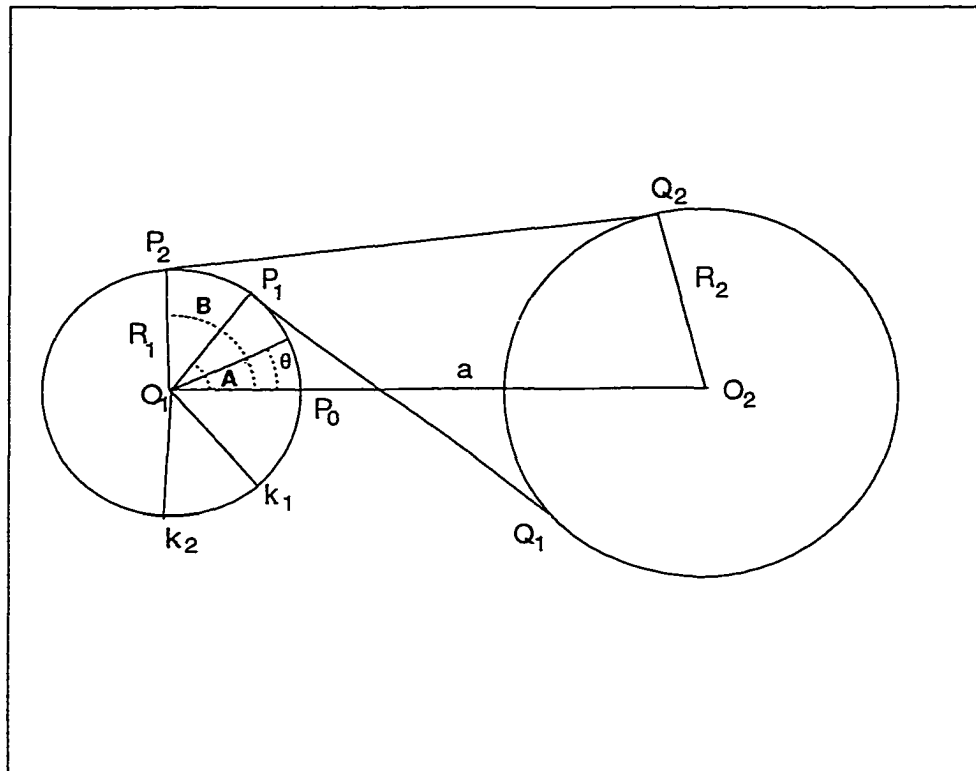


Figure 2.6: A close binary with the parameters from the Zhou and Leung irradiation theory marked. The area between P_1k_1 on the secondary is irradiated by the entire surface of the primary. The area $P_1P_2 - k_1k_2$ is irradiated by only part of the primary's surface. a is the separation distance.

are expressed as a fraction of a , the separation distance. Since r_1 and r_2 are in relative coordinates (scaled by a), their sum is always less than or equal to 1. For the angle θ in this region the disk of star 1 is irradiated by the entire disk of star 2. The angle function $F(\theta)$ becomes:

$$F(\theta) = r_2^2(\cos \theta - r_1)/D_1^3. \quad (2.12)$$

Here, $D_1 = \sqrt{1 + r_1^2 - 2r_1 \cdot \cos \theta}$. Figure 2.7, based on Figure 3, pg 71 of Zhou and Leung (1997a), highlights this region.

2) **Partial Irradiation Region - Part I.** In this region, $A < \theta < B$, where $\cos B = r_1 - r_2$. The angle $\alpha < \pi/2$. This angle represents the angle between \vec{n} (the surface normal at the angle θ) and the line which bisects the irradiating star. The angle $z = \alpha - \pi/2$, therefore $z < 0$ in this region. Figure 2.8, based on Figure 4, pg 72 of Zhou and Leung (1997) shows α . $F(\theta)$ becomes:

$$F(\theta) = \cos^3 \alpha + \frac{\cos^2 z}{2} - \frac{1}{\pi} \left\{ \cos I \cdot \sqrt{\cos^2 z - \cos^2 I} + \cos^2 z \cdot \sin^{-1} \left(\frac{\cos I}{\cos z} \right) \right\} + \frac{\cos \alpha}{\pi} \left\{ \sin^2 I \cdot \cos^{-1} \left(\frac{\tan z}{\tan I} \right) - \pi \sin^2 z - \sin z \cdot \tan^{-1} (\cos z \sqrt{\tan^2 I - \tan^2 z}) \right\}. \quad (2.13)$$

where $\cos \alpha = \frac{\cos \theta - r_1}{D_1}$, $\sin \alpha = \frac{\sin \theta}{D_1}$, $\cos I = \frac{\sqrt{D_1^2 - r_2^2}}{D_1}$ and $\sin I = \frac{r_2}{D_1}$.

3) **Partial Irradiation Region - Part II.** Here $A < \theta < B$ still, but now $\alpha > \pi/2$ and $z > 0$. $F(\theta)$ becomes:

$$F(\theta) = \frac{\cos^2 z}{2} - \frac{1}{\pi} \left\{ \cos I \cdot \sqrt{\cos^2 z - \cos^2 I} + \cos^2 z \cdot \sin^{-1} \left(\frac{\cos I}{\cos z} \right) \right\} +$$

Entire Irradiation Region

Schematic of Irradiation Model

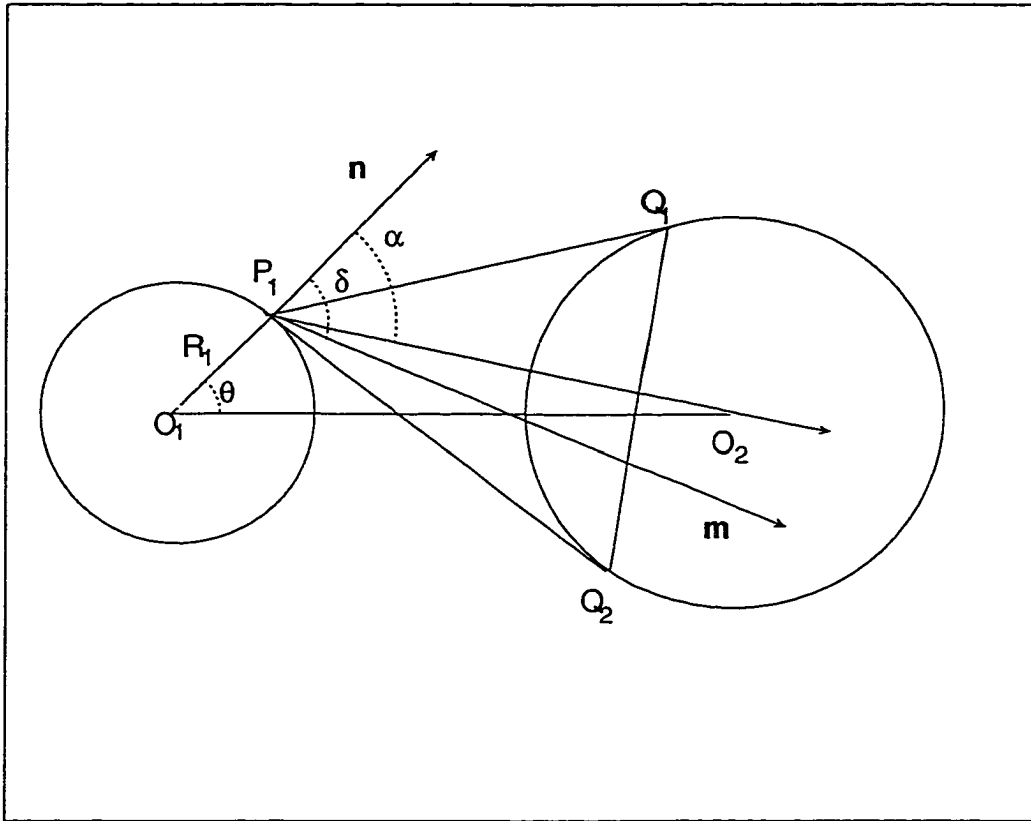


Figure 2.7: The point P_1 on the secondary is in the Entire Irradiation Region. It is irradiated by the primary with a solid angle of $P_1 - B_1B_2$.

Partial Irradiation Region

Schematic of Irradiation Model

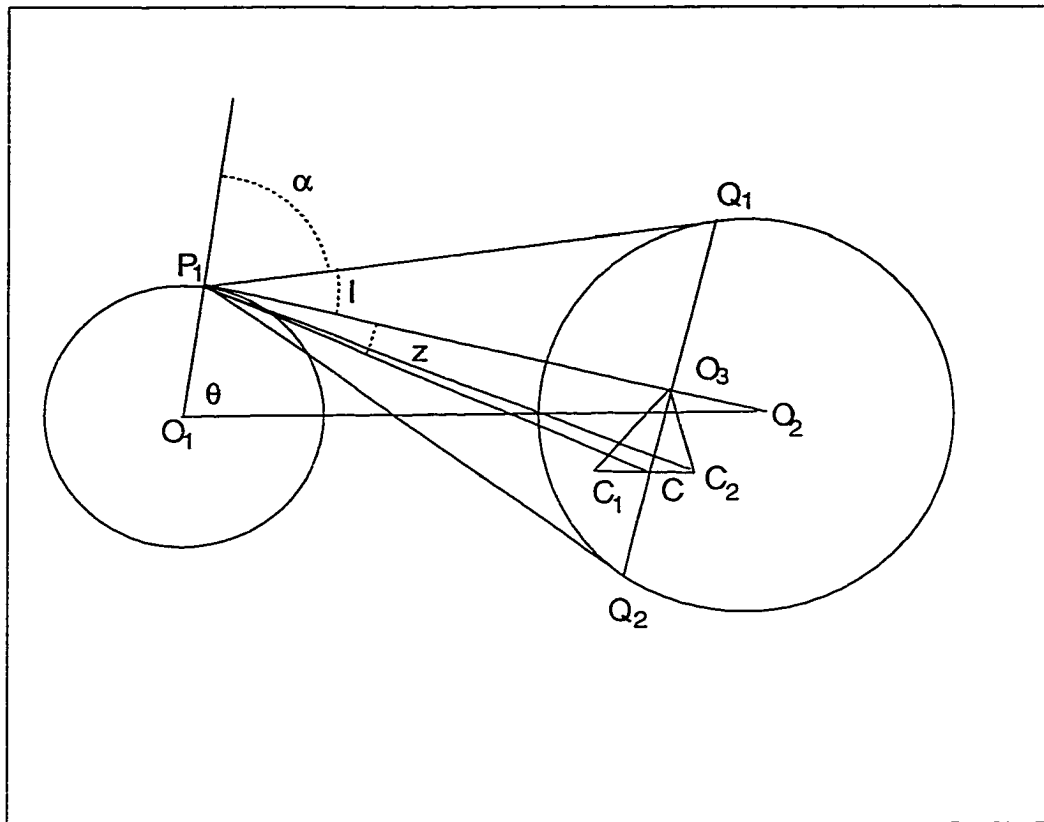


Figure 2.8: The point P_1 on the secondary is in the Partial Irradiation Region - I. It is irradiated by the primary with a solid angle of $P_1 - C_1 Q_1 C_2$. For a point in Partial Irradiation Region - II, α would be $> \pi/2$.

$$\frac{\cos \alpha}{\pi} \left\{ -\sin^2 I \cdot \cos^{-1} \left(-\frac{\tan z}{\tan I} \right) - \sin z \cdot \tan^{-1} (\cos z \sqrt{\tan^2 I - \tan^2 z}) \right\}. \quad (2.14)$$

4) **Non Irradiation Region.** This is the part of the star's surface for $\theta > B$. No emergent radiation from the other star is visible at this angle.

This model, as proposed by Zhou and Leung, may be realistic as well. Among the W subclass of the W UMa class, the fillout % is typically very small, around a few %. The amount of energy which can be transferred through the neck region compared to irradiation is small. As the fillout is increased, they propose that the flow of material through the neck will become more important. The irradiation model can then provide us a lower limit for what we would expect, at a point where little mass exchange occurs. Chapter 3 will discuss the computer model incorporating this theory.

2.6 Flow Dynamics

Systems with large fillouts ($> 30\%$) cannot be realistically modeled with the above method. Instead, we need to model the material flow through the neck region. Webbink (1977) discussed the mechanism for large-scale circulation in contact systems in great detail. The standard conservation equations that are relevant to the flow are:

Mass conservation:

$$\frac{\partial \rho}{\partial t} + \nabla \cdot (\rho V) = 0. \quad (2.15)$$

Momentum conservation:

$$\frac{\partial v}{\partial t} + (v \cdot \nabla)v = -\frac{1}{\rho} \nabla P - \nabla \psi - 2\Omega \times v + \nu \nabla^2 v + \left(\frac{\zeta}{\rho} + \frac{1}{3} \nu \right) \nabla (\nabla \cdot v). \quad (2.16)$$

Energy conservation:

$$\frac{\partial}{\partial t}(\rho(\frac{1}{2}v^2 + u)) = -\nabla(\rho v(\frac{1}{2}v^2 + h + \psi) - v \cdot \vec{\sigma} - F). \quad (2.17)$$

The large list of definitions used is: ρ , the density; v , the velocity of the mass component; P , the gas pressure; ν , the kinematic viscosity; ζ , the bulk viscosity; ψ , the gravitational potential (per unit mass); Ω , the angular velocity; u , the internal energy of the gas; h , the specific enthalpy of the gas; $\vec{\sigma}$, the viscous stress tensor; and F , the heat flux.

With these equations, we can study the flow in the system. Webbink starts with an adiabatic, isopotential, irrotational approximation of the hydrodynamic equations and proceeds to model the luminosity transfer between contact binaries. He first obtains a stationary (non-rotating) solution by neglecting four important effects: (i) the flow's coupling with the gravitational field, (ii) the Coriolis forces, (iii) viscosity effects and (iv) thermal relaxation across the flow. As we might expect, this simplifies the problem greatly. The momentum equation becomes:

$$\frac{\partial v}{\partial t} + (v \cdot \nabla)v = -\frac{1}{\rho}\nabla P. \quad (2.18)$$

and the energy equation:

$$\frac{\partial}{\partial t}(\rho(\frac{1}{2}v^2 + u)) = -\nabla(\rho v(\frac{1}{2}v^2 + h)). \quad (2.19)$$

These simplifications allowed Webbink to obtain stationary solutions to Equations 2.15-2.17. Among his assumptions, he invokes hydrostatic equilibrium for the L_1 point and assumes that the stream velocities (from Bernoulli's equation) are negligible at that limit. Webbink (1975) derived the following quantity in this scenario:

$$h + \frac{1}{2}v^2 = h_0, \quad (2.20)$$

where h_0 is the specific enthalpy of the gas far from the inner Lagrangian point, L_1 . The flow is laminar since it is frictionless and adiabatic (that is, no turbulence develops). Thus it follows:

$$v \times \nabla \times v = 0, \quad (2.21)$$

for this flow.

For Equation 2.18 we then get:

$$\nabla\left(\frac{1}{2}v^2\right) = -\frac{1}{\rho}\nabla P. \quad (2.22)$$

Here, we have used the vector identity:

$$\nabla(v \cdot v) = 2(v \cdot \nabla)v + 2(v \times \nabla \times v), \quad (2.23)$$

to simplify the final result. Webbink then includes the ignored terms and shows that the circulation responsible for luminosity transfer cannot be due to simply an entropy change. Rather, Webbink states that the flow must be due to large-scale circulation induced by rotational and tidal distortion, and by the resulting temperature change occurring within the L_1 region.

Webbink defines the null surface region as the dividing surface between the Roche lobes of the two components. In the null surface region, Webbink shows that an approximation of the flow as having sonic velocities is valid. This results in the pressure change being described as:

$$\delta P \approx P \left(\frac{v_{\text{circ}}}{c_s} \right)^2. \quad (2.24)$$

where v_{circ} is the circulation velocity required to obtain thermal and hydrostatic equilibrium. It can be approximated by:

$$v_{\text{circ}} \approx \frac{\bar{\rho} R \Omega^2 R}{\rho \tau_{KH} g}. \quad (2.25)$$

$\bar{\rho}$ is the mean density of the star, g is the local gravity and τ_{KH} is the thermal (or Kelvin-Helmholtz) time scale for the star. We will call this method I: the Webbink flow velocity.

2.7 Energy Transfer Dissipation In Contact Binaries

Hazlehurst (1985) discussed a model for the dissipation of energy resulting from mass transfer in contact binaries. His argument is based on three basic postulates:

- The heat carrying elements pass from the primary to the secondary without mixing easily with their local surroundings. Hazlehurst describes these elements as interlopers.
- These interlopers arrive with a higher temperature than the surrounding media, leading to a high buoyancy. Thus, these elements rise to the top of the secondary's convective zone. Their speeds are approximately sonic.
- The interlopers then dissipate this kinetic energy at the top of the convective zone. This extra energy is radiatively transported to the secondary's surface, leading to a luminosity enhancement.

Using v as the vertical speed of the elements and λ as the distance they travel before reaching the top of the convection zone, we obtain:

$$T_D = \lambda/v, \quad (2.26)$$

for an order of magnitude estimate for the dissipation time, T_D . The dissipation per unit mass per unit time is:

$$D = \frac{KE_m}{T_D} = \frac{1}{2}v^3/\lambda, \quad (2.27)$$

where $KE_m = \frac{1}{2}v^2$ is the kinetic energy per unit mass. Since the interlopers only comprise a fraction, f , of the material in the secondary, D becomes:

$$D = \frac{1}{2}f\rho v^3/\lambda. \quad (2.28)$$

ρ is the density. The dissipative flux, F_D can be defined as:

$$F_D = D\lambda = \frac{1}{2}f\rho v^3, \quad (2.29)$$

and finally, the dissipative luminosity, L_D as:

$$L_D = 4\pi R^2 F_D = 2\pi R^2 f\rho v^3. \quad (2.30)$$

Hazlehurst uses this theory to explain the W UMa light curve paradox (see Section 1.1).

He obtains a maximum vertical velocity v of:

$$v = 0.83c_s \quad (2.31)$$

where $c_s = \sqrt{\frac{2}{3}c_p T}$ is the speed of sound. c_p is the specific heat at constant pressure.

As the interlopers rise in the convection zone, they split into smaller bubbles, which Hazlehurst calls "descendants". As they split, some of the bouyancy energy is transferred into lateral motion. As these descendants rise, and split more, the interlopers push on each other even more, as they take up an increasing fraction of f the closer they get to the surface. Hazlehurst derives W , the bouyancy energy, per unit mass as:

$$W = \frac{3}{2}(e^{0.2\Delta S} - 1)c_0^2, \quad (2.32)$$

where c_0 is the speed of sound at the layer of contact. ΔS is the entropy excess of the interlopers. He obtains a lateral velocity u_t of:

$$u_t = 0.25c_s. \quad (2.33)$$

Hazlehurst uses an example with $M_1 = 0.85M_\odot$ and $M_2 = 0.5M_\odot$, and assuming the primary is on the main sequence, he calculates $u_t \approx 2$ km/s.

With such a high flow velocity, the bubbles can reach all the way around the secondary by the time they dissipate their energy. Thus the secondary, which should be much cooler, instead has a temperature only slightly cooler, or possibly, *warmer* than the primary. The latter case describes the W-type subclass. This flow velocity will be method II: the Hazlehurst flow velocity.

2.8 Inherent Existence Of Circumfluence

Zhou and Leung (1990) also discuss the theoretical calculation of the flow in a contact system. They first prove that the isothermal surface is not coincidental with the isobaric surface in a static model of a contact binary. This implies a baroclinic structure in a contact binary atmosphere, which means the development of circumfluence (hydrody-

namical flow) is inevitable. They suggest then, that a static model shouldn't be used to model a contact binary atmosphere. Thus the need to use a dynamic model results from the existence of this circumfluence. Using the momentum conservation Equation 2.16 without viscosity they obtain a value for the circumfluence in a contact system:

$$\left(\frac{\partial(\nabla \times v)}{\partial t}\right)_0 = C_0 F(q, \alpha)(a \times r). \quad (2.34)$$

C_0 is a constant made up of various physical constants and system parameters:

$$C_0 = \frac{3G\kappa\rho_0}{16\pi c a_{rad} T^4} \frac{M_1 L_2}{R_1^3 R_2^3} > 0. \quad (2.35)$$

κ is the opacity and a_{rad} the radiation constant. Figure 2.9 (From Figure 2, pg 272 of Zhou and Leung (1990)) illustrates \vec{a} and \vec{r} . $F(q, \alpha)$ is called the direction function:

$$F(q, \alpha) = (1 - q^{1-\alpha}) - \frac{1 - q^{1+\alpha/2}}{(1 + q^{\alpha/2})^3}, \quad (2.36)$$

where q is the mass ratio and α is derived from the mass-luminosity relationship for the two stars. Zhou and Leung find, that for a large range of q , α is about the same: for $0.2 < q < 1.0$, $\alpha = 0.82$. As q drops to 0.07, $\alpha = 0.81$. Since only a handful of W UMa systems have $q < 0.2$, we can assume $\alpha = 0.82$. A plot of $F(q, \alpha)$ vs q for $\alpha = 0.82$ is shown in Figure 2.10.

From this we can then determine a flow velocity for the system. A later paper (Zhou and Leung (1997b)) shows a numerical simulation of 2-D circulation. After letting the calculation go for 6733 minutes, they reach a characteristic velocity of 1 km/s. This is for an A type system, with the primary's mass, $M_1 = 1.5M_\odot$ and $q = 0.5$. This velocity is consistent with those obtained by the above methods.

Potential on an Arbitrary Point

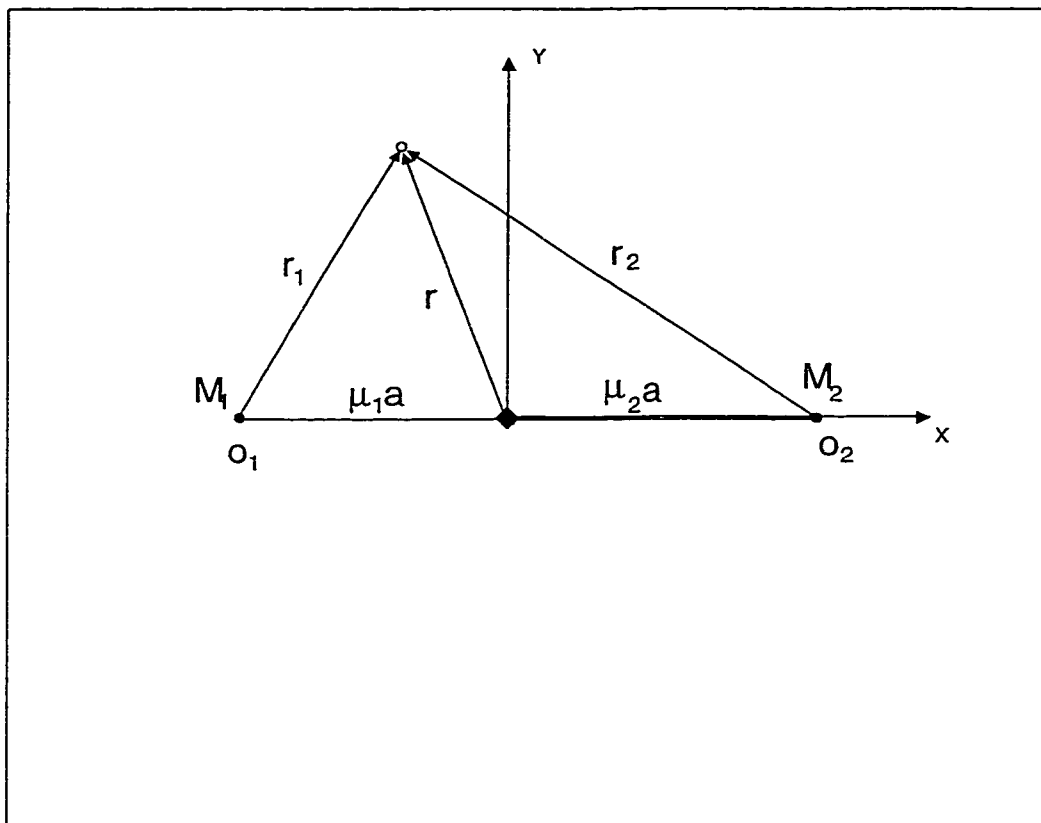


Figure 2.9: This is a plot of the variables used for the $\vec{a} \times \vec{r}$ term in Zhou and Leung's model. The μ 's are reduced masses.

The Direction Function vs Mass Ratio

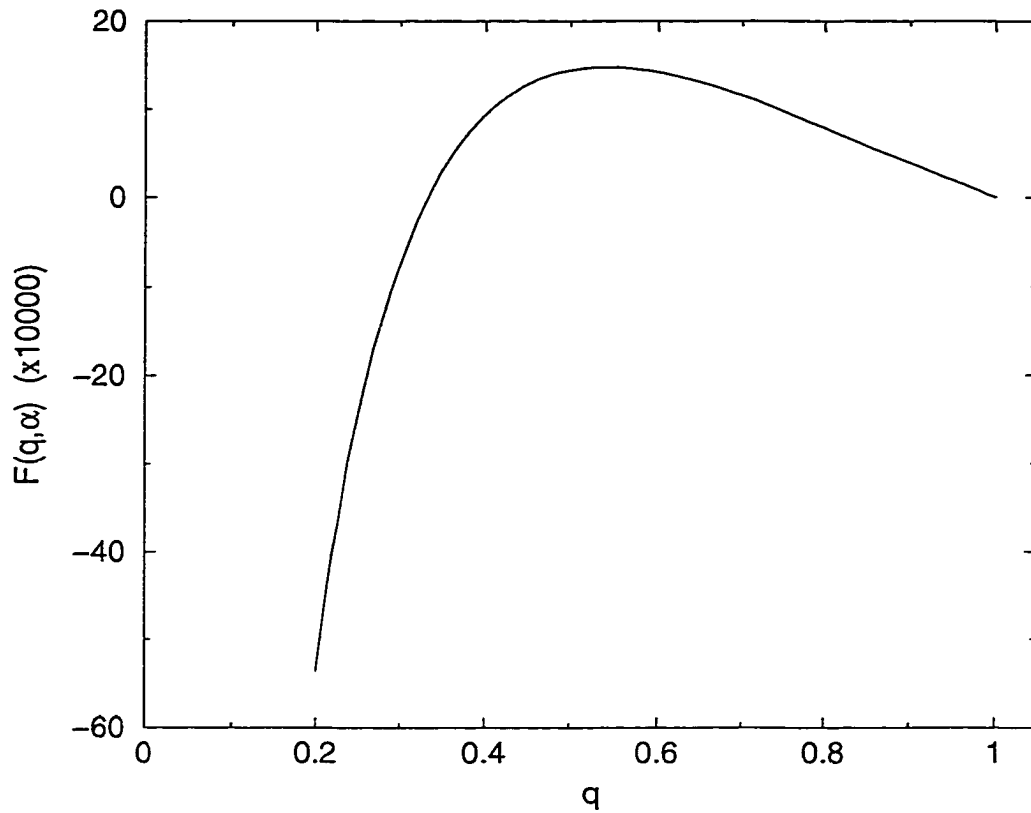


Figure 2.10: A plot of $F(q, \alpha)$ vs q . As stated in the text, we can assume a constant $\alpha = 0.82$ over the range of q involving W UMa systems.

2.9 The Coriolis Force

Zhou and Leung's 1990 theory incorporates the Coriolis force. Unfortunately, their 1997 model does not. So, we need to find some way to calculate the effect the coriolis force has on the flow. The proper way is to incorporate $\nabla \times v$ into a 3-D model. In order to gain insight into future work in three dimensions, a 2-D approximation will be used. We are primarily concerned with how the coriolis force affects the bouyant interlopers in assisting or restricting their rise in the convection zone.

Hazlehurst (1999) used streamlines to show how the velocity field would be altered by the Coriolis force. Starting with Equation 2.16 above (again without viscosity):

$$\frac{1}{2}\nabla v^2 - v \times \nabla \times v + 2\Omega \times v = -\nabla\phi - \frac{1}{\rho}\nabla P, \quad (2.37)$$

he takes the vector product of this with \hat{r} to obtain the component equations:

$$\frac{\partial}{\partial\theta}(\phi + \frac{1}{2}v^2) = (\eta_r + 2\Omega \sin\theta \cos\phi)v_\phi, \quad (2.38)$$

$$\frac{1}{\sin\theta} \frac{\partial}{\partial\phi}(\phi + \frac{1}{2}v^2) = -(\eta_r + 2\Omega \sin\theta \cos\phi)v_\theta. \quad (2.39)$$

The vorticity component perpendicular to the surface is represented as:

$$\eta_r = \frac{1}{R \sin\theta} \left(\frac{\partial v_\theta}{\partial\phi} - \frac{\partial}{\partial\theta} \sin\theta v_\phi \right). \quad (2.40)$$

Hazlehurst's (1997) view is that there is no hydrodynamical argument favoring a constant Jacobi energy (the sum of the kinetic and potential energies) as derived from the consideration of the symmetry-breaking caused by the Coriolis force. Further topological changes in the flow may result. If we assume that the Jacobi energy ($\Phi + \frac{1}{2}v^2$) is

constant everywhere then Equations 2.38 and 2.39 result in the following:

$$\eta_r + 2\Omega \sin \theta \cos \phi = 0. \quad (2.41)$$

Hazlehurst show that this results in solutions of the form:

$$v_\theta = \frac{A}{\sin \theta} - \Omega R \sin \phi, \quad (2.42)$$

$$v_\phi = -\Omega R \cos \theta \cos \phi. \quad (2.43)$$

He assumes approximate sphericity to make his calculations remain analytic, setting $A = 0.1\Omega R$. This allows for a maximum rms radius variation of 10% of the average radius for the star. Next, Hazlehurst relaxes the constant Jacobi energy condition, which means now:

$$\eta_r + 2\Omega \sin \theta \cos \phi = F, \quad (2.44)$$

where $F \neq 0$. This alters the velocity componets thusly:

$$v_\theta + u_\theta = \frac{A}{\sin \theta} - R \sin \theta \left\{ \Omega - \frac{F}{1 + \sin \theta \cos \phi} \right\}, \quad (2.45)$$

$$v_\phi + u_\phi = -R \cos \theta \cos \phi \left\{ \Omega - \frac{F}{1 + \sin \theta \cos \phi} \right\}. \quad (2.46)$$

Using the same A limit with $F = -0.5\Omega$, he calculates stagnation points for both cases. For the constant case, $\theta = 5.74^\circ$ and $\theta = 174.26^\circ$. Relaxing the constant condition results in $\theta = 3.82^\circ$ and $\theta = 176.18^\circ$ for the location of the stagnation points. Hazlehurst's interpretation is that the area covered by closed streamlines increases slightly as

we relax the energy condition. Obviously then, the open streamline region has shrunk. So, we have here an idealized point source or sink for a 2-D flow field. The velocity increases to very high values whenever a source or sink is approached.

With the stagnation points we have a meeting point for the open streamlines. Where these lines meet, the Jacobi energy will be the same for all the streamlines. Therefore, if we could connect every point on the surface via an open streamline with this stagnation point, we would have a situation where the Jacobi energy was constant over the whole surface.

Hazlehurst's argument is in response to the work of Kahler (1995, 1997a, 1997b and 1997c), who argues that the Jacobi energy is constant. Using this condition, he shows that contact binaries evolve on *thermal* time scales, in cycles oscillating between marginal contact and semi-detached configurations. Standard models for common envelope systems have them evolving slower than thermal time scales and thus have the contact configurations being stable and long term. For our purposes the correctness of either argument is not of primary importance. Both methods result in material streams that move rapidly from the hot to cool component during the contact phase. During the Kahler semi-detached phase, the irradiation model of Zhou and Leung would apply. Kahler's flow velocities, while not identical to Hazlehurst's values, are similar enough that we need not consider both methods in the current simple model, where all we wish to use this theory for is the flow velocity value. Thus an approximation of Hazlehurst's method for finding the flow velocity will be used in the code.

Chapter 3

Modeling Code

In the case where the components in a binary system do not have strong tidal interactions, sphericity with minor perturbations can usually be assumed. Thus, spherical symmetry can be used to determine locations on and in the star. However for very close and contact binaries, this approximation breaks down. Due to the differential tidal forces, the components distort significantly so the spherical symmetry can no longer be used. Instead, the Roche equations are used to describe the system (see e.g. Kopal, 1958). Tassoul (1992) outlined a set of Roche harmonics to utilize in contact systems. It is with these harmonics that a simple code model has been developed.

3.1 The Irradiated Model

The code based on the Zhou and Leung irradiation model (1997a) is outlined below. As stated in Chapter 2, it can be used to look at the *W* type subclass in particular, due to the low fillout ratio those systems have, on average. For *A* types, this approximation breaks down, due to the large fillout ratio. Their model will be covered in Section 3.2. The code, written in C, can be broken into five main areas:

- 1) The temperature profile.
- 2) The flow velocity.
- 3) Coriolis force effects.
- 4) Calculation of the luminosity of the irradiated star.
- 5) Calculation of a synthetic light curve.

Important parameters, such as the masses of the components, their temperatures and sizes, will be read in and used by the code to generate the final result, a theoretical light curve which can have OER measured for it. Since we are assuming spherical symmetry for the irradiated case, the light curve will not qualitatively resemble a system with distorted components. For this model we are primarily interested in showing the trends – that is, how the irradiated model OER varies as we change one of the parameters. Then we will compare this with systems in the database that (ideally) only vary significantly for the same parameter.

3.1.1 Calculation Of The Irradiated Temperature Profile

To begin, a set of data is read in which contains parameters we will need during calculation. The Roche lobe radii, r_1 and r_2 , of each component are used to calculate the angles A and B , which are used to obtain the region for which one of the three irradiation equations (2.12, 2.13 and 2.14) apply. $F(\theta)$ is then calculated, with θ having one degree steps from 0° to B° . This $F(\theta)$ value is then plugged into Equation 2.10. The other parameters of this equation, s , the absorption factor, and surface temperature of each star (T_{10} and T_{20}) are also fed in as known values. It should be noted that the temperatures are not the same as the ones shown in Appendix A. This is because Zhou and Leung’s hypothesis is to assume two normal systems, which just happen to be close enough to heat each other via irradiation. Since in general we assume the components are somewhere between ZAMS and TAMS in their evolution, the mass-luminosity rela-

relationship for main sequence stars will be used to estimate a surface temperature for each component.

For the larger mass component, this will turn out to be very close to its model temperature. This is because if we have two stars, both on the main sequence, then the more massive one is more luminous. The hotter star's energy falling on the cooler component has a bigger effect on the secondary's final luminosity than the reverse. The code calculates the radiation of each star on the other anyway.

Thus for a system with $M_p = 1.0M_\odot$ and $M_s = 0.4M_\odot$ we would have $T_p(= T_{20}) = 5800\text{K}$ and $T_s(= T_{10}) = 3400\text{K}$. This is much larger than the observed temperature differences, typically from 100-500K. Therefore if the Zhou and Leung model is to be valid, it must predict the surface temperature over most of the cool component rising dramatically. Figure 3.1 is a plot of the above situation, showing the increase in T_{10} . As can be seen, the original ΔT has changed from 2400K to 750K. Perhaps a higher absorption coefficient is needed for such a cool star. While the magnitude of the theoretical value may be off, the relationship should remain consistent, that is, we would expect the temperature distribution to follow the same functionality, regardless of the choice of s . In order to calculate an exacting model for a given system, we would need to determine a better s . But for comparing two systems, the profile should still increase if the primary temperature increases.

3.1.2 The Flow Velocity

Since this irradiation creates a temperature profile, this temperature gradient will therefore lead, by necessity, to a heat flow and the calculation of the velocity of this flow is our next step. Since we are dealing with an irradiation case, the flow here would simply be flow along the equator of the irradiated star. Using Equation 2.24 can give us an estimate for the flow velocity. Substituting the perfect gas law ($P = \frac{k}{\mu H} \rho T$) into the

Surface Temperature

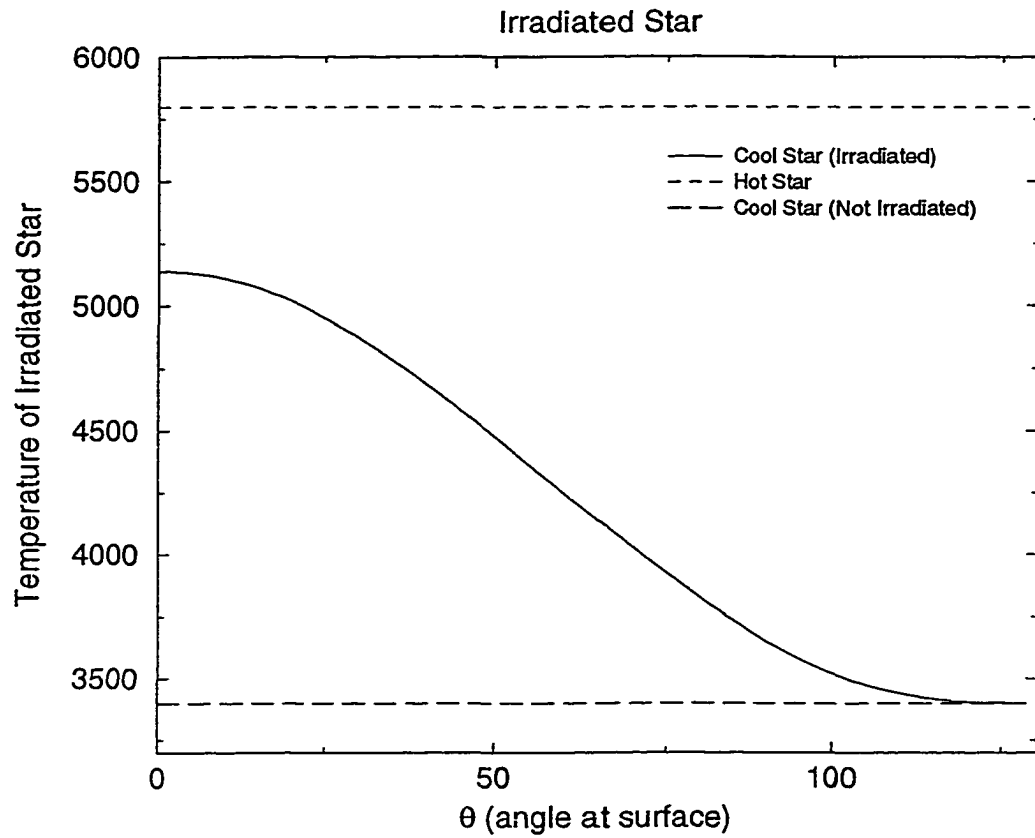


Figure 3.1: The effect of a hotter star on the temperature of the cooler star. This is for the example in the text. At the limit of no irradiation, the temperature goes to the unaffected temperature.

above equation, we get:

$$\frac{\delta P}{P} = \frac{\delta(\rho T)}{\rho T} = \left(\frac{v}{c_s}\right)^2. \quad (3.1)$$

Let us assume the density is constant, that is, the heating doesn't change the local ρ .

The above becomes:

$$\frac{\delta T}{T} = \left(\frac{v}{c_s}\right)^2. \quad (3.2)$$

If we consider density changes along the gradient, then $\delta\rho$ changes in the opposite direction as the temperature. That is, as the temperature decreases, the local density would increase. This would lower the flow velocity. Therefore v is an upper limit. Since the problem of integrating the flow velocity must really be done by models which can develop over time, this can become a tedious exercise (see, for example Zhou and Leung (1997b)). Thus, we will use the above method (from Webbink, Section 2.6) to obtain an upper limit and parameterize the flow as well, with lesser values.

3.1.3 Application Of The Coriolis Force

The irradiated material will move along the surface, since this is the direction of the temperature gradient caused by the excess radiation. Since the star is rotating, the Coriolis term should be kept in the conservation Equation 2.16. This term is a cross product:

$$a_{cor} = 2\Omega \times v. \quad (3.3)$$

Ω is the angular velocity. For a spherical star, if the material moves along the surface, v will be perpendicular to Ω . This means that a_{cor} will be maximal:

$$a_{cor} = 2\Omega v. \quad (3.4)$$

Since we are staying in the plane, v remains perpendicular to Ω .

This a_{cor} will accelerate the irradiated material vertically. From a view over the pole of the star, we would have material flowing in a clockwise direction on one side of the star, while the material would flow in a counter-clockwise direction on the other side (see Figure 3.2). Thus a_{cor} would accelerate the material down on one side, and lift it up on the other side as it moves along. Countering this would be the buoyant force. On the side where the material is driven down by the coriolis acceleration, the buoyancy will increase as the material falls. Eventually, the force up due to buoyancy will be greater than the downward force due to the coriolis acceleration.

The buoyancy acceleration on the irradiated mass can be approximated by:

$$a_{buoy} = \frac{GM_*}{R_*^2}, \quad (3.5)$$

where M_* is the mass of the irradiated star and R_* is the radius of the irradiated star. This approximation assumes that the density of the bubble of heated material is very close to the density of the surrounding media. If this is not true, a factor of $\rho_{media}/\rho_{material}$ would be introduced. From Equation 3.5, we can see that as we go into the star, the radius will decrease as will the mass contained within that radius. Looking at standard polytropes for main sequence stars, we find that the radius term dominates the change in the upper regions of the star. Thus, a_{buoy} will increase as the radius decreases.

So at the point that $a_{cor} = a_{buoy}$, the acceleration is zero. However, the vertical velocity of the material isn't zero, it still has a downward velocity. The material will eventually be decelerated to zero velocity, due to the buoyant acceleration. Thus the

Flow In The Irradiated Star

With Direction Of Coriolis Acceleration

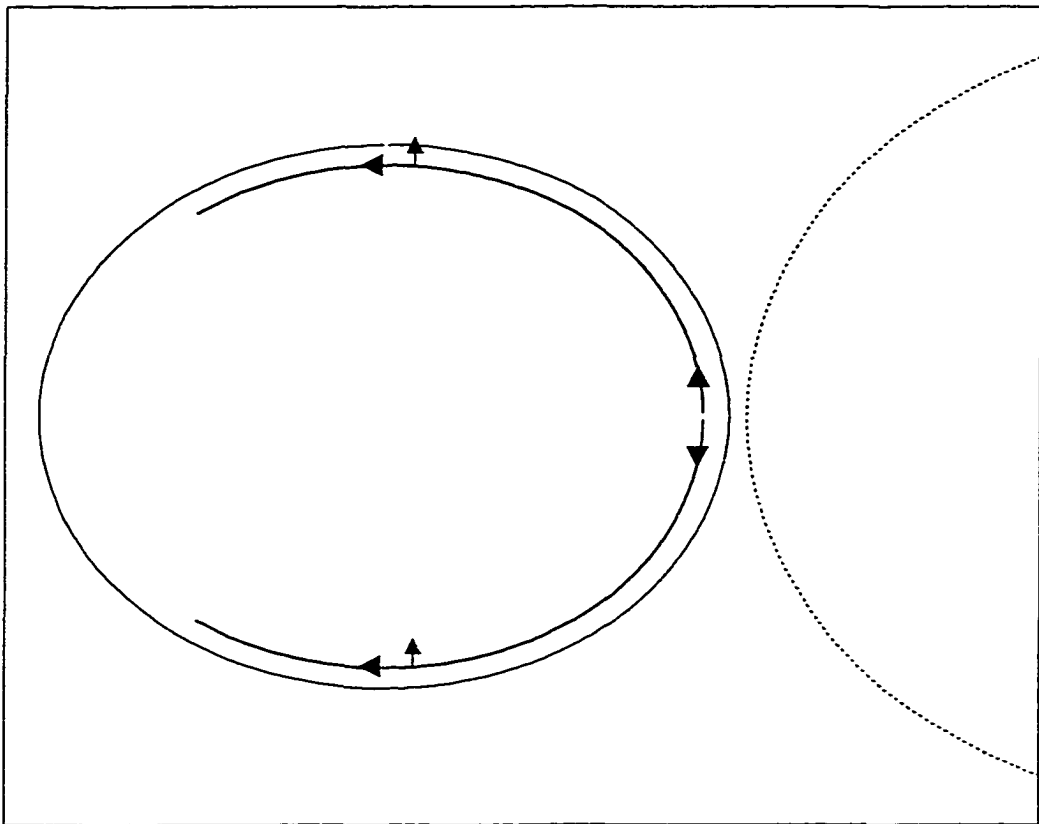


Figure 3.2: A plot of the flow and the coriolis effect upon it for an irradiated star. The bold lines represent the irradiated material, with the direction of flow indicated. The material is hottest at the point closest to the other star. The small arrows indicate the direction of the coriolis acceleration. The system is being viewed from the top and has clockwise rotation.

varying velocity will be integrated to find the total travel distance. The heated material will now be at a higher optical depth, τ than before. If we assume some mean opacity, $\bar{\chi}$, then the relationship between the optical depth and the radial coordinate is:

$$d\tau = -\bar{\chi}dr. \quad (3.6)$$

The optical depth gets bigger at smaller radius. We can find the change in radius, since we know the flow velocity. Then we can get the new optical depth by:

$$\tau_{new} = \tau_{old} + \bar{\chi}(r_{old} - r_{new}), \quad (3.7)$$

where we will use $r_{old} = R_*$ and $\tau_{old} = 2/3$, which is the base of the photosphere.

Now we can calculate the new effective temperature at $\tau = 2/3$ by:

$$T(\tau)_{new}^4 = \frac{3}{4}T_{eff}^4\left(\tau + \frac{2}{3}\right). \quad (3.8)$$

$T(\tau)_{new}$ is the temperature of the irradiated material, which has been sunk to its new optical depth τ . We then solve this equation for T_{eff} . Now we have the Coriolis adjusted temperature profile at the base of the photosphere (see Figure 3.3).

For the rising side of the star, the situation reverses. The buoyant force is in the opposite direction from before since the material doesn't want to rise naturally as the material is too heavy. The coriolis acceleration drives it to rise. Eventually a point is reached where the material will be so heavy that the upward coriolis accieration won't lift it anymore.

The final step in this calculation is to realize that the material at lower optical depths will be irradiated by some diminishing exponential factor. Thus we need to integrate this extra radiation over some reasonable range in τ . A value of $\tau = 3.67$ results in

Coriolis Effect On Temperature Profile

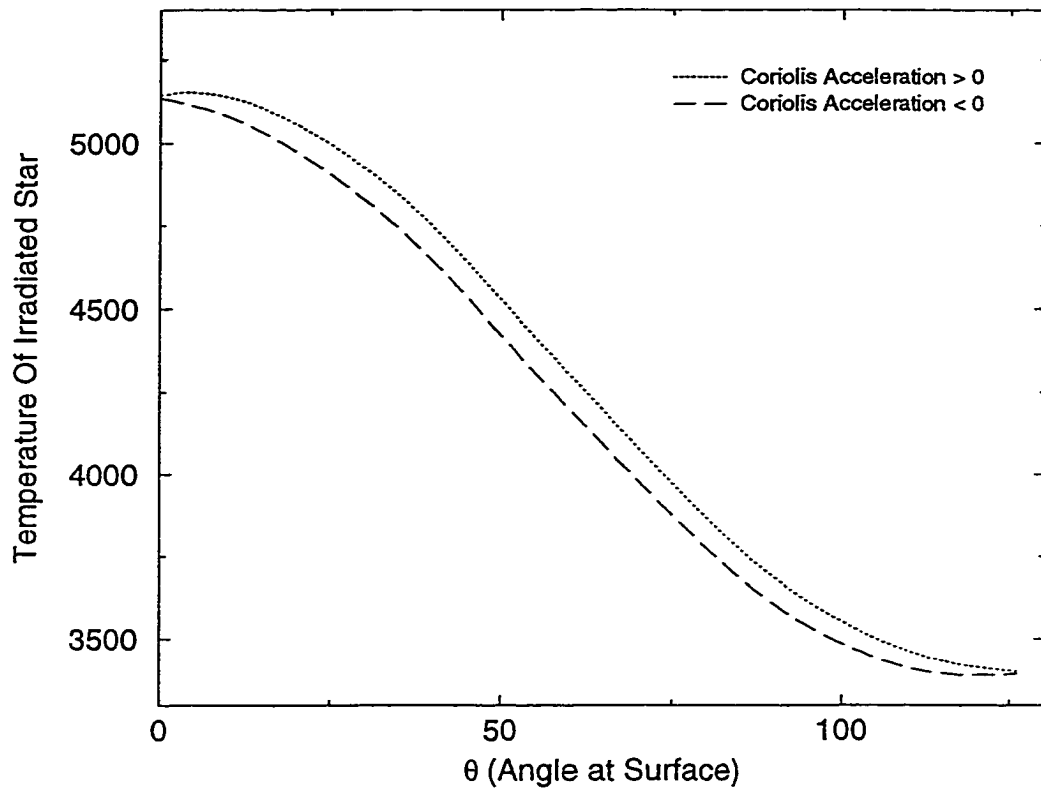


Figure 3.3: A plot for the example from Figure 3.1, with the Coriolis Acceleration on the heated material figured in. The difference is very small, but this is reasonable, since no large changes in $B - V$ for most W UMa systems are observed, during the eclipse cycle.

the irradiated flux being 1% of its $\tau = 2/3$ value. This is the range over which we will integrate.

3.1.4 Luminosity Calculation

Once we have a temperature profile, the next step is to calculate the new luminosity for that part of the surface. Since we are dividing the surface up into 1° slices, each pre-irradiated slice has luminosity 1/360th of the total luminosity. If, $T_{slice} \neq T_{surrounding}$ we get:

$$L_{slice} = \frac{L_*}{360} \left(\frac{T_{slice}}{T_*} \right)^4 \quad (3.9)$$

Summing over the surface of the star would then give the total luminosity. However, we need something different, the visible luminosity for the part of the star facing us. We also have to add the luminosity from the other component, and take into account the eclipses. A synthetic light curve will be calculated for each theoretical model. This will be done by adding up the luminosity of the 180 visible 1° slices for each star. Any slices obscured by the other star will not be added into the luminosity sum. From this a light curve can be constructed. This light curve will then have an OER calculated as detailed in Chapter 2. These theoretical OERs will then be compared with the database values. For simplicity, an inclination angle of 90° (eclipses seen edge on) will be used.

3.2 The Contact Model

The code based on the Hazlehurst contact model is outlined in the following subsections. This code is also written in C and will be used to look particularly at the A-type subclass. The method of calculation is similar with the differences detailed below for the contact case.

3.2.1 Tassoul's Coordinate System

Tassoul's system is a Roche coordinate system, which allows an easier way to express the location of the bubbles (see Hazelhurst (1996)) and their eventual superposition onto the local luminosity of the unheated (but spherically distorted) Roche lobe star. In this system, the radial component is replaced with the coordinate a , which is not spherically symmetric. Rather, the symmetry is based on the shape of the surface derived from the Roche potentials. That is, all points on the surface are at the same a , even though they are obviously not at the same radial distance from the center of mass. Tassoul begins by stating the Coriolis force components for a simple spherical case:

$$C_r = 2\Omega_0(\sin \phi v_\theta - \cos \theta \cos \phi v_\phi), \quad (3.10)$$

$$C_\theta = -2\Omega_0(\sin \phi v_r + \sin \theta \cos \phi v_\phi), \quad (3.11)$$

$$C_\phi = 2\Omega_0(\cos \theta \cos \phi v_r + \sin \theta \cos \phi v_\theta). \quad (3.12)$$

Then the temperature structure can be viewed as a deviation from spherical symmetry:

$$T = T_0(r) + T_1(r, \theta, \phi) + \dots, \quad (3.13)$$

Spherical harmonics can be used to handle this deviation from perfect sphericity.

However, for a close or contact binary case, this approximation will not work. Due to the greatly distorted shape of the components, Tassoul describes a similar method, but using Roche harmonics rather than spherical harmonics. Tassoul defines the Roche coordinate system with:

$$\frac{1}{a} = \frac{1}{r} + q \sum_{j \geq 2} r^j P_j(\lambda), \quad (3.14)$$

where λ being the usual designation for $\cos \theta$, and the P_j 's are Legendre polynomials. A similar equation exists for η , the angular coordinate:

$$\eta = \lambda + q(1 - \lambda^2) \sum_{j \geq 2} \frac{r^{j+1}}{j+1} P_j'(\lambda). \quad (3.15)$$

The final coordinate, ζ , coincides exactly with the azimuthal angle ϕ . From this, Tassoul derives a similar temperature structure equation:

$$T = T_0(a) + T_1(a, \eta, \phi) + \dots, \quad (3.16)$$

The biggest hurdle to Tassoul's work is proper consideration of the boundary conditions. Whatever expansion we use to express T , the values must match up at the opposite ends of the stars. That is, if we use an expression for T to express the temperature on one side of the star, it must match up for value at the point where we are on the back side of each component (this would be the part of the star we see directly at 0.0 and 0.5 phase).

We will use Tassoul's coordinates to provide a first order correction to the spherical star models generally used. This will result in change in the temperature distribution on the surface, since the surface has changed shape. For the first order expansion to Equation 3.14 ($j = 2$), we have:

$$\frac{1}{a} = \frac{1}{r} + qr^2 P_2(\lambda). \quad (3.17)$$

Using $P_2(\lambda) = \frac{1}{2}(3\lambda - 1)$, we get:

$$a = r\left\{1 + \frac{qr^3}{2}(3\lambda^2 - 1)\right\}^{-1}. \quad (3.18)$$

Here, a is the Roche coordinate equivalent of radius. For a common envelope, the distance from the center of mass of the binary will be the constant value a . Equation 3.6 becomes:

$$\eta = \lambda + q(1 - \lambda^2)\frac{r^3}{3}P_2'(\lambda), \quad (3.19)$$

where now, $P_2'(\lambda) = 3\lambda$. Finally for, η we get:

$$\eta = \lambda\{1 + q(1 - \lambda^2)r^3\}. \quad (3.20)$$

As above, η is the Roche equivalent of θ , measure from the line connecting the two stars, with a vertex at the center of mass. These relationships for a and η will be used for the contact model.

So, if we assume the first order approximation, we get:

$$T(\eta) = T_0 + T_1(A\eta + B\eta^3), \quad (3.21)$$

where A and B depend on the boundary conditions. As previously stated, this is the primary weakness of the Tassoul coordinate method. We do have two boundary conditions: $T(-1) = T_H$, on the backside of the hot star, and where the two stars meet $T(\eta_{contact})$ is the same for each system, since the stars are coincidental. If we use a guess for the backside temperature of the secondary, $T(1) = T_C$, we can determine A and B for each model. Preferably, we don't want to have to do this, we would rather determine T_C from the model. Because of this problem, we will use the same ΔT method as outlined for the irradiated model.

3.2.2 The Contact Flow Velocity

Hazlehurst's method will be used to find the lateral flow velocity of the interloper material. We will also use his assumption that the material spreads laterally in evenly sized bubbles along the surface. Thus, for reasonable guesses of the specific heat in the envelope, the flow velocity will be calculated using Equation 2.33. The difference between this situation and the irradiated case above, is that here we are using the Tassoul coordinate system, which means we first need to convert back to a system based on r and θ to find the velocity component perpendicular to the old radial coordinate. This is the velocity that will be used in Section 3.3.3 to find the Coriolis acceleration on the interlopers.

3.2.3 Application Of The Coriolis Force

The Coriolis acceleration will be calculated in the same manner as Section 3.1.3 above, using the velocity as outlined in Section 3.3.1. The primary difference between the two methods is that only the component of the velocity tangent to the velocity is used, since the original term is really $2\Omega \times v$. This results in an altered version of Equation 3.4:

$$a_{cor} = 2\Omega v \sin \theta. \quad (3.22)$$

3.2.4 Transferred Luminosity Calculation

The transferred energy is calculated using Hazlehurst's dissipation theory outlined in Chapter 2. Since we are assuming even distribution of the bubbles along the surface, we can assume the dissipative luminosity, L_D (Equation 2.30) is spread evenly as a function of the angle $\sin^{-1} \eta$. The luminosity will be diminished on one side and enhanced on the other, due to the Coriolis acceleration. Then, $L_D(\eta)$ will be added to the underneath

static luminosity and this new total luminosity (per angle slice) will then be used to calculate the theoretical light curve, as in Section 3.1.4. For this case, we will sweep the angle $\sin^{-1} \eta$, rather than θ .

3.3 Grid Sweeping

For each of the above two models, a sweep of the important parameters will be done. The independent parameters varied will be: $M_{1,2}$ (and thus q), $R_{1,2}$, $T_{1,2}$ and P . A reasonable range of values for each of these parameters would be:

- $M_{1,2}$: Maceroni and Van't Veer's method (1996) calculate values between $0.2M_{\odot} - 2.2M_{\odot}$. This will be the range used, with the additional constraint of $0.1 < q < 1.0$.
- $R_{1,2}$: The physical radii (in R_{\odot}) are determined from the given masses (above) and the WD scaled radii. Thus the value of $r_{1,2}$ will be varied. The important constraint here is that $r_1 + r_2 \leq 1.0$. Also, if $r_1 + r_2 \ll 1.0$ we have a system which isn't a close binary. Referring to the database shows that most WD models for W UMa systems have $r_1 + r_2 > 0.75$. We will use a range of $0.65 \leq r_1 + r_2 \leq 1.00$ for this parameter. The two radii will be varied separately, subject to the above constraint.
- $T_{1,2}$: As shown in the example above, the temperatures used for the irradiated model will be the ZAMS value for a detached system. Since the mass is already determined, this will fix the value of T_1 used for the primary. For the contact case, the temperature of the secondary will be determined by a temperature difference relative to the primary, as determined by Hazlehurst's method. A range of 3000K - 7500K will be used.

- *P*: For the period, the range for W UMa systems is from 0.22 d up to 1.15 d. We will use 0.2 d to 1.2 d.

A spacing no bigger than 1% of the range will be used in each case. Chapter 5 will detail the results, as well as the comparisons with the database.

Chapter 4

The W Ursae Majoris database

4.1 Database Details

A large database of W UMa systems has been gathered, and is displayed in Appendix

A. This database has been collated to serve many purposes:

- To be the single largest collection of fundamental parameters of W UMa systems. A number of systems have data published that were not included in an exhaustive paper by Maceroni and Van't Veer (1996). The present database attempts to remedy this by using the neglected systems, as well as the Maceroni and Van't Veer systems. This will allow a search with the largest available statistics to check for correlations between the various parameters.
- Include the measurements of what we call the O'Connell effect Ratio (*OER*) and the Light Curve Asymmetry (*LCA*), as outlined below. A method has been used, developed by McCartney, Leung and Herczeg, to provide a more detailed measure of the O'Connell effect than the historical method used by O'Connell and later researchers.

- To allow for a comparison between the Coriolis modeling code (discussed in Chapter 3) and the observational data.

The data set has come from the literature, where a wide variety of sources were used. Most important were those systems which had observations with well separated epochs (e.g. VW Cep, AM Leo, and RZ Com), allowing for a check in variations of the *OER* and *LCA* with time. The model parameters come from published models, usually determined by the Wilson-Devinney method.

4.1.1 Derivation Of Physical Properties

Maceroni and Van't Veer (1996) (hereafter MV) utilize an angular momentum argument to determine a (hopefully) consistent set of physical parameters for W UMa systems, such as the radius (in R_{\odot} units) and mass (in M_{\odot}). The method is based on two assumptions: 1) the total luminosity of the system is not affected by the interaction between the components, and thus the common envelope radiates the same luminosity as the sum of the internal luminosities. This means the total luminosity is the same as for two detached components of the same mass and age. 2) The components of W types are considered ZAMS, while for A types they are considered as Terminal-Age Main Sequence (TAMS). The total luminosity is then determined by:

$$L = 4\pi\sigma a^2(r_1^2 T_1^4 + r_2^2 T_2^4). \quad (4.1)$$

If we use Kepler's third law, we can express this as:

$$L = c m^{2/3} P^{4/3} (r_1^2 T_1^4 + r_2^2 T_2^4), \quad (4.2)$$

with $c = (4\pi)^{1/3} G^{2/3} \sigma$, $r_{1,2}$ are the fractional radii and $T_{1,2}$ are the effective temper-

atures of the primary and secondary components. Then, using isochrones from Vandenberg (1985), they looked for the intersection of the solution from the locus for the luminosity-mass relationship with the isochrone. Maceroni and Van't Veer used isochrones between 1 and 8 Gyr. These derived values will be used in the present study as well; in addition the systems not included in Maceroni and Van't Veer's study have had their physical parameters calculated in this way.

4.1.2 Relationships Of Non-*OER* Parameters

Several parameters have had relationships plotted by previous authors. One of the more significant is color vs period (Mochnacki (1985)). In Figure 4.1, we see a clear relationship between these values. The hotter stars have the longer orbital period. This diagram also serves to show one fundamental difference between the A and W subtypes, namely their temperatures (or colors).

Thus, the more massive and physically larger stars have longer rotation periods. Since the primaries are main sequence, this also implies they are hotter. We see that a few of the A types mix in with the W types. These systems will be plotted with the W types when we look at the results from the irradiation model in Chapter 5. A similar plot results for density vs temperature (see Figure 4.2). Color and temperature are directly correlated and as we move up the main sequence, the stars are less dense. This plot affirms the previous differences between the A and W types.

A final plot (Figure 4.3) shows the relationship between the total mass of the system and q . This data does not have the same tight correlation of the above examples. However, if we look at just the W type, a weak correlation exists. For the A type, it seems that there are two populations, which split around $q = 0.4$. A plot of the two subsets shows that they tend to have different temperatures. The higher q value systems are cooler (see Figure 4.4).

Color vs Period Diagram

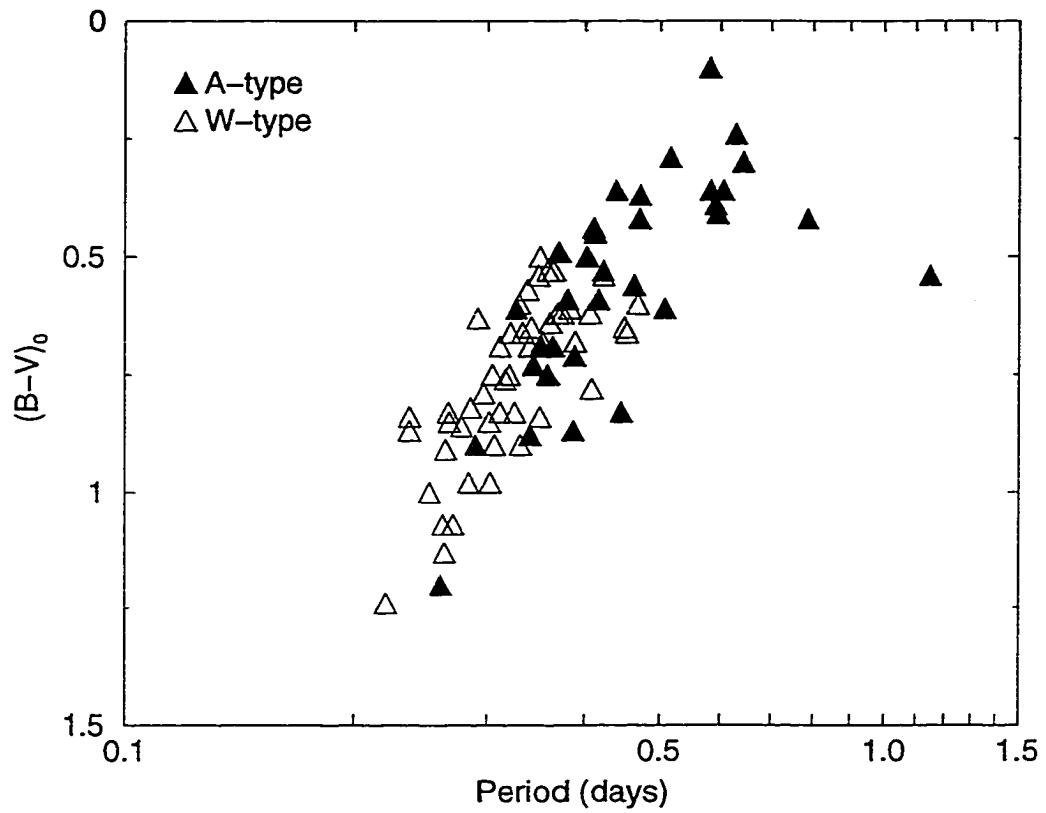


Figure 4.1: A plot of the $B - V$ color vs period for both subclasses. The separation between A and W types is readily apparent.

Temperature vs Density

For the more massive component

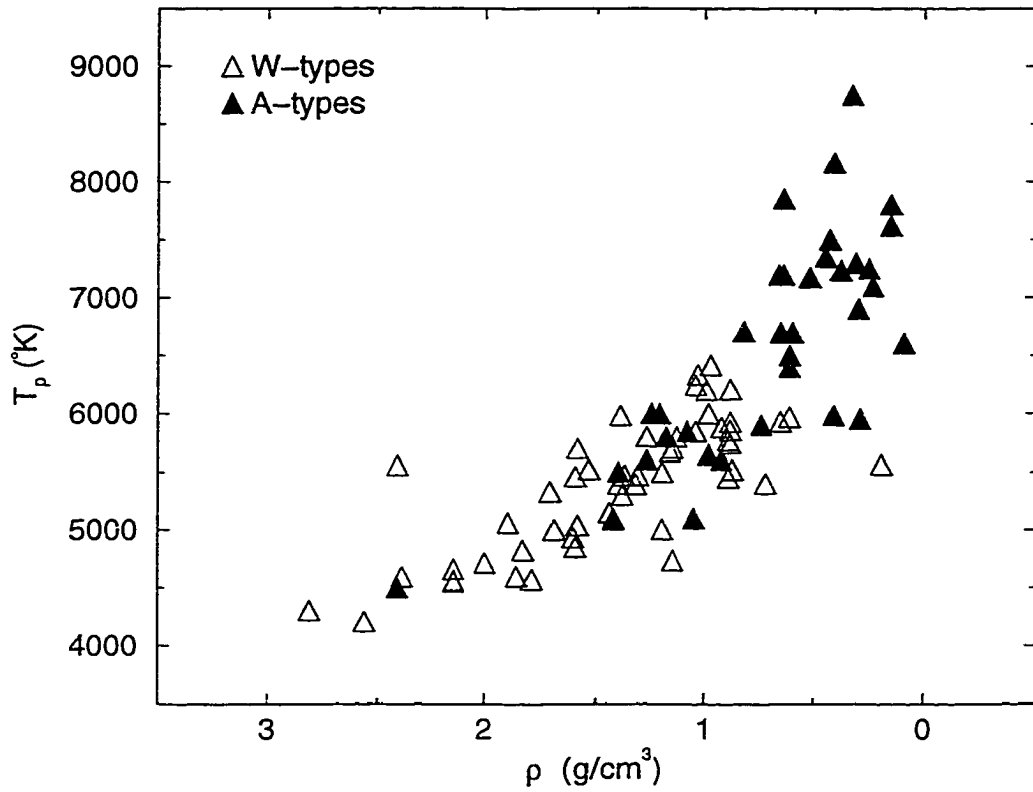


Figure 4.2: The relationship between temperature and density, again showing a difference between A and W types.

Total Mass vs q

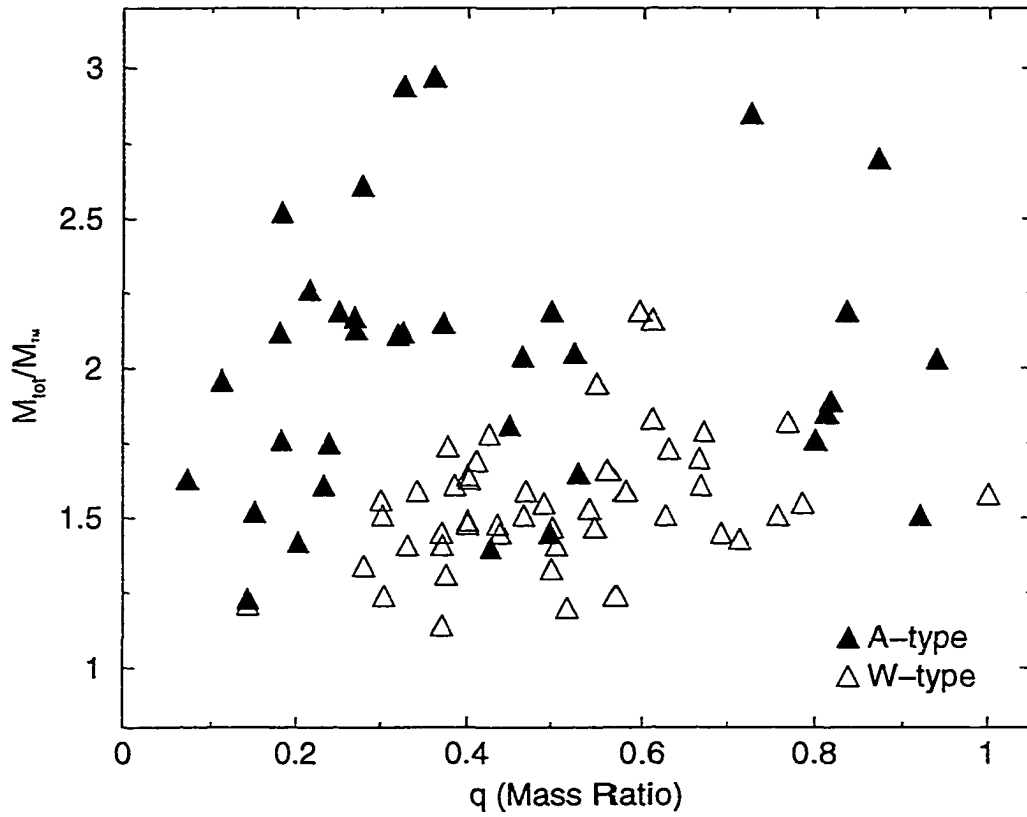


Figure 4.3: This original plot is from Maceroni and Van't Verr (1993). The W types seem to have a weak correlation of higher total mass for the high q systems. For the A types, it appears a bifurcation may exist. Figure 4.4 highlights this difference.

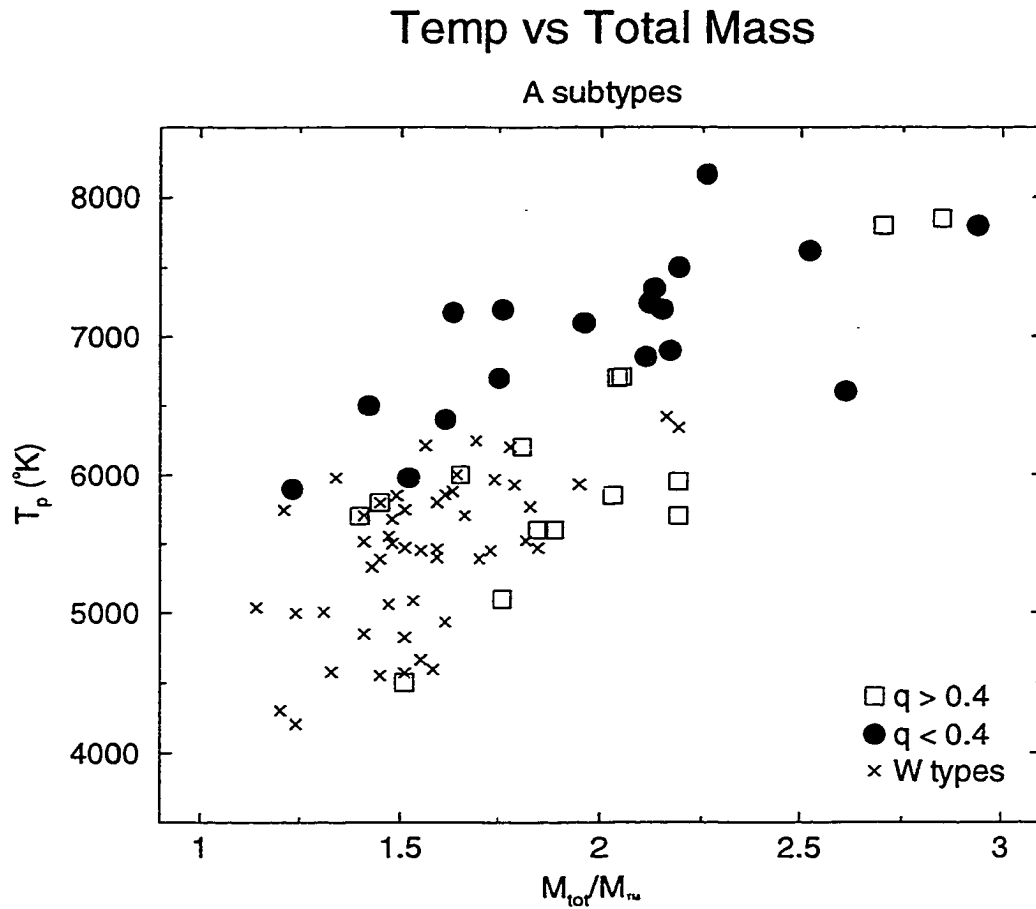


Figure 4.4: The A types are split according to the apparent bifurcation in Figure 4.3. A distinct difference is that the high q value systems tend to have a cooler temperature at a given mass. The W types are plotted for reference. The high q value A types coincide with the W types. As stated previously, this behaviour will be discussed in more detail in Chapter 5.

4.2 Determination Of The O'Connell Effect Ratio

The usual way to plot a light curve (LC) is to place the primary (or deepest) eclipse at phase = 0.0, which occurs in *W* UMa's when the *cooler* component is in front (see Figure 1.3). A phase = 0.25 corresponds to the system being completely out of eclipse, as if the viewer is seeing the system from the 'side'. Then, at a phase = 0.5, the secondary eclipse occurs, when the hotter star passes in front of the cooler star. Phase = 0.75 is a repeat of phase = 0.25, except the viewer now sees the 'other side' of the two stars. If there are no flux asymmetries, the intensity at these two phases should be equivalent. Finally, by definition, a phase = 1.0 is just phase = 0.0 again, and a new cycle begins. O'Connell's method (Figure 1.3) measured the difference in magnitude at the peaks (i.e. phase = 0.25 and phase = 0.75). While a useful diagnostic, this method excludes some possibly important information. If the largest asymmetry between the two halves of the LC (phase 0.0-0.5 vs 0.5-1.0) occurs away from the 0.25 vs 0.75 phase, then insight into *where* a spot is located is made more difficult.

The *OER* method will also identify light curves where the asymmetry isn't greatest at 0.25 vs 0.75 phase, which does not always offer the largest variation. This method (McCartney 1997), groups the photometric data into small phase bins (see Figure 4.5). The light curve is broken up into n bins, where each bin is a phase = $1/n$ wide region. The mean intensity for bin i is I_i . It is calculated from the average of the intensities for each photometric observation in that particular bin. The bins are then normalized by subtracting the intensity at primary minimum (I_1) from the given bin intensity. Next, the bins are summed from phase 0.0 to 0.5 and from phase 0.5 to 1.0. Bins 1 through $n/2$ cover the first half of the LC while bins $n/2 + 1$ through n cover the last half. *OER* is the ratio of the 0.0 to 0.5 bin sum over the 0.5 to 1.0 bin sum:

B–Light Curve of BB Peg

Showing Bins For Measuring OER

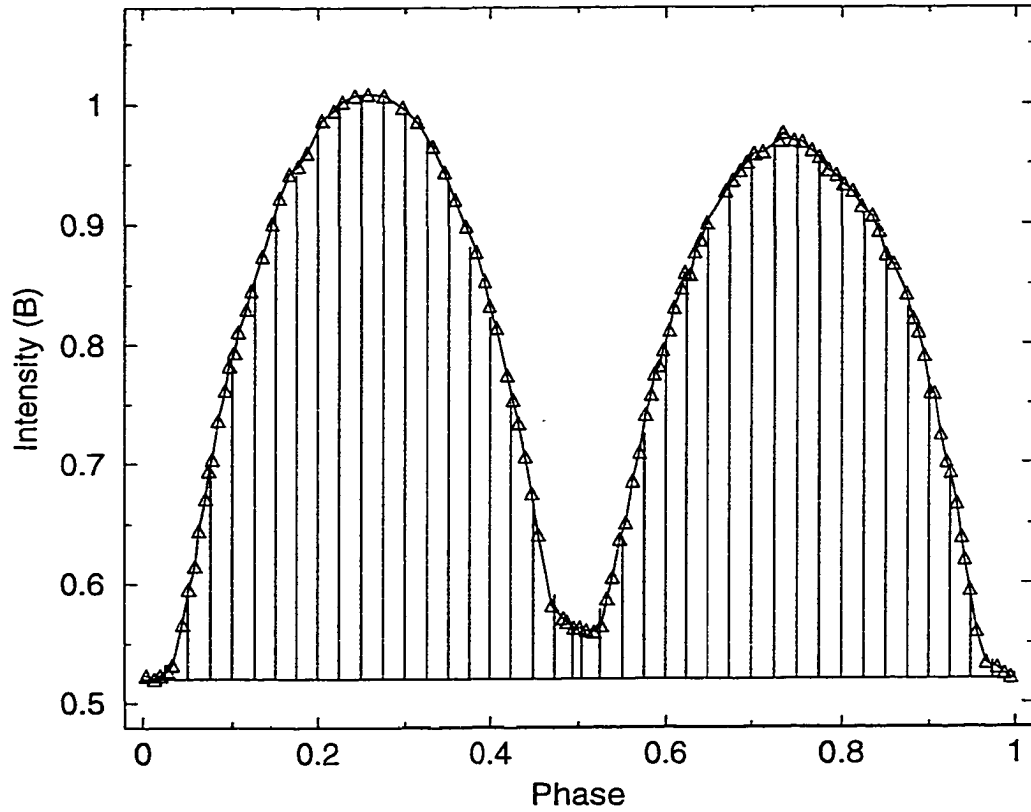


Figure 4.5: An example light curve of BB Peg (Leung, *et al.* (1985)). In this case, the phase bin width = 0.025, for a total of 40 bins. Using the *OER* method, we get: $OER_B = 1.088$. The measured asymmetry by the old method yields: $\Delta m_B = 0.048$.

$$OER = \frac{\sum_{i=1}^{n/2} (I_i - I_1)}{\sum_{i=n/2+1}^n (I_i - I_1)}. \quad (4.3)$$

An $OER > 1$ corresponds to the first half of the light curve having more total flux. A good correlation exists between the OER and Δm , the historical method used by O'Connell (see Figure 4.6). A $\Delta m > 0.0$ means, as noted above, peak I is brighter than peak II. This is not surprising, since a higher maximum at phase = 0.25 should result in more total flux in the first half of the light curve. The OER will be listed as greater or less than 1 in the database, indicating which half of the light curve has more total flux (as outlined above). However, for modeling comparisons, an $OER < 1.00$ will be reexpressed as $1/OER$. The motivation for this comes from the work of Zhou and Leung (1990), who state that this might be indicative of an inversion in the flow direction. That is, the circulation direction sets up in the opposite direction for some systems. This problem could be as simple as the binary system rotating in the opposite direction. Since the relationship between OER is similar for $\Delta m > 0$ and $\Delta m < 0$, this should be explored in future work.

As mentioned in Chapter 2, third light is a problem that has to be resolved. By calculating the bin intensity as $I_i - I_1$, we are looking at only the part of the light curve containing the intensity variation. Thus, this works to subtract out third light effects, and OER is measuring only the variation due to asymmetries, no matter what constant background fluxes exist.

Previously, it was stated that one motivation for a thermodynamic explanation vs a MHD explanation for the O'Connell effect was the stability of the magnitude difference for many systems. Two such systems, RW Com and AM Leo are detailed in Table 4.1.

OER vs Magnitude Difference

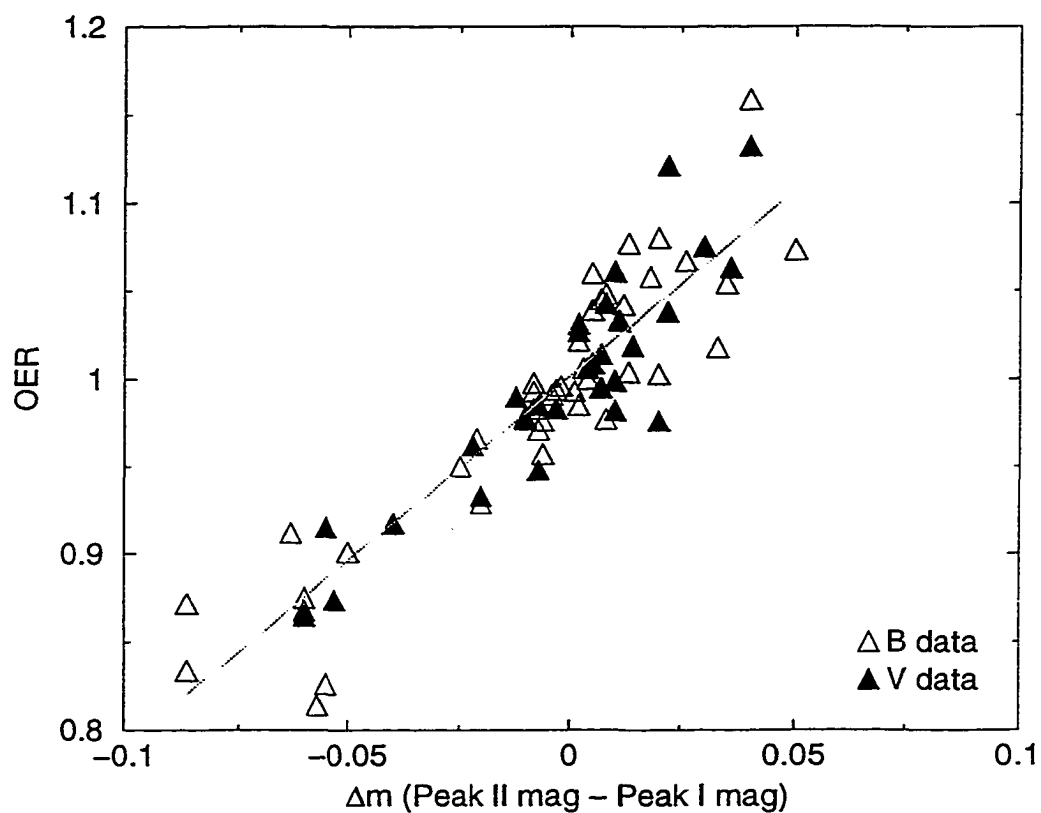


Figure 4.6: A comparison of the *OER* method with the Δm method. The line represents a least squares fit to both the B and V data. The correlation coefficient is 0.902. The equation for the line is: $OER = 2.193\Delta m + 1.001$.

System	Year	Δm	System	Year	Δm
RZ Com	1911	-0.10 (photographic)	AM Leo	1959	0.03 (visual)
	1923	-0.08 (photographic)		1969	0.00 (V-filter)
	1937	-0.07 (visual)		1969	0.00 (B-filter)
	1949	-0.08 (visual)		1977	-0.10 (B-filter)
	1969	-0.12 (V-filter)		1981	0.02 (V-filter)
	1969	-0.14 (B-filter)		1981	0.07 (B-filter)
	1976	-0.10 (V-filter)		1983	0.00 (V-filter)
	1976	-0.15 (B-filter)		1983	0.01 (B-filter)

Table 4.1: The Δm values for two variables, each of which has been observed on many widely separated occasions.

For RW Com, we see good stability between the different eras, even without considering a transformation from a photographic magnitude to the either the B or V filters. For AM Leo, there is dramatic change, but it is worth noting that at the two very separate times (1959 and 1983) the light curves are very similar. The 1977 data would seem to be evidence of a temporary superluminous bump, possibly a temporary magnetic effect. The point here is that the observations show that the light curves retain a similar O'Connell effect that is difficult to explain with short-term MHD effects. Observations over a long time span must be used to eliminate the effects of temporary bumps, which seem to be unrelated to the more stable O'Connell effect.

4.3 Determination Of The Light Curve Asymmetry

The bin method allows the additional information of knowing where the asymmetry is greatest. To find this information, a given bin is compared with its reflected bin in the other half of the light curve. For a 40 bin total example, bin 2 covers phase 0.025 to

0.050 and is compared to bin 39, which covers phase 0.950 to 0.975. If we reflect the light curve about the phase = 0.5 point, we can better visualize where the light curve deviates the most from symmetry (Figure 4.7).

In this way, the location of maximum asymmetry can be compared with phase (see Figure 4.8). By using as many systems as possible, we can then make a determination of the preferred statistical location for the asymmetric flux. This bin asymmetry is used to calculate the Light Curve Asymmetry (*LCA*). Here each bin is compared with its reflection and the square of the difference is summed over each bin pair:

$$LCA = \sqrt{\sum_{i=1}^{n/2} \frac{(I_i - I_{(n+1-i)})^2}{I_i^2}}. \quad (4.4)$$

At first glance it may seem that *OER* and *LCA* measure the same thing. However, since *LCA* measures the deviance from symmetry rather than the amount of flux under the curve, it contains different information. That is, one could imagine a light curve with little peak asymmetry, but the brighter peak being narrow while the fainter peak is shallower. In this situation, the *OER* could be almost exactly 1.00, despite the obvious asymmetry of the curves. Yet, measuring the *LCA* will show a large asymmetry. An observed example of this is V566 Oph (see Figure 4.9). A plot of *OER* vs *LCA* is shown in Figure 4.10.

"Folded" Light Curve

AE Phe Light Curve Reflected About Phase = 0.5

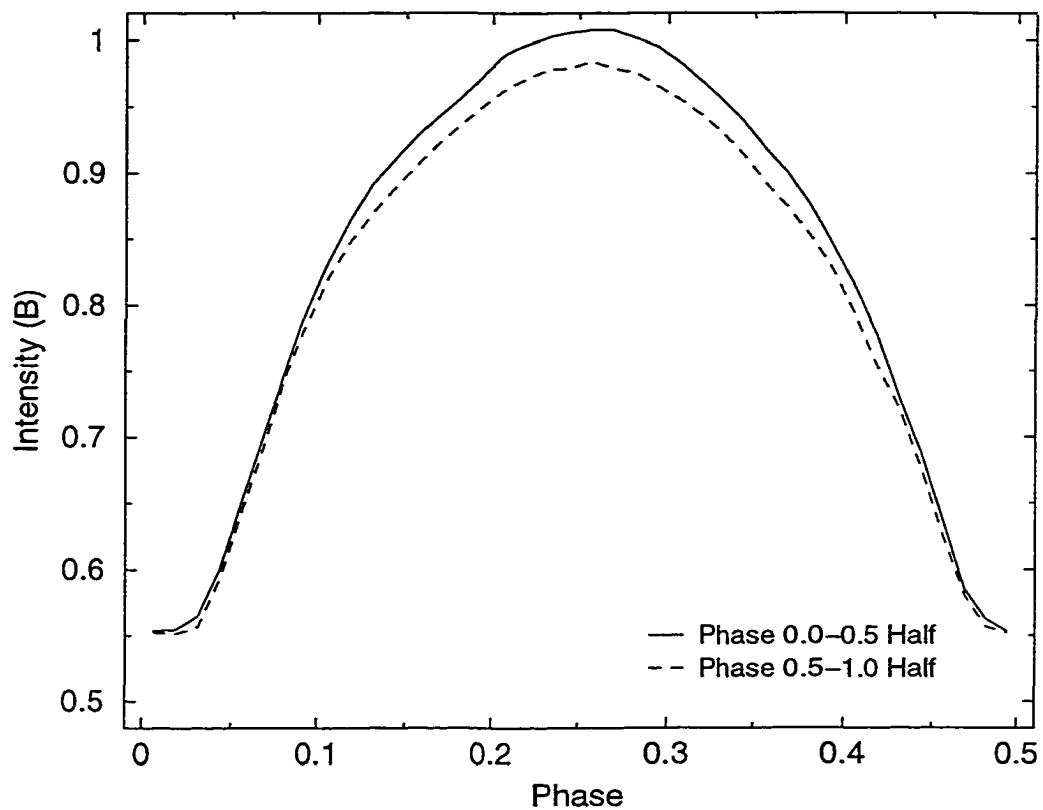


Figure 4.7: A plot of the light curve of AE Phe. This shows visually where the light curve is most asymmetric. The quantity LCA , described above, measures the asymmetry as a function of phase. For this data, the maximum asymmetry is $\Delta\text{Intensity} = 0.028$ at a phase of 0.3063. The LCA_B for this system is calculated as 0.02148. For reference, $OER_B = 1.068$.

Maximum Asymmetry Phase Location

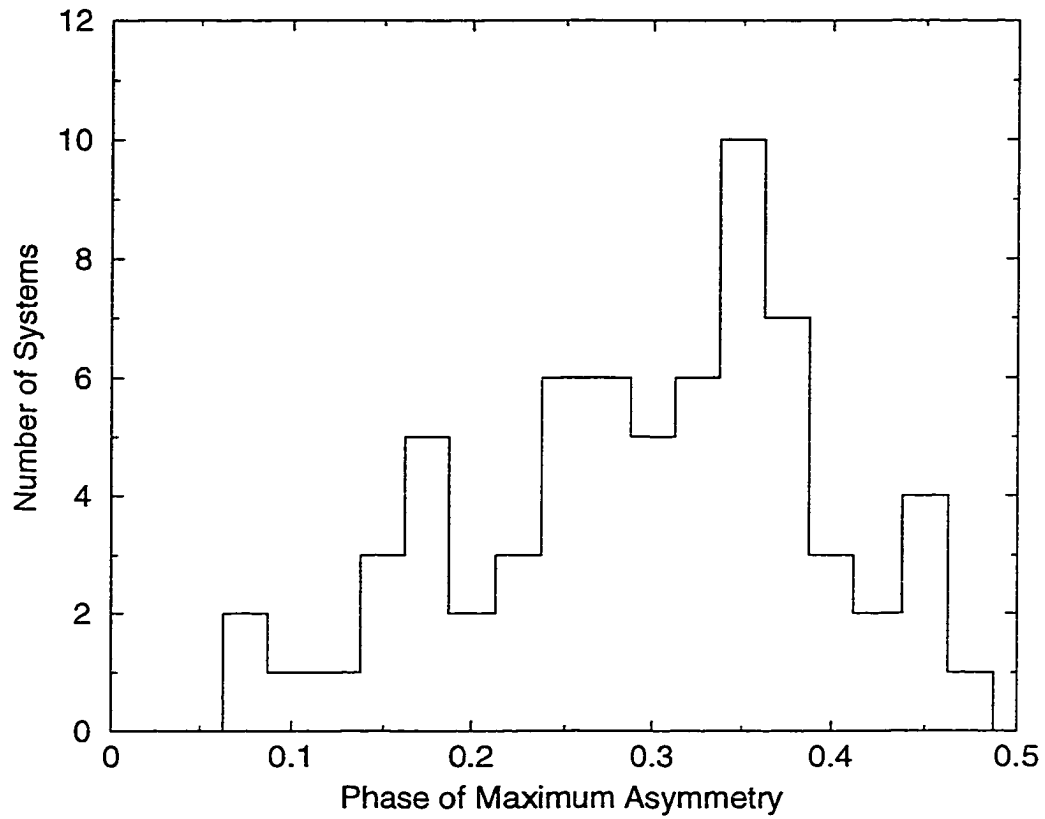


Figure 4.8: A plot of the phase location of maximum *LCA*. A solid peak appears just around the phase 0.35, which would be just after the first maximum. At this phase, we are primarily seeing the 'sides' of the two components. We are seeing slightly in towards the cooler star's region facing the hotter component.

Light Curve of V566 Oph

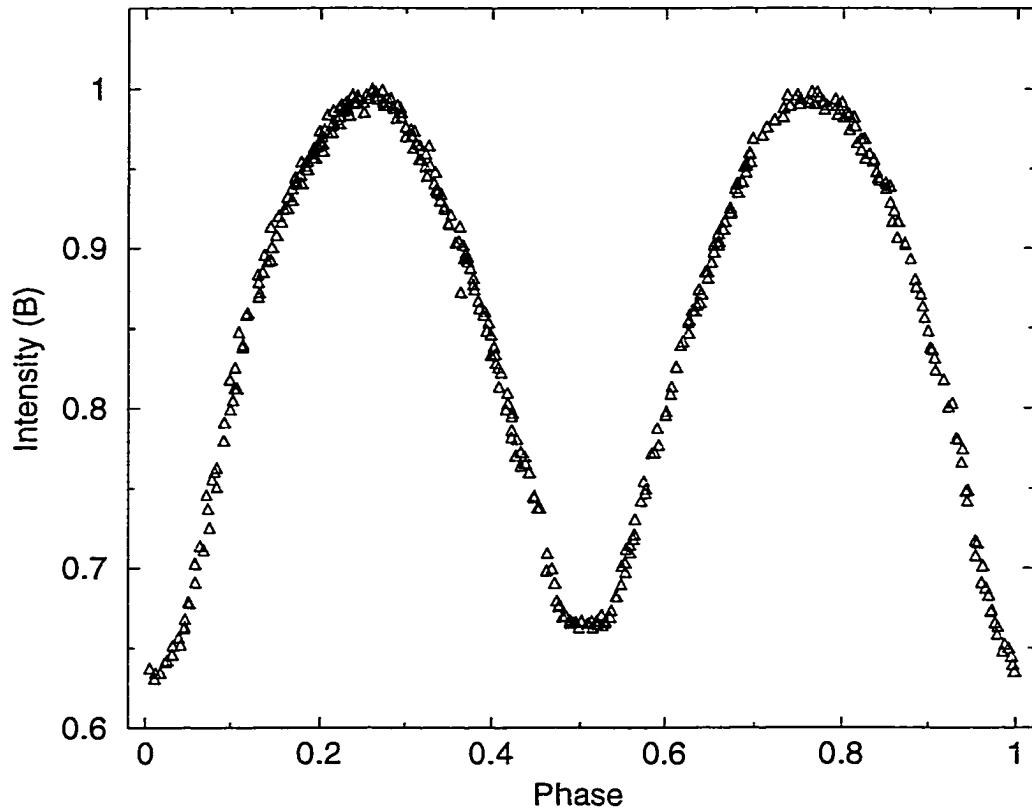


Figure 4.9: A plot of V566 Oph, which has $OER = 0.993$ (or $OER = 1.007$, see text) and $\Delta m = 0.00$, yet has an appreciable $LCA = 0.042$. This implies that even though the peaks are similar, the shape of the light curve is fundamentally different for the first half vs the second half.

OER vs LCA

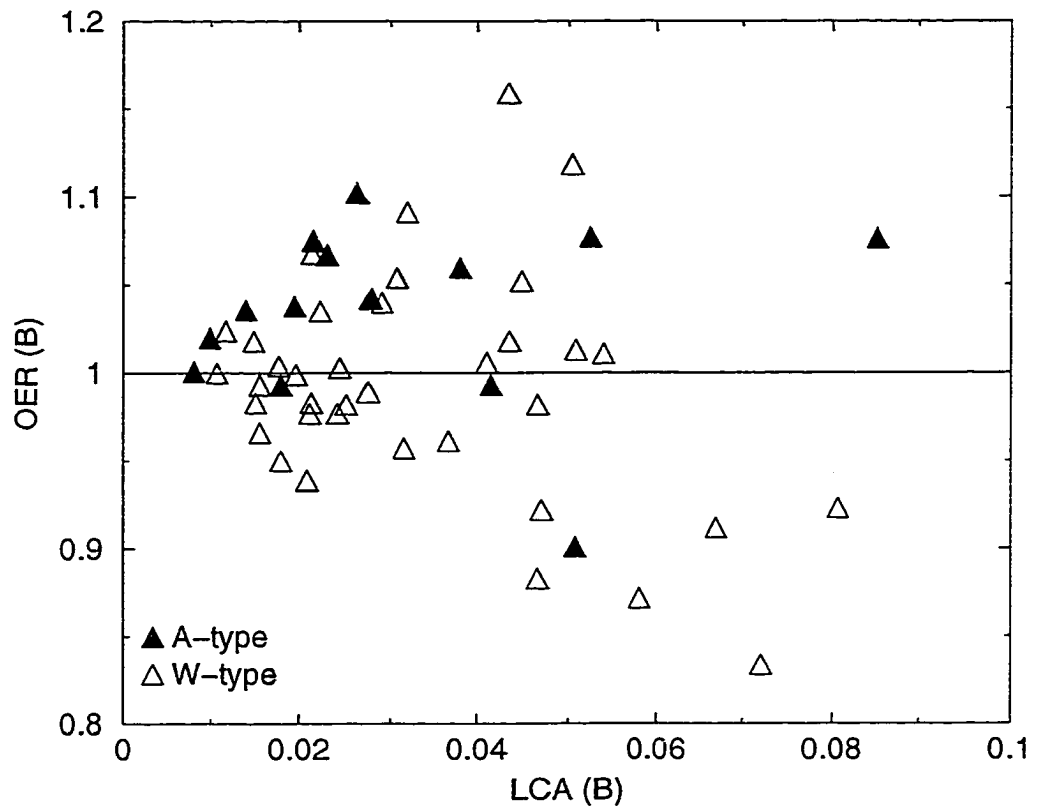


Figure 4.10: The relationship between *OER* and *LCA* is shown. A given *LCA* will result in an *OER* between two extremes. V566 Oph is the black triangle near the middle of the plot.

Chapter 5

Model Results

The results of fitting the theoretical model with the observational database is detailed below. As shown in Chapter 4, several observational differences exist between the W and A types. This was the original motivation for creating two separate models. The irradiation model is compared with the observational values for the W types, while the contact model is used for analyzing the A type data. A summary of the work, as well as a discussion of possible future work is included as well.

5.1 Results For The Irradiated Model

The Zhou and Leung irradiation model, as discussed in Section 3.1 was used to calculate theoretical *OERs*. The grid sweep method detailed in Section 3.3 was used to generate a series of curves by varying one of the primary parameters and holding the others constant. The parameters varied were discussed in the above section. An in depth paper on the evolution state of W UMa systems by Rovithis-Livaniou, Rovithis and Bitzaraki (1992) (RRB) provides useful information for the assumptions used during the parameter sweep. One of the bigger problems with computer modeling is keeping the

parameters in a reasonably astrophysical range. One of the assumptions discussed earlier stated that W UMa stars are typically thought of as being ZAMS objects. RRB provide H-R diagrams of W UMa stars for their sample of 31 systems (which are contained in the current database) and they find that the WD modeling technique typically predicts that indeed, the primaries are main sequence objects. An H-R diagram of the systems in the current database is shown in Figure 5.1.

With this information in mind, the grid sweep was set up to account for those parameters that had strong empirical relationships. Since we can assume the primaries are main-sequence, the radius is known if the mass is known. Thus, as the mass parameter was varied, the radius of the primary was varied according to the mass-radius relationship (see, for example Kippenhahn and Weigert (1990)). The relationship of:

$$R \sim M^\xi, \tag{5.1}$$

where typically $\xi = 0.8$ for the lower main sequence. Since a mass-luminosity relationship also exists, this can be combined with the above result to also derive a mass-temperature relationship for the main sequence as well. Kippenhahn and Weigert use:

$$L \sim M^\eta, \tag{5.2}$$

and for the lower main sequence derive $\eta = 3.88$. After using the basic luminosity law, this yields $T \sim M^{1.21}$, which was used for these models.

The period was considered a completely independent variable. No mass-radius or mass-luminosity relationships were used for the secondary, since RRB's data showed them to not be on the main sequence. Rather, the heating of the primary caused them to appear under the main sequence. This behavior is because they have increased their temperature, but not their radius (at least not enough) for them to move up the main

H-R Diagram For W UMa Primaries

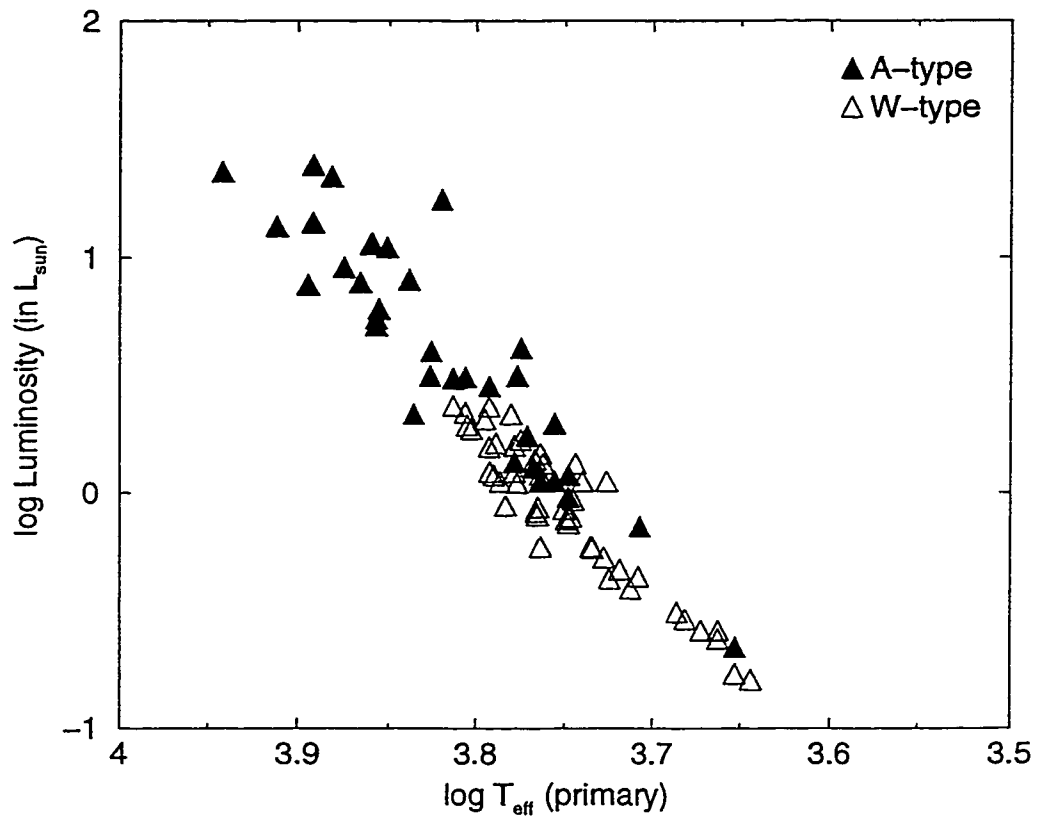


Figure 5.1: The primaries plotted on the H-R diagram. Since the primaries are main sequence objects, the mass-luminosity and mass-radius relationships for main sequence stars will be used for the primaries. The exact relationship is detailed in the text.

Irradiation Theory OER vs q

Varying Mass of the Primary

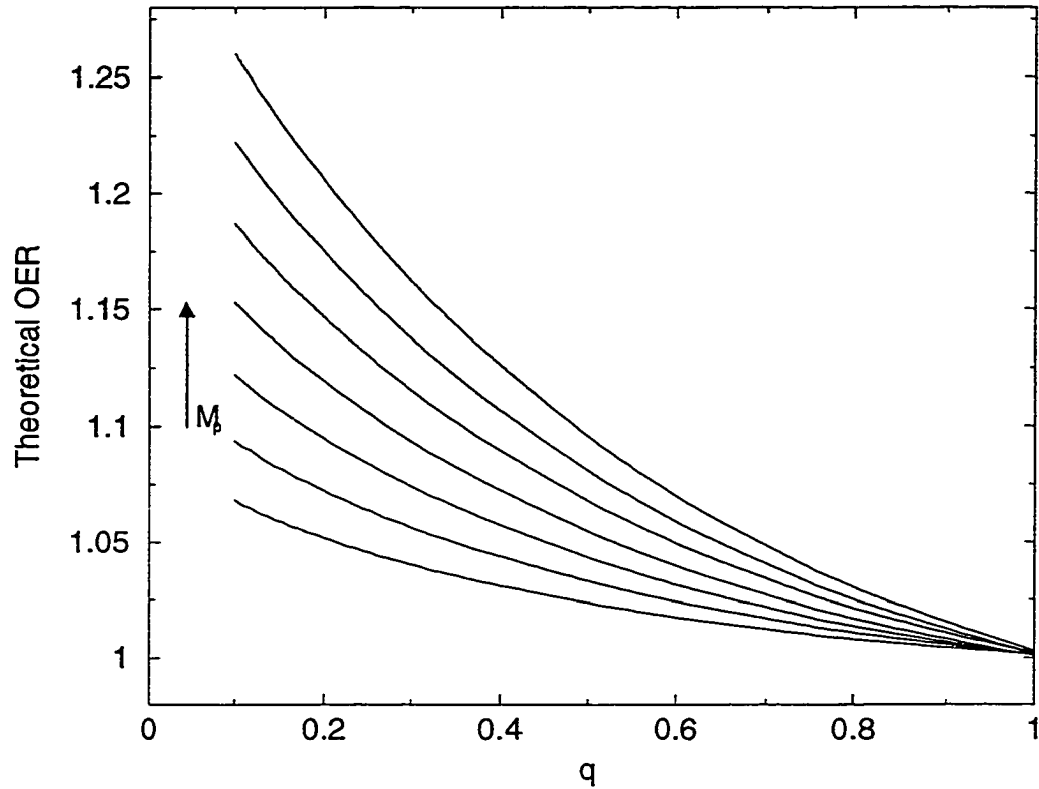


Figure 5.2: The variance of the theoretical OER with q is shown. In each case, $\Delta T = 200\text{K}$, $r_1 + r_2 = 0.75$ and $P = 0.6$ d. The lines represent constant mass of the primary. As the primary mass was increased, the OER increased in value by: $OER \sim M^\alpha$, with $\alpha = 1.4$. This is the relationship used in Equation 5.3. M_p has been varied from $0.6 - 1.8M_\odot$, in steps of $0.2M_\odot$.

Irradiation Theory OER vs q

Varying Temperature Difference

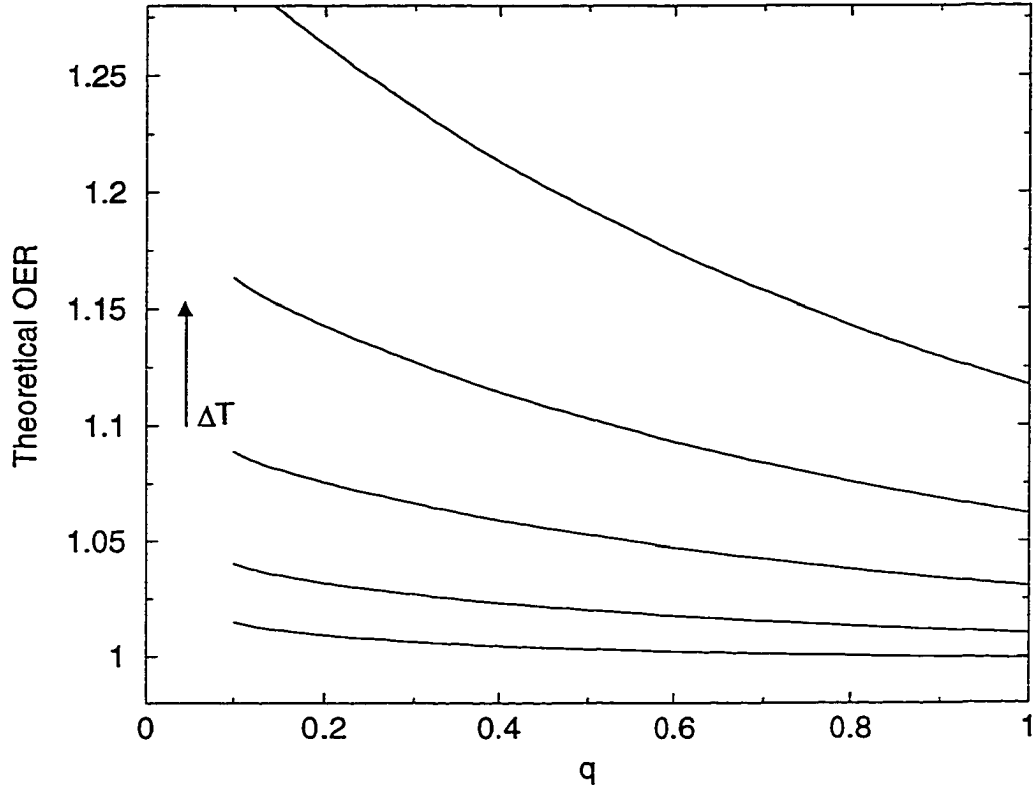


Figure 5.3: As before, the variance of the theoretical *OER* with q is shown. In each case, $M_p = 1.0M_\odot$, $r_1 + r_2 = 0.75$ and $P = 0.6d$. The lines represent constant between temperature difference the two components. As the temperature difference was increased, the *OER* increased in value by: $OER \sim (\Delta T)^\beta$, with $\beta = 3.5$. This is the relationship used in Equation 5.4. The lines don't meet at $q = 1.0$ since the constant temperature is somewhat unrealistic as we sweep q . A $q = 1$ system would ideally have a $\Delta T = 0K$. The ΔT 's range from 100 – 500K, in 100K increments.

Irradiation Theory OER vs q

Varying The Wilson–Devinney Radius Sum

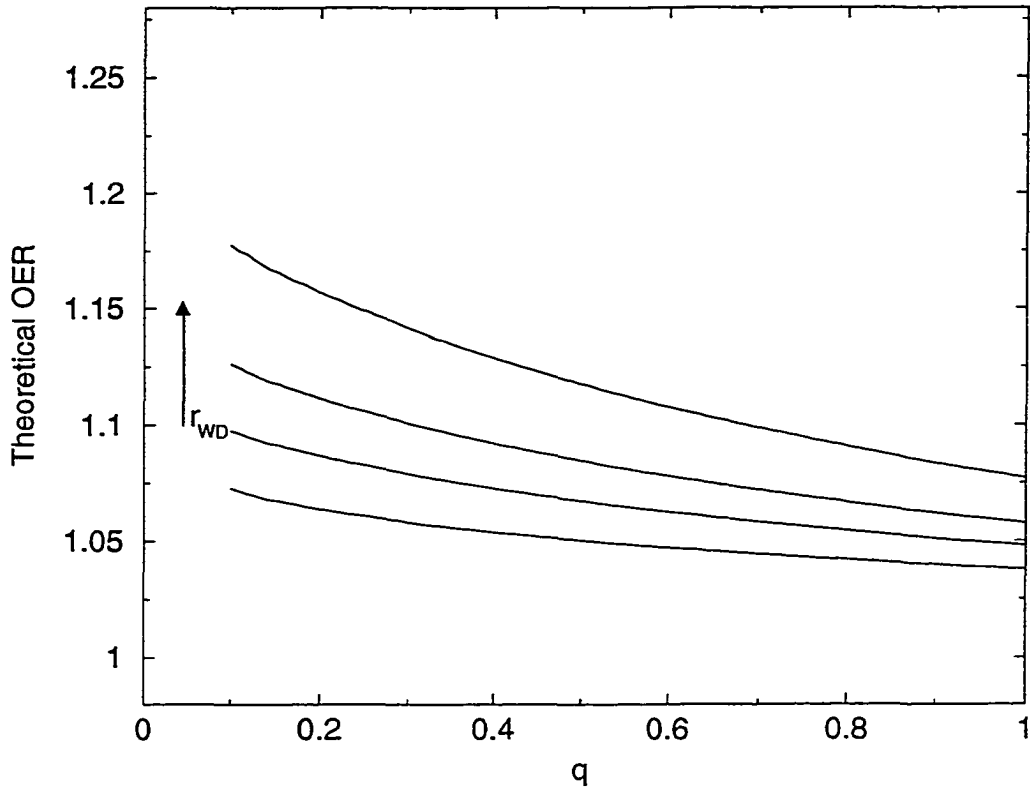


Figure 5.4: Again, the variance of the theoretical *OER* with q is shown. In each case, $M_p = 1.0M_\odot$, $\Delta T = 100\text{K}$ and $P = 0.5\text{d}$. The lines represent constant radii sum between the two components. As the radii sum was increased, the *OER* increased in value by: $OER \sim (r_1 + r_2)^\gamma$, with $\gamma = 2.1$. This is the relationship used in Equation 5.5. The sum varies between 0.65 and 0.95.

Irradiation Theory OER vs q

Varying Rotation Period

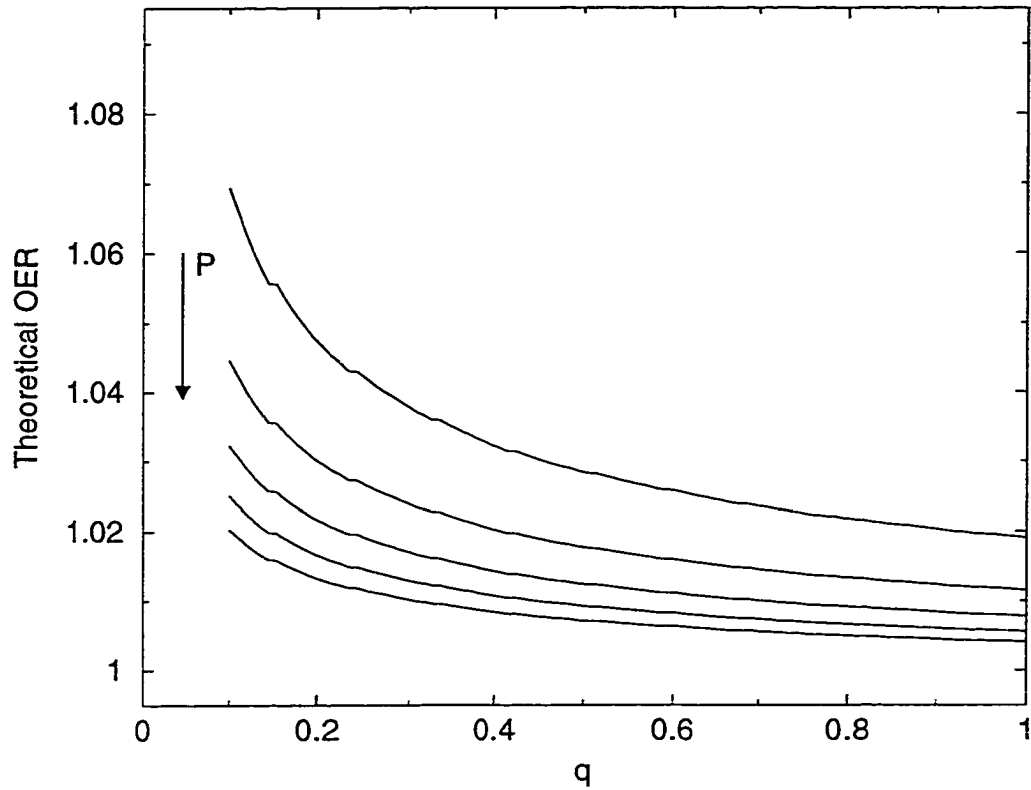


Figure 5.5: Once again, the variance of the theoretical OER with q is shown. In each case, $M_p = 1.0M_\odot$, $\Delta T = 100K$ and $r_1 + r_2 = 0.75$. The lines represent constant rotation period. As the period was increased, the OER decreased in value by: $OER \sim P^\delta$, with $\delta = -1.3$. This is the relationship used in Equation 5.6. A period range of 0.3 d to 0.7 d is shown.

sequence. Instead it appears that the effect of the primary on the secondary is for the secondary to shift to the right on the H-R diagram. Thus the secondary mass was a free parameter, subject only to the constraint that the mass ratio must be between 0.1 – 1.0. This range was used since no systems in the database have $q < 0.1$.

The temperature difference between the components was also considered an independent variable. This is a result of the fact that no mass-luminosity relationship exists for the secondary. As such the secondary's temperature has no direct relationship to the secondary's mass either. So, for ΔT , the temperature difference of the components, a range between 100K and 1000K was used. Again, the motivation is based on the fact that almost all the systems had ΔT 's in this range. The final variable to be addressed was the fillout. Systems that had many similar physical parameters could have very different fillouts. As such the WD radii of the components was varied, as discussed in Section 3.3. Values between 0.65 and 0.95 were used for the sum of the radii. Systems with larger radii sum correspond to higher fillouts.

The results are plotted in Figures 5.2-5.5. In each case the variance of OER with respect to q is plotted. For each line, only the mass of the secondary was varied. Then, a step was made in one of the other independent parameters (primary mass, period, radii sum or temperature difference), and a new line was plotted. From this we can calculate the theoretical variance of OER with each of our critical parameters. OER relationships have been derived from the plots for each of the independent parameters:

$$OER \sim M_p^{1.4}, \quad (5.3)$$

$$OER \sim (\Delta T)^{3.5}, \quad (5.4)$$

$$OER \sim (r_1 + r_2)^{2.1}, \quad (5.5)$$

$$OER \sim P^{-1.3}, \quad (5.6)$$

and have been used to fit the observational data.

5.1.1 Observational Fits

To fit the observational data, the preceding relationships have been applied to the values shown in the database. A simple plot (Figure 5.6) of *OER* with respect to the primary mass will show the scatter caused by the other parameters. This diagram is very messy since the competing effects of temperature difference, period, and radii sum are all mixed in. Ideally, the way to analyze the observational data is to plot it versus one independent parameter and bin the data with respect to the other parameters.

However, with four parameters a very large sample would be needed. Not enough W UMa types have adequate light curves to allow this. Instead a method of applying the theoretical relationships was used. The data has been plotted with respect to a combination of the free parameters. Since simple power law relationships were obtained for *OER* with each parameter, these were used to calculate Λ , a quantity defined as:

$$\Lambda = M_p^\alpha (\Delta T)^\beta (r_1 + r_2)^\gamma P^\delta, \quad (5.7)$$

where α , β , γ , and δ are obtained from the theoretical relationship derived above. Thus for all cases with the irradiated model, we will assume: $\alpha = 1.4$, $\beta = 3.5$, $\gamma = 2.1$, and $\delta = -1.3$. In Figure 5.7 a plot of *OER* vs Λ is shown. The values for each variable were obtained from the database, and the data was fit with a least squares fit. However it looks like an exponential fit might be better, but the one outlier makes it difficult to determine if this is a curve or scatter. The y-axis is plotted as $(OER(B) - 1) \times 100$ to make the scale convenient to read. A value of 15 corresponds to a measured *OER* of 1.150. This follows the method used in the work of Davidge and Milone (1984), in

OER(B) vs Mass Of Primary

W Types

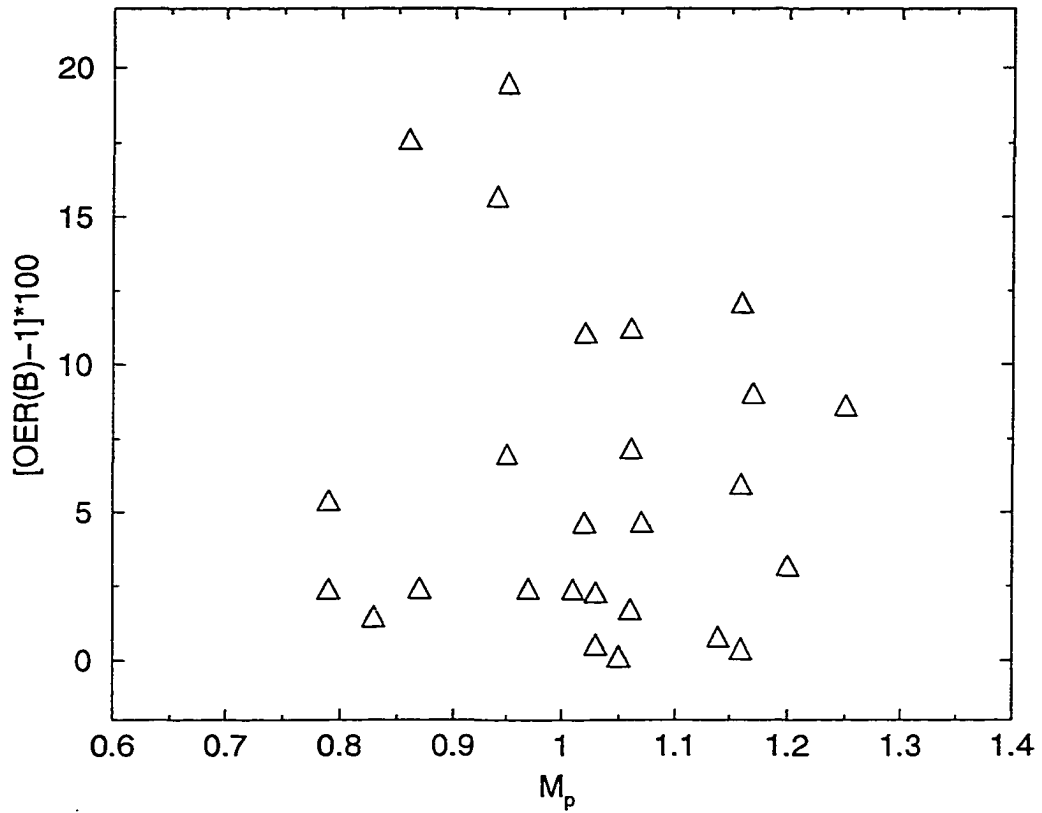


Figure 5.6: *OER* plotted vs mass of the primary. This data is for just the W types. No relationship can be discerned, since the other independent parameters are still mixed in.

their study of the O'Connell effect. They plotted the various parameters vs $\Delta m \times 1000$, typically obtaining values between -40 and 40.

Since the theoretical data is plotted vs q we should look at a plot of the observational data as well (see Figure 5.8). At best, a weak correlation of high q implying a lower *OER* is present. This roughly agrees with Zhou and Leung's contact theory concerning the direction function, stating that there should be almost no *OER* for systems with high q . A better plot is to show *OER* vs $q \times \Lambda$, removing the effects of the other independent parameters. This relationship is shown in Figure 5.9.

Several other parameters have been plotted (Figures 5.10- 5.15), some showing good correlations, some none at all. The plots involving the secondary's parameters show poor correlations, but this is not surprising, since no easy mass-luminosity relationship exists for these objects. *LCA* is plotted in Figure 5.13. Although *LCA* and *OER* are not well correlated (see Figure 4.10) a reasonable agreement results for the same relationships that were used for *OER*.

Several interesting relationships result. From Figure 5.11, we would expect the lower density systems to have higher *OERs*. For main sequence stars, this implies that the earlier spectral type systems would have a higher O'Connell effect. In the WD model, the reflection coefficient goes to one when we reach hot stars. This means that s , the absorption coefficient goes to zero. At this point, the irradiation model would no longer be useful. However, the hottest W type systems are cool enough to still use an absorption coefficient around 0.5.

As shown in Figure 4.2, the primary temperature is well correlated with the primary density. Thus we can infer from Figure 5.11 that the hotter W types have higher *OERs*. In Figure 5.13 the cool A types which are interlopers in most of the diagrams plotted in Chapter 4 are plotted here as well. The hottest of the group, V566 Oph, is quite far from the best fit line. Perhaps this system, at $T_{eff} = 6700\text{K}$, is too hot to have a high

OER(B) Correlation With Primary Parameters

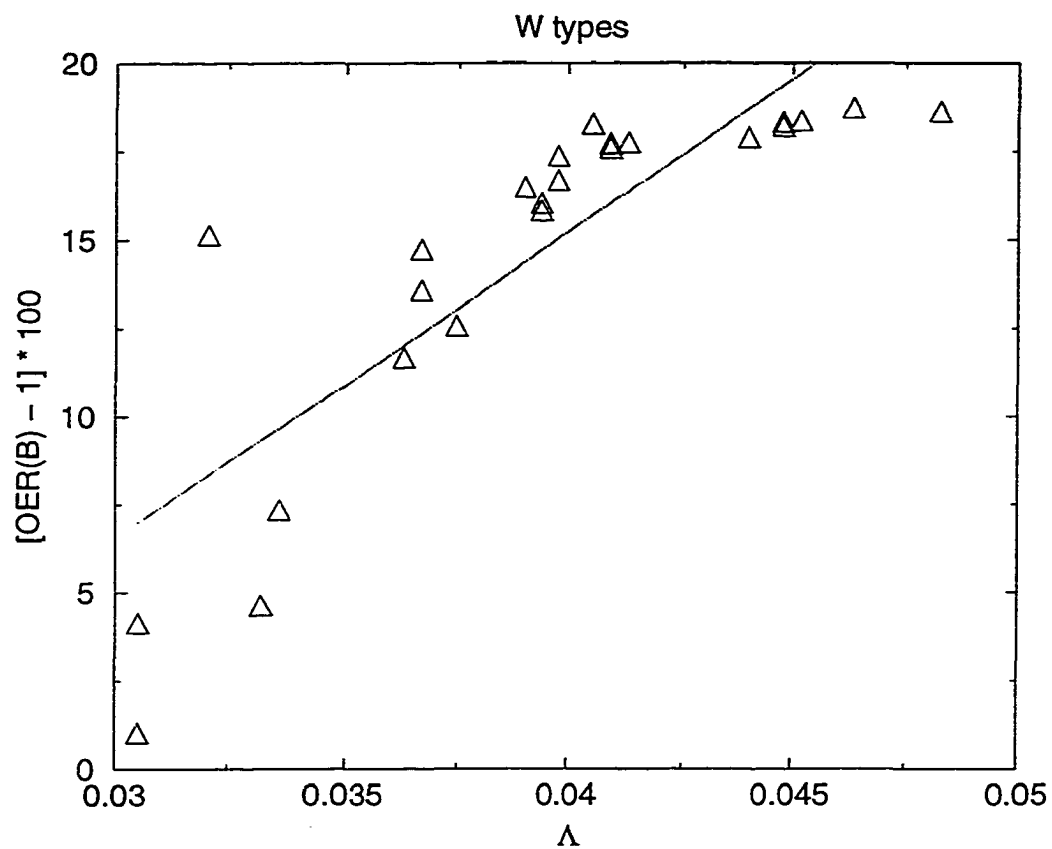


Figure 5.7: The correlation of OER with the primary parameters, as determined by the theoretical predictions. This quantity is defined as Λ in the text, and will be used in later figures. A linear regression yields a correlation coefficient of 0.844.

OER vs q

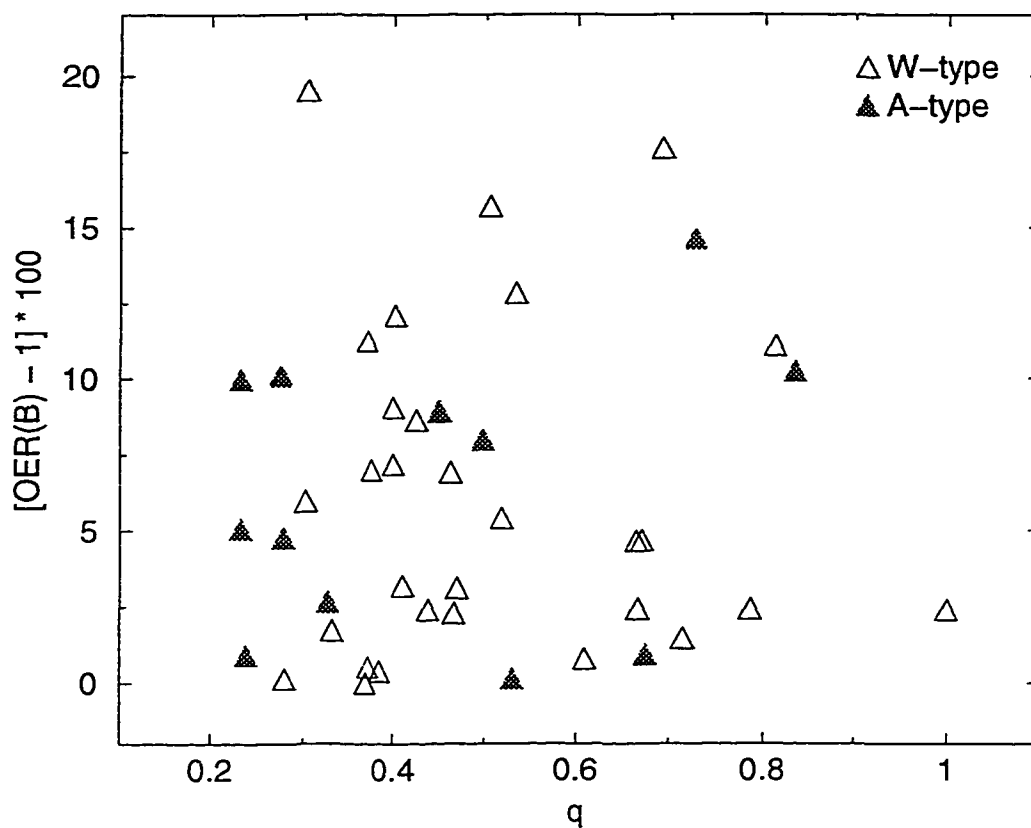


Figure 5.8: Similar to Figure 5.6, this *OER* vs *q* plot shows little correlation. Both A and W types which have a complete independent parameter data set are plotted. As with the plot vs primary mass, the effects of the independent variables are mixed in.

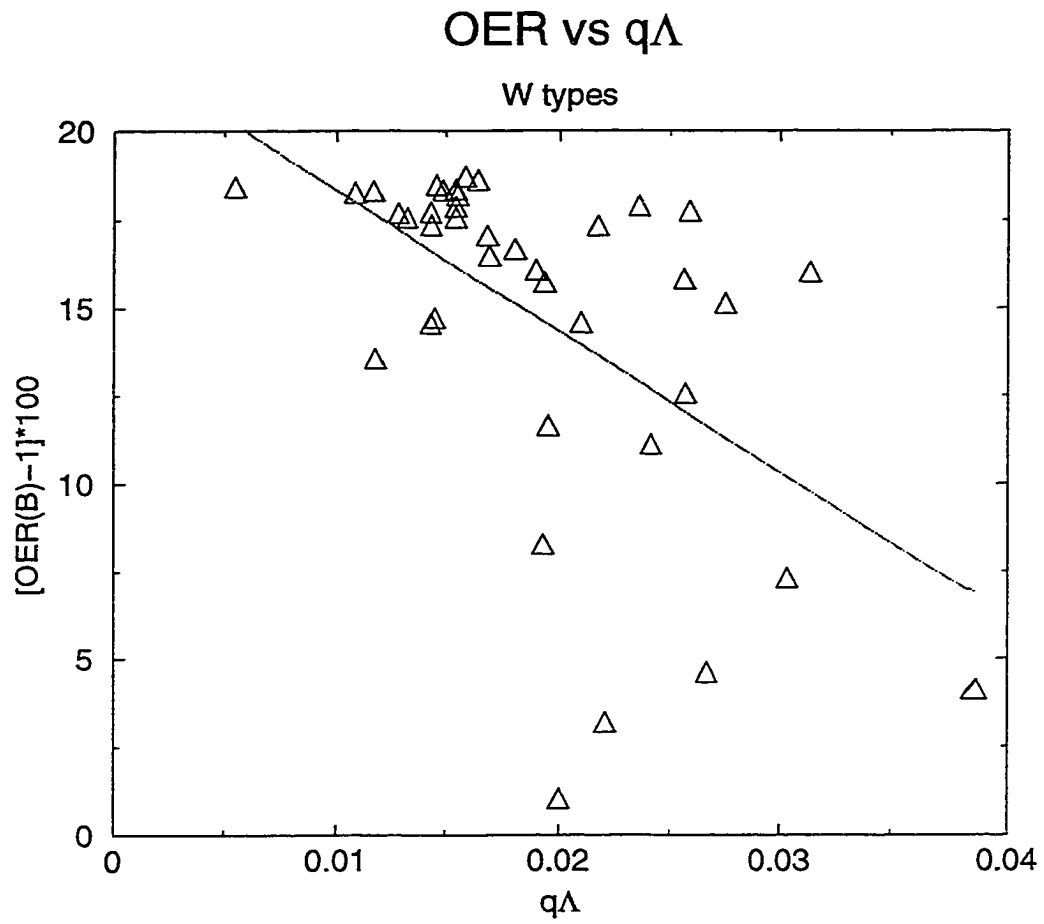


Figure 5.9: A plot of the W types for $q \times \Lambda$. This shows a better correlation (coefficient = 0.56) than Figure 5.8, since the four independent variables have been sorted out.

enough absorption. The W type closest to it, at $\Lambda = 0.048$, is AH Cnc, which is also quite hot for a W type, with $T_{eff} = 6400\text{K}$.

5.2 Results For The Contact Model

For the A types, the contact model discussed in Section 3.2 was used to fit the observational data. Since A type primaries also obey the mass-luminosity relationship for main sequence stars (see Figures 5.1), the same relationships as outlined in Section 5.1 were used: $R \sim M^{0.8}$, $L \sim M^{3.88}$ and $T \sim M^{1.21}$. For the grid sweeps a similar set of ranges for each independent parameter was utilized. The theoretical data was plotted with the same method as outlined in Section 5.1. Figures 5.16-5.19 show the *OER* vs *q* plots for each independent parameter for the contact model.

For this scenario, ΔT should be determined as a non-free parameter, based on Hazlehurst's method. However, using the Tassoul coordinates to approximate the non-spherical distortions leads to a boundary condition problem, discussed in Section 3.2. Thus until we have a better determination of boundary conditions, ΔT will unfortunately still be a free parameter.

We end up defining Λ as the same quantity,

$$\Lambda = M^\alpha (\Delta T)^\beta (\tau_1 + \tau_2)^\gamma P^\delta, \quad (5.8)$$

except the values of the exponents are now different. Using the various theoretical *OER* vs *q* plots results in the following relationships:

$$OER \sim M^{2.2}, \quad (5.9)$$

$$OER \sim (\Delta T)^{3.2}, \quad (5.10)$$

OER vs Mass Of The Secondary

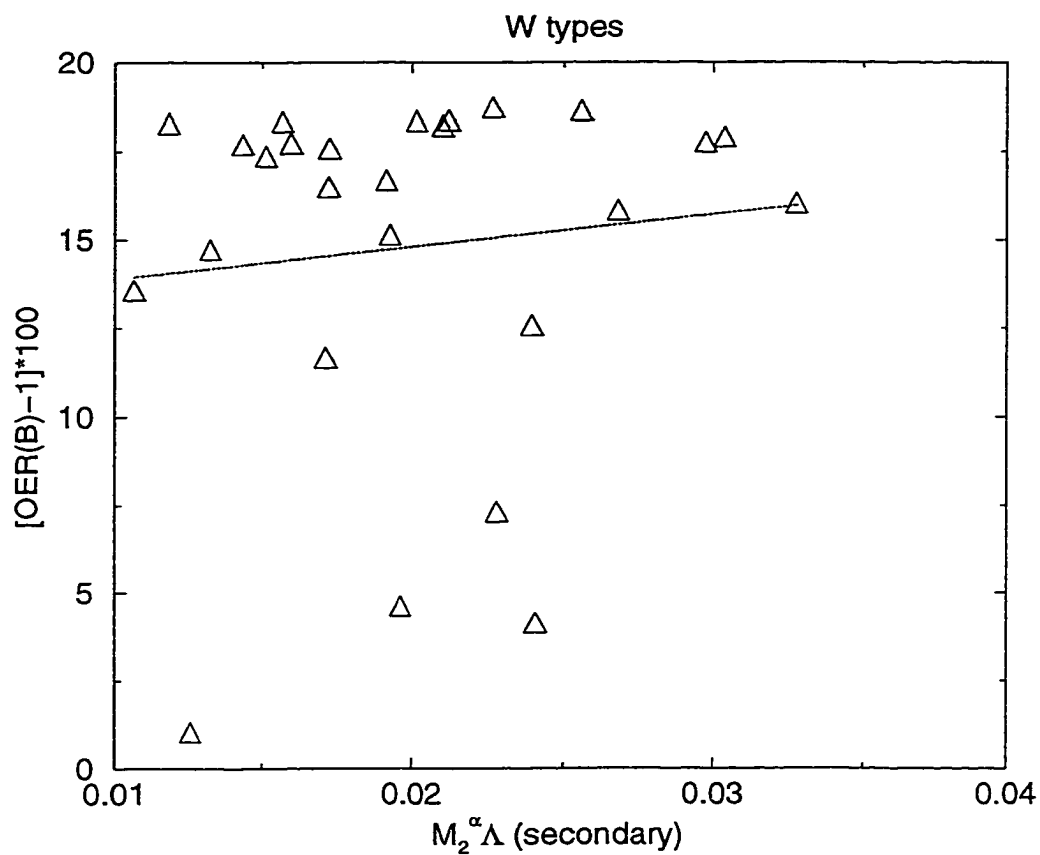


Figure 5.10: At best, a weak agreement exists. Here the correlation coefficient = 0.10 was calculated. As discussed in the text, this result isn't surprising, since the secondaries do not fit a ZAMS relationship. The exponent α has been set to 1.4, the same as the relationship for the primary mass.

OER vs Density Of The Primary

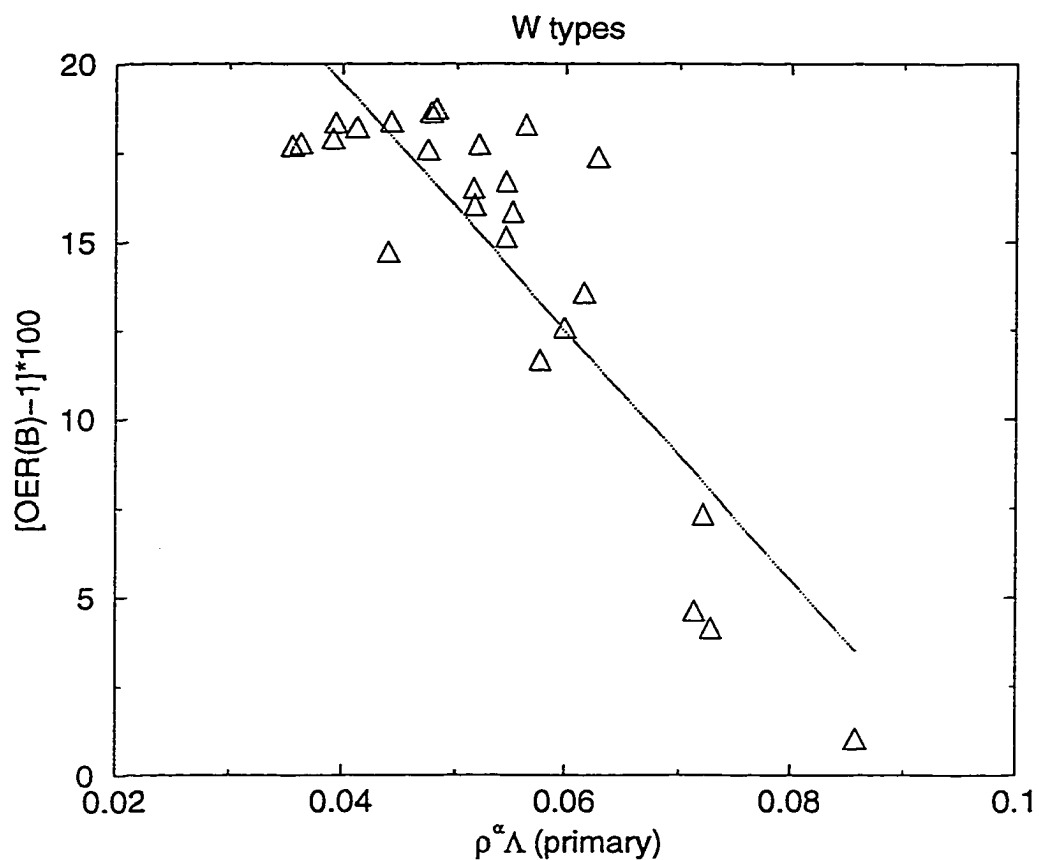


Figure 5.11: A plot of OER vs the density of the primary. The correlation (0.862) is very high, but since ρ_p depends on M_p and R_p , a good fit with OER is expected. The α parameter for this case was just set equal to 1. The plot predicts that the lower density (higher mass and earlier spectral type) systems will have a higher OER

OER vs Density Of The Secondary

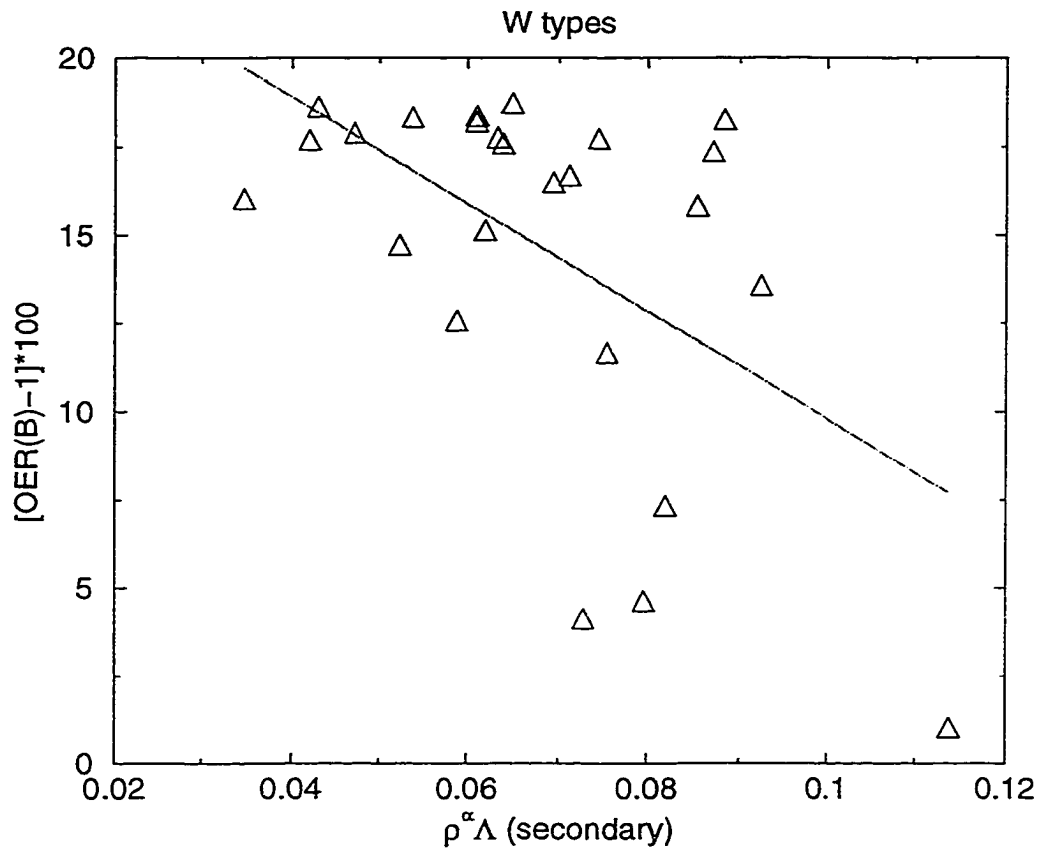


Figure 5.12: As with the secondary mass, a poor correlation (0.42) results for this relationship.

LCA Correlation For W Types

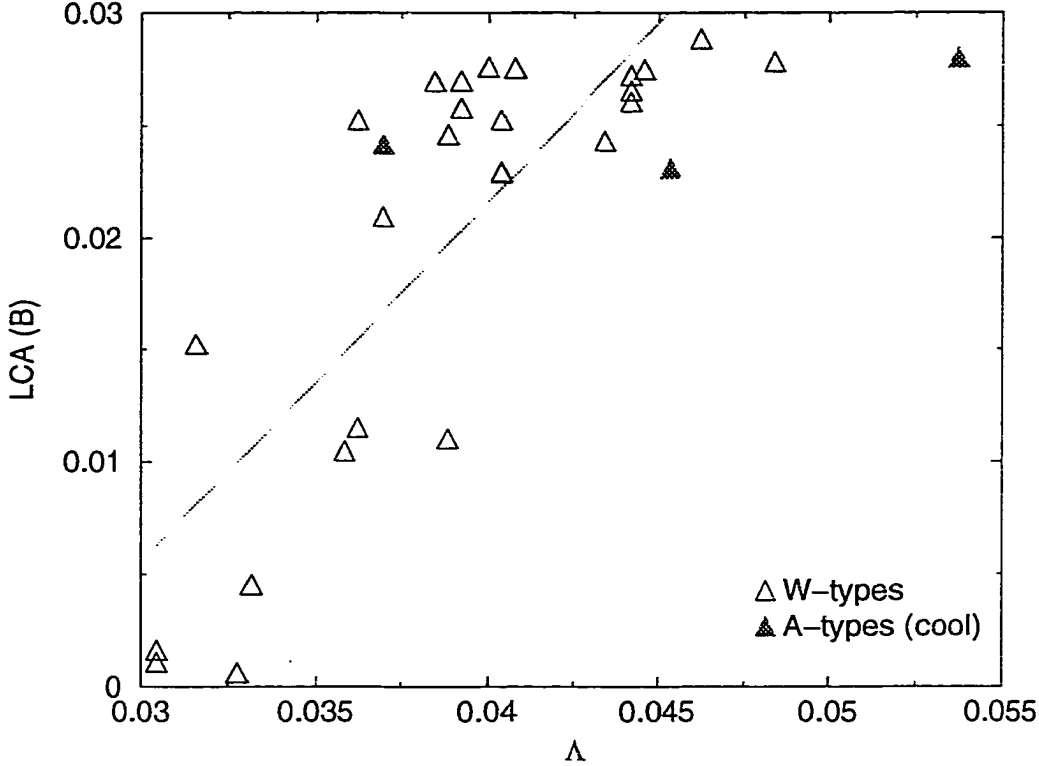


Figure 5.13: *LCA* plotted against Λ . As with the *OER* vs ρ_p , this relationship predicts that the higher mass systems will have a higher *OER*. The correlation here is 0.817.

OER(V) Correlation With Primary Parameters

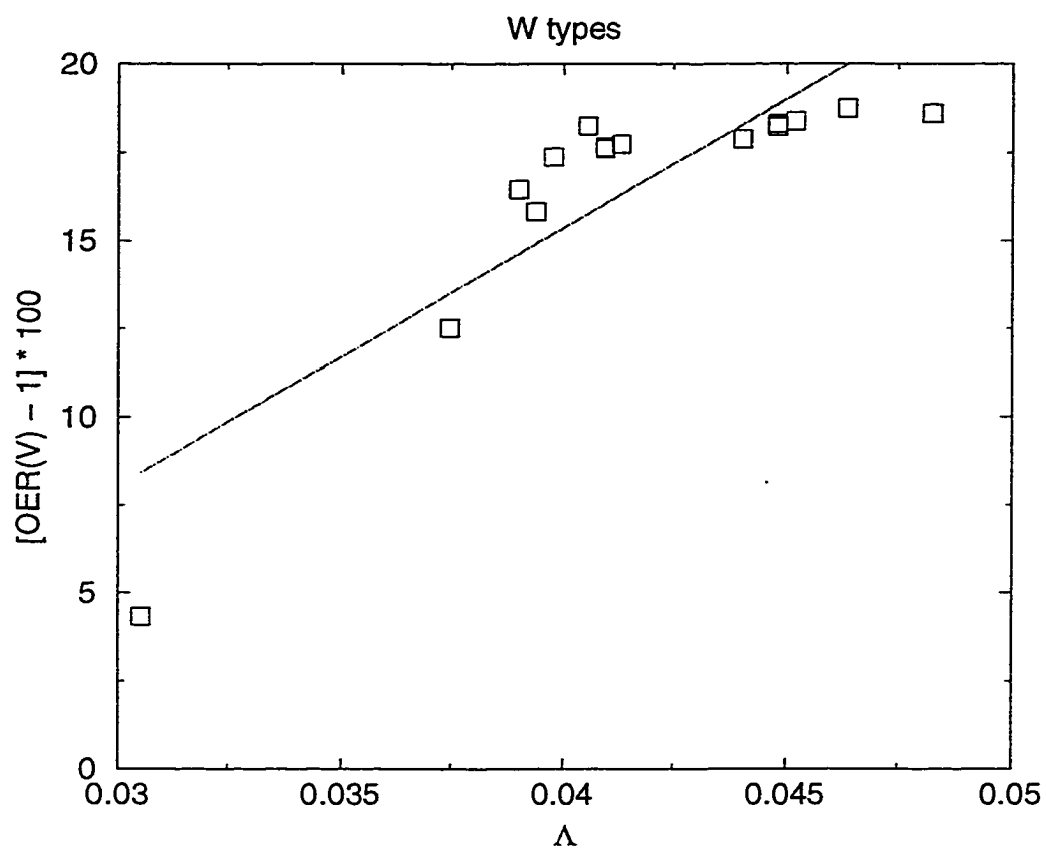


Figure 5.14: The V data for OER vs Λ is shown. The correlation of 0.86 is similar to the B value. Due to the similar agreement of OER with Δm regardless of color, this is expected.

OER(U) Correlation With Primary Parameters

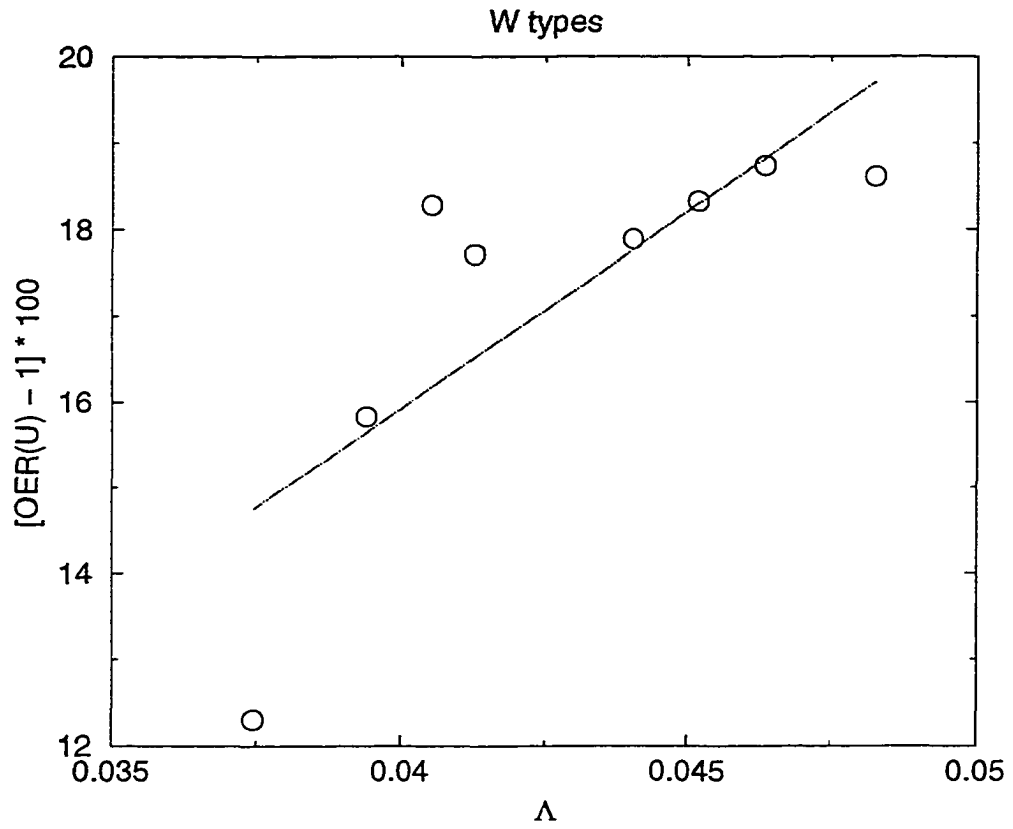


Figure 5.15: The U data for *OER* vs Λ . Similar to the V plot, the correlation here is 0.78.

Contact Flow Theory OER vs q

Varying Mass of the Primary

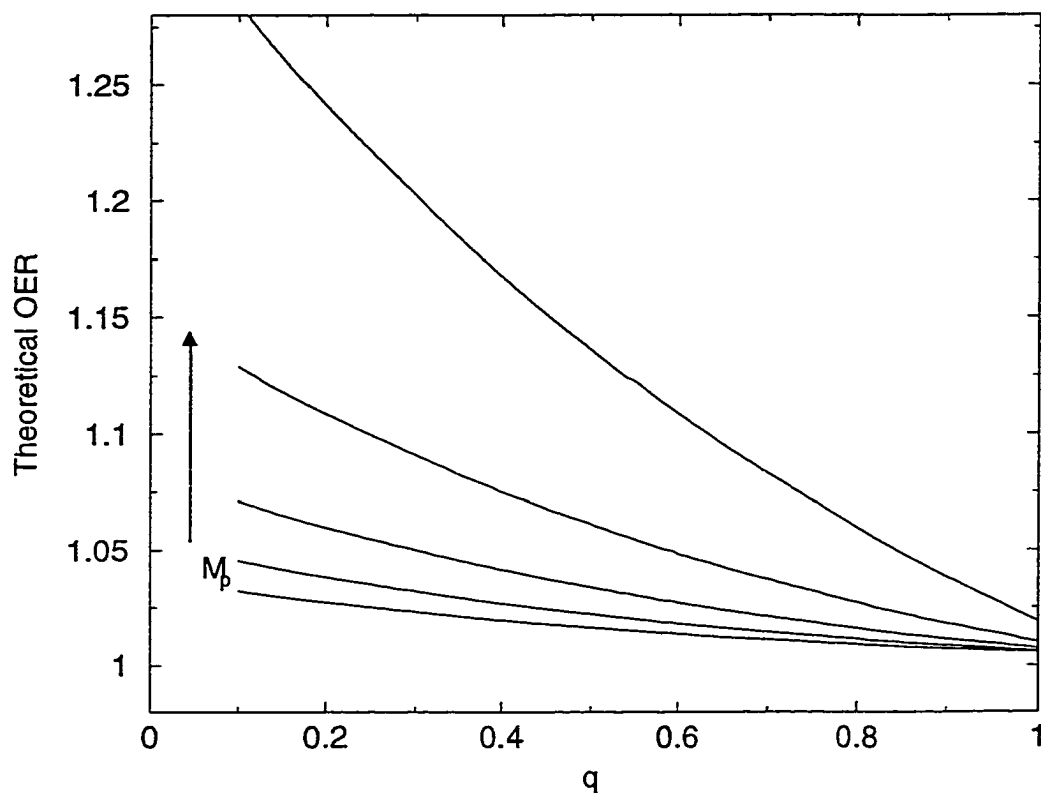


Figure 5.16: Plotted here is the contact model's OER variance with respect to q . In each case $\Delta T = 200\text{K}$, $r_1 + r_2 = 0.95$, and $P = 0.6$ d. The primary mass was increased from $0.8 - 1.6M_\odot$. The derived relation is: $OER \sim M^\alpha$ where $\alpha = 2.2$. This is the relationship used in Equation 5.9.

Contact Flow Theory OER vs q Varying Temperature Difference

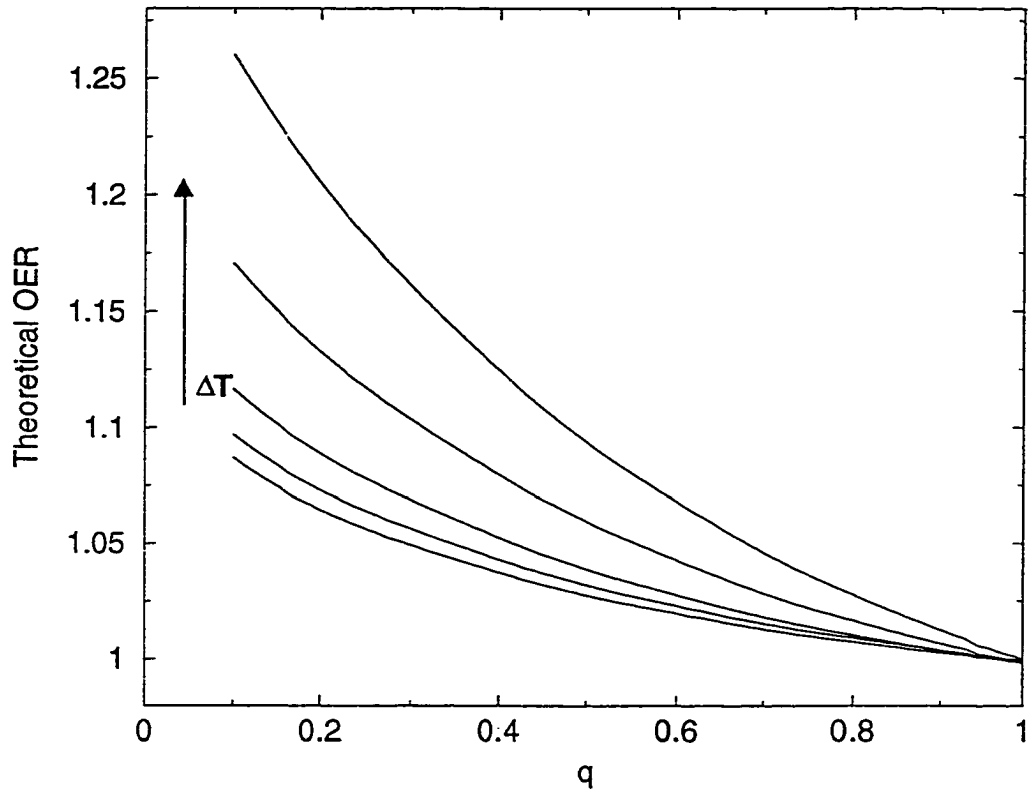


Figure 5.17: The contact model's OER variance is plotted with respect to q . In each case $M_p = 1.2M_\odot$, $r_1 + r_2 = 0.95$, and $P = 0.6$ d. The temperature difference was increased from 200-600K. The derived relation is: $OER \sim (\Delta T)^\beta$ where $\beta = 3.2$. This is the relationship used in Equation 5.10.

Contact Flow Theory OER vs q

Varying The Wilson–Devinney Radius Sum

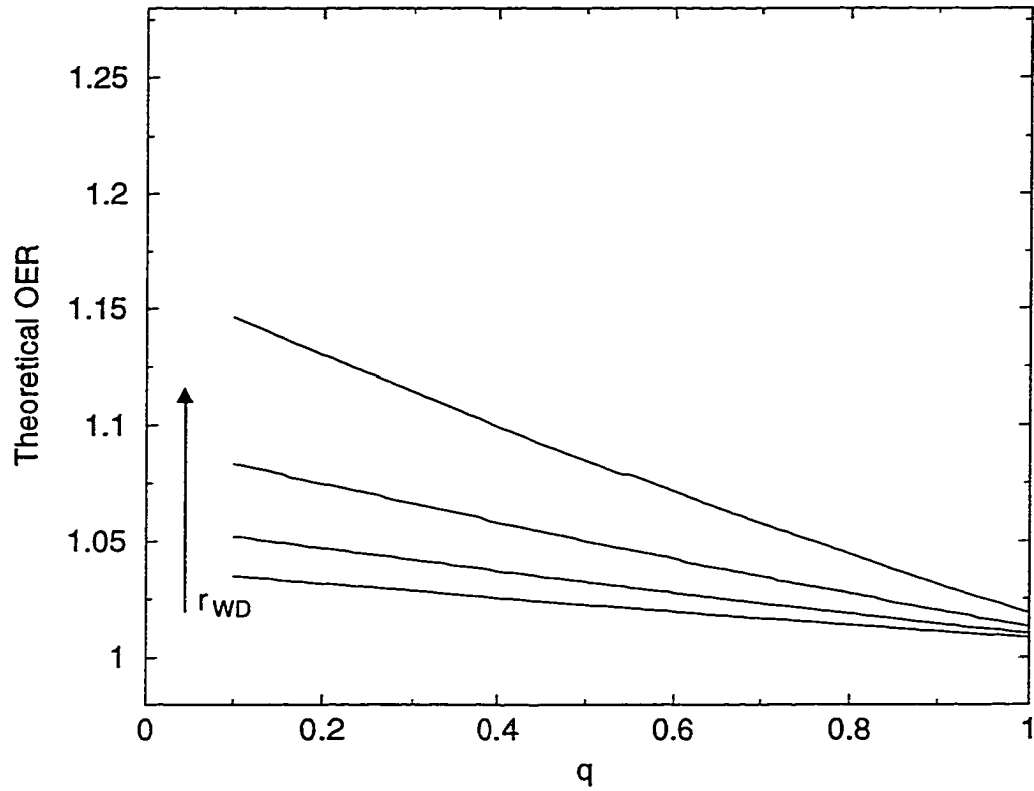


Figure 5.18: Again, OER variance is plotted with respect to q . In each case $M_p = 1.2M_\odot$, $\Delta T = 200\text{K}$, and $P = 0.6$ d. The radii sum was increased from 0.65 - 0.95. The derived relation is: $OER \sim (r_1 + r_2)^\gamma$ where $\gamma = 0.5$. This is the relationship used in Equation 5.11.

Contact Flow Theory OER vs q

Varying Rotation Period

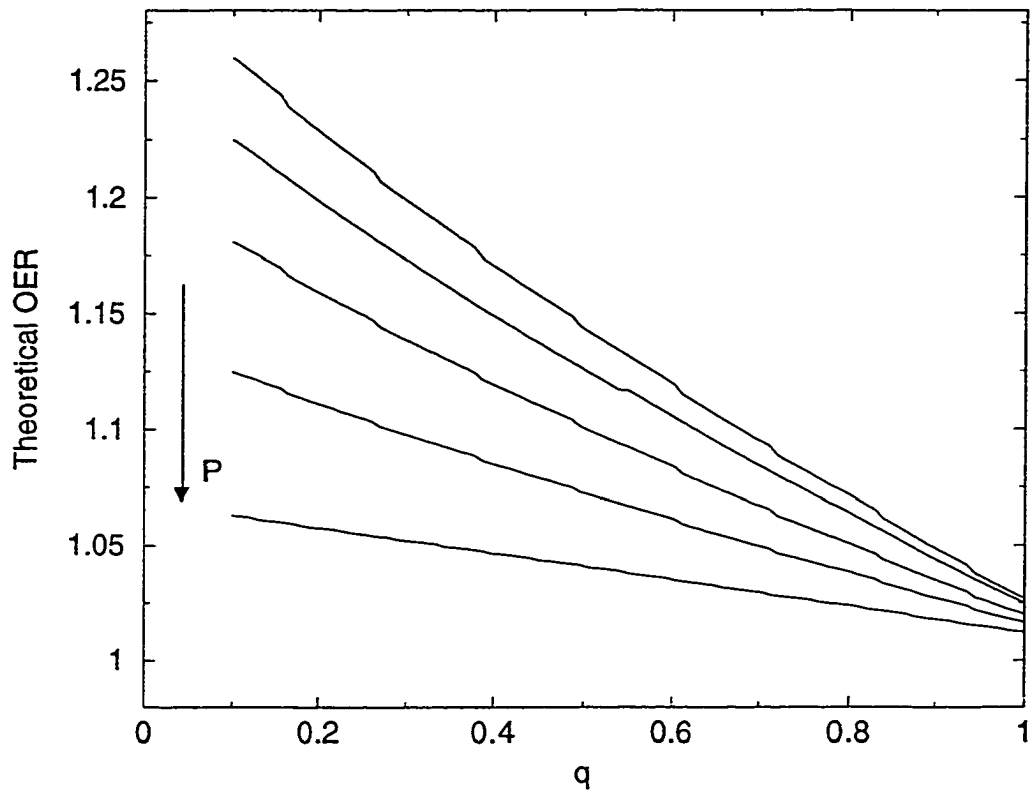


Figure 5.19: OER variance is once again plotted with respect to q . In each case $M_p = 1.2M_\odot$, $\Delta T = 200\text{K}$ and $r_1 + r_2 = 0.95$. The period was increased from 0.4 - 1.2 d. The derived relation is: $OER \sim P^\delta$ where $\delta = -1.6$. This is the relationship used in Equation 5.12.

$$OER \sim (r_1 + r_2)^{0.5}, \quad (5.11)$$

$$OER \sim P^{-1.6}. \quad (5.12)$$

As with the irradiated case, these power laws were used to fit the observational data. Figures 5.20-5.25 plot the A type observational data for quantities.

5.2.1 Observational Fits

At first glance, it is apparent that the data fit for the contact model is not as good as for the irradiated model. Several reasons exist for this. The contact model is not nearly as well developed as the irradiated one. The boundary condition problem introduces more uncertainty into a model which already includes many approximations. Clearly, the best way to proceed is to do a full-blown 3-D model which properly intertwines the temperature gradient and the flow velocity. This was not done for this model since the computational time would have been too extensive for the large parameter space used. Zhou and Lueng (1997b) present results for a preliminary *static* (non-rotational) model, and their computational time was well over 6000 minutes for just one model.

The situation is not a complete loss. The observational data shows similar trends with the previous set of data. In particular, the Figure 5.20 plot shows a reasonable fit. As with the irradiated case, it would appear that possibly a better fit would be exponential. This most likely implies that the exponents determined by the *OER* vs *q* plots are not quite correct for the contact case.

Another factor which might be influencing the data is that A types are often considered TAMS rather than ZAMS objects (see, e.g. MV). Thus, evolutionary effects could be causing some of the scatter.

OER(B) Correlation With Primary Parameters

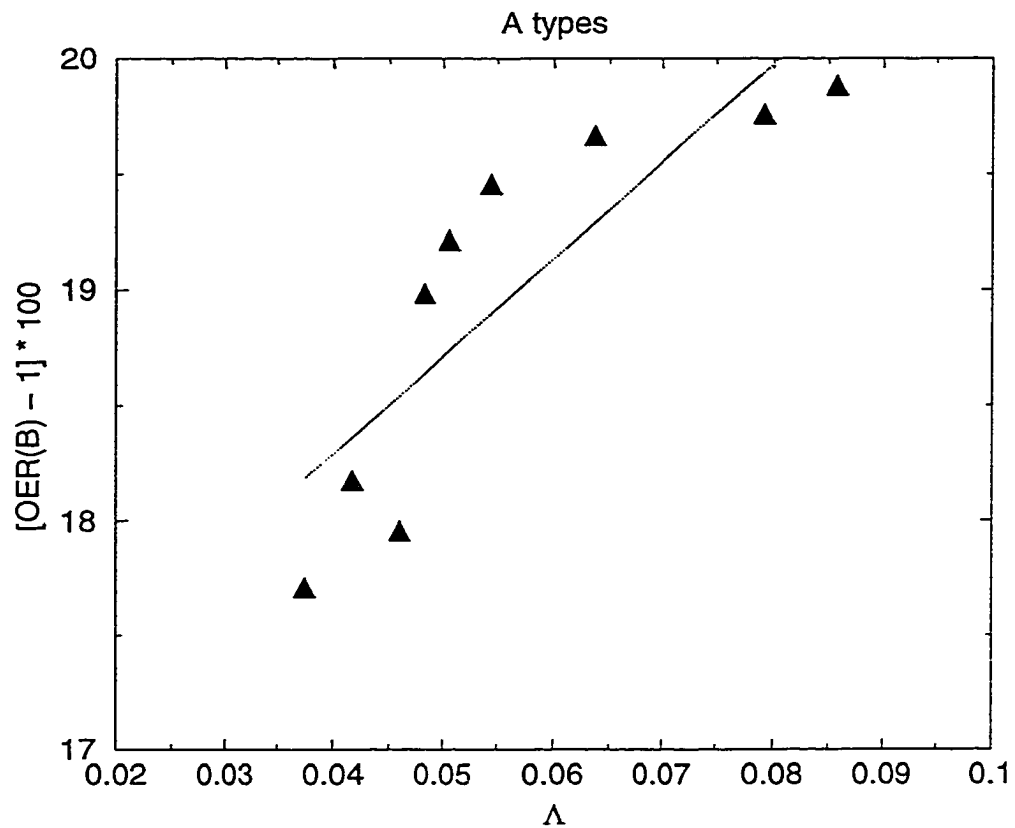


Figure 5.20: The fit for OER with Λ for the A types is not as good as for the W types. In this case the theory does not seem to be as well developed as for the irradiation case. The correlation coefficient = 0.84.

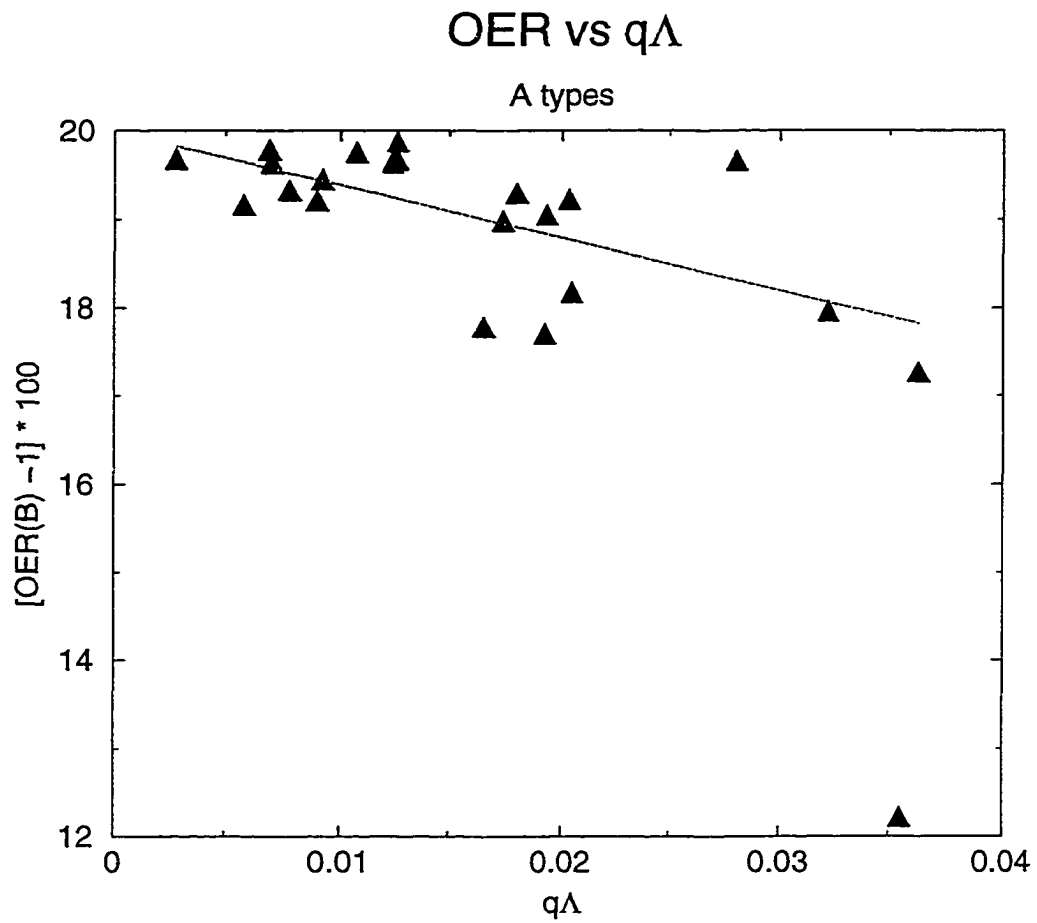


Figure 5.21: A plot of the A types for $q \times \Lambda$. This shows a better correlation (coefficient = 0.67) than Figure 5.8, since the four independent variables have been sorted out. The outlier has not been included in the best fit line.

LCA Correlation for A Types

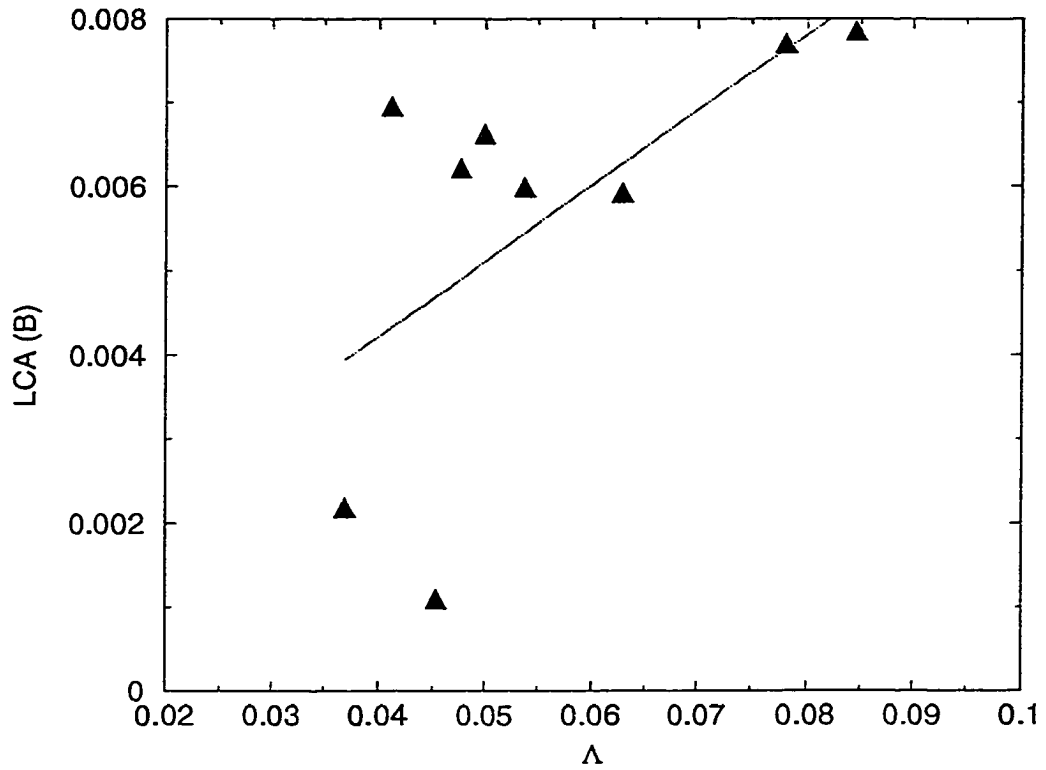


Figure 5.22: For the A types, the LCA- Λ plot is shown. Again, as with the previous figure, the correlation (coefficient = 0.62) is not as good as the W type correlation.

OER vs Density Of The Primary

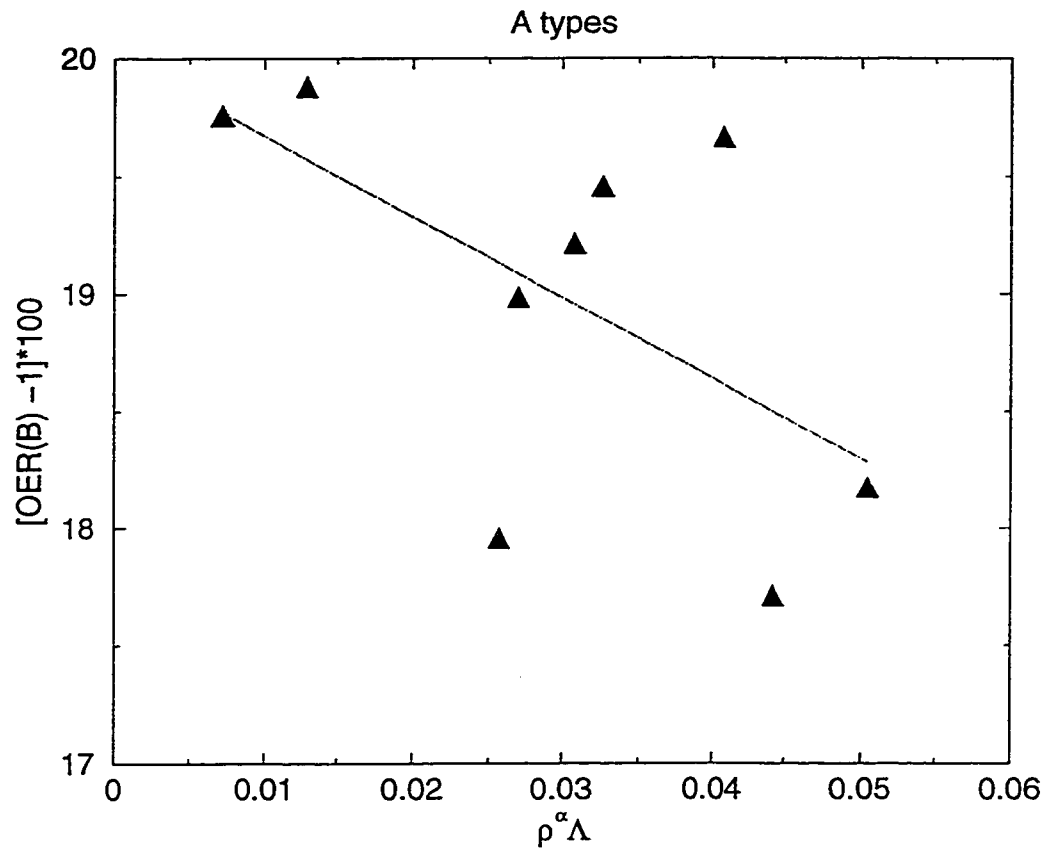


Figure 5.23: The OER vs density of the primary. As with the irradiation case, α has been set equal to 1. The scatter is fairly high, for the reasons discussed in the text. The correlation is 0.58.

OER vs Density Of The Secondary

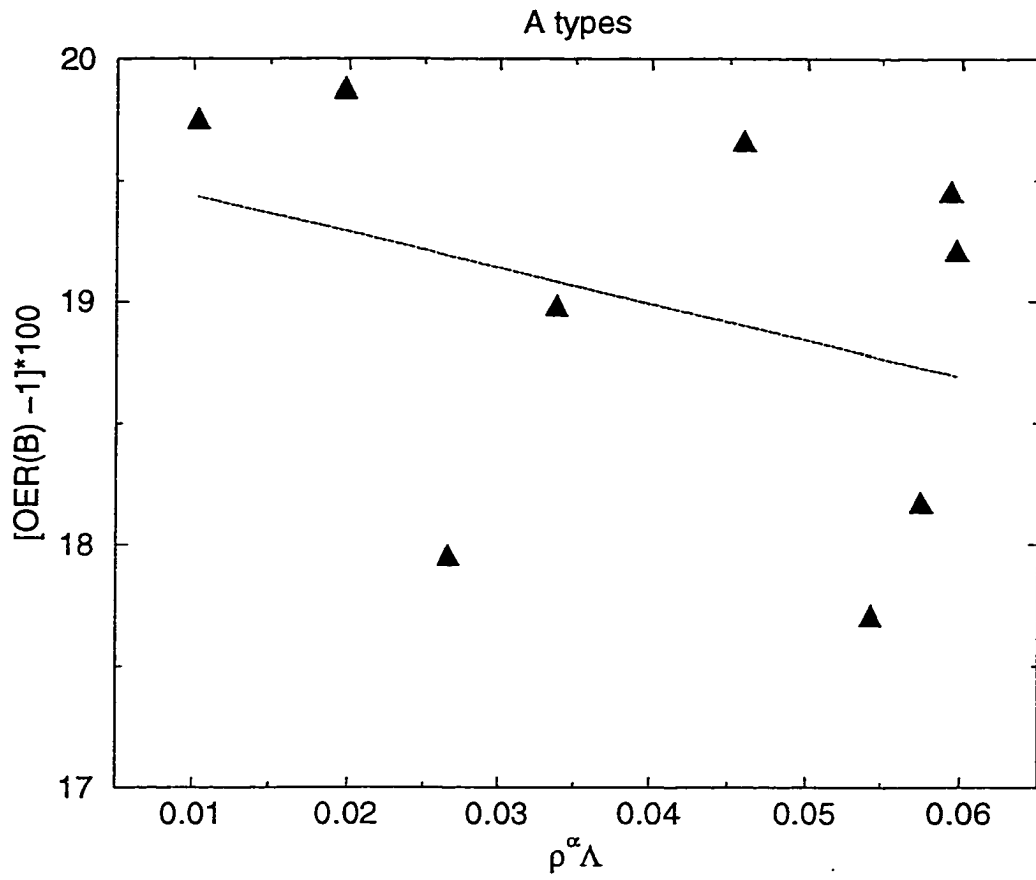


Figure 5.24: The OER vs density of the secondary. Again, $\alpha = 1$. A very weak correlation (0.34) exists.

OER vs Mass Of The Secondary

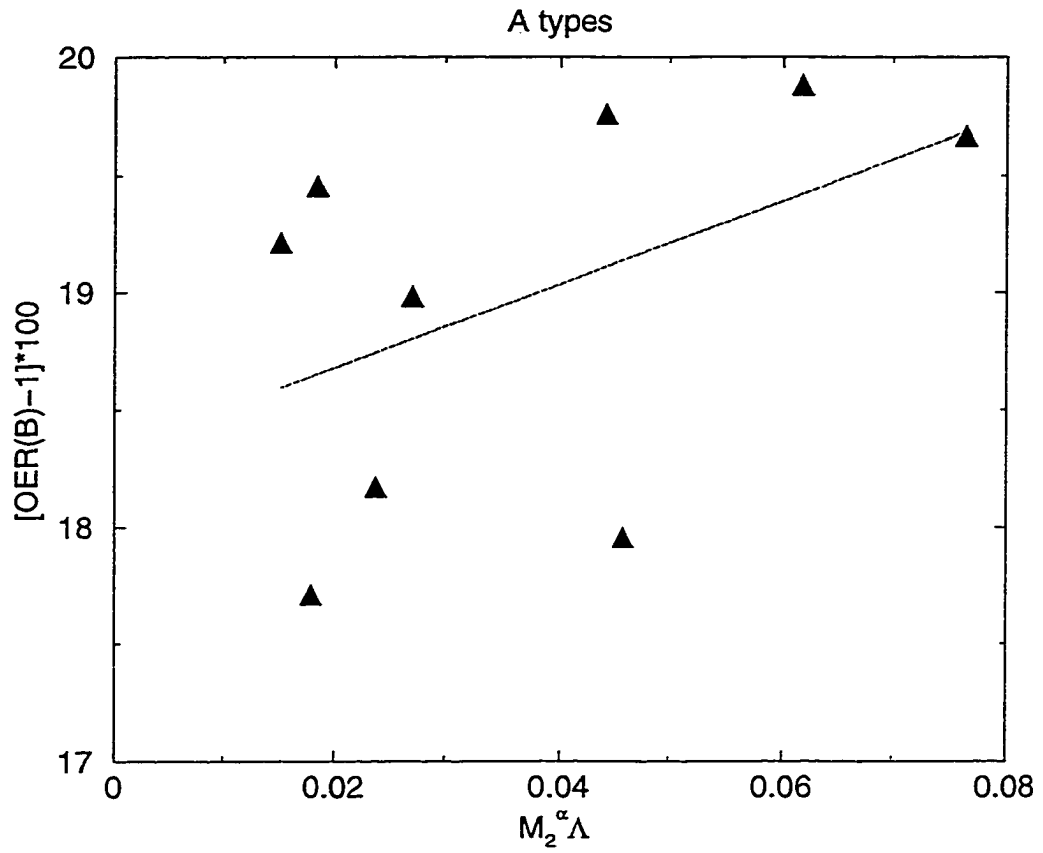


Figure 5.25: The OER vs mass of the secondary. As with the density cases, the correlation of 0.46 is weak. In this case, $\alpha = 2.2$, in keeping with the relationship for M_p .

5.3 Conclusions

The O'Connell effect has been known for many years, but no adequate explanation has been published yet. The long term stability of the asymmetry in many systems seems to indicate a thermodynamic explanation. The irradiation model of Zhou and Leung offers a reasonable fit to the observational data for the *W* types. The correlation shown in Figure 5.7 indicates that the parameters that were used (primary mass, temperature difference, sum of the radii and period) do influence the O'Connell effect in *W* types. The relationship indicates how a combination of important quantities would change *OER*. As primary mass (and thus effective temperature), overall radius and temperature difference increase, and the period decreases, the O'Connell effect becomes more pronounced in the *W* types. Other parameters might also be important, and should be analyzed in the future. In particular, ρ_p , the primary density shows a very good correlation when plotted with the above parameters (see Figure 5.11). The code should be re-ran with density as a free parameter as well. The simple 2-D model presented here offers a preliminary look and hopefully motivates the development of a 3-D model.

The non-O'Connell effect asymmetries in the light curves (the 'bumps' and 'dimples') remain unmodeled. The best course of action for these phenomena seem to be spot modeling, which implies a probable MHD origin. However a good determination of the O'Connell effect with the current model should help to greatly reduce the parameter uniqueness problem inherent in the spot modeling method. Zhou and Leung's irradiation model should be included in the WD model, so that the calculations are intertwined. This would provide a physically consistent model, which conserves energy, rather than the "slapping on" method inherent in current spot modeling. The derived relationships for *OER* with the various parameters would allow for a reasonable first guess for these parameters, thus at least closing the range of some of the free values. As a result, this

would reduce the ambiguity brought on by spot modeling, which is still the primary weakness of the WD method.

Using the *LCA* method, a reasonable guess for the location of the flux asymmetry can be obtained. This would help in obtaining a constraint on the longitude value for the spot. Since the normalized *LCA* vs phase is known from this method, similarly sized asymmetries at more than one location could justify the introduction of multiple spots for a solution. The reduction in ambiguity of one of the spot(s) parameters would help with the uniqueness problem outlined by Maceroni and Van't Veer (1993).

The current model could also be applied to another class of eclipsing binaries, the near-contact systems. These are systems known to have fillouts just less than 0%, implying that they are in a detached state, but are very close. The irradiated model could be applied to these systems, many of which were studied in the 1984 study by Davidge and Milone. For the *W* type *W* *UMa* systems, many have fillouts of only a few percent, while a few have *negative* fillouts, which implies they are actually near contact systems. Including the data set of close, near contact binaries would greatly increase the statistics.

For the contact model, the observational fit was not nearly as good. Perhaps this is a result of the simple model not incorporating the complete theory of Zhou and Leung, which is still a work in progress. However, the weaker correlation doesn't show a complete failure for the simplified version of this model used here. As with the irradiated model, an increase in primary mass, radius sum and temperature difference, couple with a period decrease, still indicates an *OER* increase. One should note however, that the relationships for the two models are slightly different, which reinforces the hypothesis that the *A* and *W* types have different mechanisms responsible for the asymmetry. As with the irradiation case, additional parameters may need to be included in the analysis. From Figure 5.21, it would seem that q should be included, since addition of the mass

ratio provided a good correlation. Zhou and Leung's direction function, discussed in Chapter 2 (see Equation 2.36 and Figure 2.10), shows that the circumfluence depends heavily on the mass ratio. As the contact model becomes more sophisticated, the mass ratio should also be used as an additional free parameter. A complete 3-D model which calculates the flow velocity more rigorously should provide a better correlation. Hopefully, when their model is complete, a reassessment of the *OER* data will be done.

It is necessary that in order to formulate a better 3-D model, the observational data set will need to grow. Also, the quality of the data needs to improve. More W UMa systems need to have q spectroscopically determined. Also broad band UBVR photometry should be done, since the size of the O'Connell effect is weakly wavelength dependent. Consistent monitoring of a few, bright well determined systems would help greatly in smoothing out the light curve asymmetries that are caused by the short term MHD effects. Similarly, the neglected systems need to be reobserved with modern CCD photometry. As mentioned above one way to increase the data set would be to include other types of binaries, in particular the near contact class. The justification for this is the close agreement in fillout %'s between the W type W UMa systems and the near contact systems.

Most of the systems analyzed in this data set had enough observations to allow 40 or 80 bins for calculating the *OER*. However, for some of the systems, the published photometry only allowed for a smaller set of 20 bins. This introduces a scatter into the calculation of *OER* that can be removed by more extensive photometry. In their recent publication, Kallrath and Milone (1999) mention some tips for observers. For the needs of this database, the most important recommendation they make is that observations need to be easily available to other astronomers. As they note, sometimes only the observations remain worthwhile 5 or 10 years after publication, since the methods of interpretation can change enough to render the analysis no longer useful.

The models introduced here justify further examination into a thermodynamic cause for the O'Connell effect in W UMa systems. Much work remains to be done before the models are robust enough to yield a complete, 3-D dynamic construct of these systems. Ongoing advances in hydrodynamical modeling will be very useful in creating more realistic models of close and contact binary stars. The interesting physical problems these systems bring to astrophysics provide a very good test environment for computational methods used in the field.

Bibliography

- [Ahn, Hill, and Khalessheh (1992)] Ahn, Y., Hill, G., and Khalessheh, B. 1992 Studies of Late-type Binaries V. The Orbit and Physical Parameters of V1073 Cygni. *A&A* **265**, 597.
- [Al-Away (1993)] Al-Away, A.A. 1993 FZ Orionis: A Short Period W UMa System. *Ap&SpSc* **207**, 171.
- [Al-Naimiy (1978)] Al-Naimiy, H.M. 1978 Linearized Limb-Darkening Coefficients for Use in Analysis of Eclipsing Binary Light Curves. *Ap&SpSc* **53**, 181.
- [Aslan and Derman (1986)] Aslan, Z. and Derman, E. 1986 Photoelectric observations of CK Bootis. *A&AS* **66**, 781.
- [Aslan and Herczeg (1984)] Aslan, Z. and Herczeg, T.J. 1984 On the Periods of RZ Comae and V1073 Cygni. *IBVS* **2478**.
- [Awadalla and Yamasaki (1984)] Awadalla, N. and Yamasaki, A. 1984 A photometric study of the contact binary XY Boo. *Ap&SpSc* **107**, 347.
- [Barker and Herczeg (1979)] Barker, L.A. and Herczeg, T. 1979 Photoelectric Observations and Period Study of AK Herculis. *PASP* **91**, 247.
- [Barone, *et al.* (1993)] Barone, F., DiFiore, L., Milano, L., and Russo, G. 1993 Analysis of Contact Binary Systems: AA Ursae Majoris, V752 Centauri, AO Camelopardis, and V677 Centauri. *ApJ* **407**, 237.
- [Batten, Fletcher and McCarthy (1989)] Batten, A., Fletcher, J. and McCarthy, D. 1989 Eighth Catalogue of the Orbital Elements of Spectroscopic Binary Systems. *Publ D.A.O.* **XVII**.
- [Bell, Hilditch and Edwin (1993)] Bell, S.A., Hilditch, R.W., and Edwin, R.P. 1993 CCD photometry of the eclipsing binary RU UMi. *MNRAS* **260**, 478.

- [Bell, Hilditch and King (1984)] Bell, S.A., Hilditch, R.W., and King, D.J. 1984 Asymmetric Light Curves of the Contact Binary AB Andromedae. *MNRAS* **208**, 123.
- [Bell, Rainger and Hilditch (1990)] Bell, S.A., Rainger, P.P., and Hilditch, R.W. 1990 Spots on AG Vir - paradigm or panacea? *MNRAS* **247**, 632.
- [Binnendijk (1970)] Binnendijk, L. 1970 The Orbital Elements of W UMa Systems, in *Vistas in Astronomy*, Vol. 12, p 217.
- [Binnendijk (1972)] Binnendijk, L. 1972 The light variation of AU Ser. *AJ* **77**, 603.
- [Bradstreet (1981)] Bradstreet, D.H. 1981 Analyses of a Light Curve of V523 Cassiopeiae. *AJ* **86**, 98.
- [Bradstreet (1985)] Bradstreet, D.H. 1985 K-type Overcontact Binaries. *ApJS* **58**, 413.
- [Branly, *et al.* (1996)] Branly, R.M., Athauda, R.I., Fillingim, M.O., and Van Hamme, W. 1996 Light Curve Solutions for Eclipsing Binaries in NGC 188. *Ap&SpSc* **235**, 149.
- [Broglia and Conconi (1983)] Broglia, P. and Conconi, P. 1983 Seasonal Light Curves of TY UMa: Observations and Solutions. *A&AS* **51**, 97.
- [Budding (1977)] Budding, E. 1977 The Interpretation of Cyclical Photometric Variations in Certain Dwarf ME-type Stars *Ap&SpSc* **48**, 207.
- [Budding, *et al.* (1996)] Budding, E., Butler, C.J., Doyle, J.G., Etzel, P.B., Olah, K., Zeilik, M., and Brown, D. 1996 Basic stellar parameter determination for active cool eclipsing binaries. *Ap&SpSc* **236**, 215.
- [Burchi, Milano and Russo (1977)] Burchi, R., Milano, L., and Russo, G. 1977 Analysis of the V Light Curve of the System CW Cas. *Ap&SpSc* **47**, 35.
- [Claret and Gimenez (1992)] Claret, A. and Gimenez, A. 1992 Circularization and Synchronization Times in Detached Main Sequence Eclipsing Binaries. In *Evolutionary Processes in Interacting Binary Stars*. Kondo, Y. *et al.* (eds.), 269.
- [Covino, *et al.* (1988)] Covino, E., Milano, L., de Martino, D., and Vittone A.A. 1988 UVRI Photometry of the Short-period Eclipsing Binaries EE Aqr, RV Gru and RW PsA. *A&AS* **73**, 437.
- [Cranmer (1993)] Cranmer, S.R. 1993 Some Aspects of Illuminated Model Atmosphere Theory as Applied to Close Binary Systems. *MNRAS* **263**, 989.
- [Davidge and Milone (1984)] Davidge, T.J. and Milone, E.F. 1984 A study of the O'Connell Effect in the Light Curves of Eclipsing Binaries. *ApJS* **55**, 571.

- [Demircan, Demircan and Akalin (1993)] Derman, E., Demircan, O., and Akalin, A. 1993 UBV Photometry of BX Andromedae. *Ap&SpSc* **205**, 327.
- [Demircan, *et al.* (1994)] Demircan, O., Derman, E., Akalin, A., Selam, S., and Muyesseroglu, Z. 1994 Light-Curve and Period Changes of AB Andromedae. *MNRAS* **267**, 19.
- [Demircan, Demircan and Selam (1991)] Derman, E., Demircan, O., and Selam, S. 1991 Light Curve and Period Variations of a W Ursae Majoris System LS Delphini. *A&AS* **90**, 301.
- [Demircan, Selam and Derman (1991)] Demircan, O., Selam, S., and Derman, E. 1991 1990 Photometry of a Small Amplitude W UMa System LS Delphini. *Ap&SpSc* **186**, 57.
- [Djurasevic (1993a)] Djurasevic, G. 1993 An Analysis of Close Binaries (CB) Based on Photometric Measurements (IV). *A&SpSc* **206**, 119.
- [Djurasevic (1993b)] Djurasevic, G. 1993 An Analysis of Close Binaries (CB) Based on Photometric Measurements (V). *A&SpSc* **206**, 129.
- [Djurasevic (1993c)] Djurasevic, G. 1993 An Analysis of Close Binaries (CB) Based on Photometric Measurements (VI). *A&SpSc* **206**, 145.
- [Djurasevic (1993d)] Djurasevic, G. 1993 An Analysis of Close Binaries (CB) Based on Photometric Measurements (VII). *A&SpSc* **206**, 207.
- [Eaton (1991)] Eaton, J.A. 1991 Ultraviolet Light Curves of V535 Arae. *Ap&SpSc* **186**, 7.
- [Frasca, Sanfilippo and Catalano (1996)] Frasca, A., Sanfilippo, D., and Catalano, S. 1996 H α Observations of VW Cephei. *A&A* **313**, 532.
- [Garcia and Gimenez (1992)] Garcia, J.M. and Gimenez, A. 1992 Mass Transfer Characterization in Close Binary Stars, in *Evolutionary Processes in Interacting Binary Stars*. Kondo, Y. et al. (eds), 337.
- [Giuricin, Madrossian and Mezzetti (1983)] Giuricin, G., Madrossian, F., and Mezzetti, M. 1983 Statistics of categorized eclipsing binary systems. Light curve shapes, periods, and spectral types. *A&AS* **54**, 211.
- [Goderya, Leung and Schmidt (1995)] Goderya, S.N., Leung, K.C., and Schmidt, E.G. 1995 A Photometric Study of V508 Cygni. *AJ* **110**, 346.
- [Goeking and Duerbeck (1993)] Goeking, K.D. and Duerbeck, H.W. 1993 The spectroscopic orbit of ϵ Coronae Austrinae, an evolved W UMa system. *A&A* **278**, 463.

- [Goecking, *et al.* (1994)] Goecking, K.D., Duerbeck, H.W., Plewac, T., Kaluzny, J., Schertt, D, Weigett, and Flin, P. 1994 The W Ursae Majoris System ER Ori, a Multiple Star. *A&A* **289**, 827.
- [Goldman and Mazeh (1992)] Goldman, I. and Mazeh, T. 1992 Tidal Circularization of Short Period Binaries, in *Binaries as Tracers of Stellar Formation*, 82.
- [Gonzales, *et al.* (1996)] Gonzales, J.F.; Lapasset, E; Gomez, M; and Ahumda, J. 1996 Photometric Analyses of the Contact Binary BF Pav. *PASP* **108**, 338.
- [Grobel (1989)] Grobel, R. 1989 A Major Period Change in the System TZ Bootis. *IBVS* **3299**.
- [Guinan (1993)] Guinan, E.F. 1993 New Directions in Eclipsing Binary Research, in *New Frontiers in Binary Star Research*. ASP Conference Series, V 38. Leung, K.C. and Nha, I.S. (eds), 1.
- [Guinan and Bradstreet (1988)] Guinan, E.F. and Bradstreet, D.H. 1988 Kinematic Clues to the Origin and Evolution of Low Mass Contact Binaries, in *Formation and Evolution of Low Mass Stars*. Dupree, A.K. and Lago, M.T.V.T. (eds), 345.
- [Hall and Henry (1990)] Hall, D.S. and Henry, G.W. 1990 Circularization, Synchronizations and Differential Rotation in Chromospherically Active Binaries. In *Active Close Binaries*. Ibanoglu, C. (ed), 287.
- [Hazelhurst (1985)] Hazelhurst, J. 1985 The Dissipation Factor in Contact Binaries. *A&A* **145**, 25.
- [Hazelhurst (1993)] Hazelhurst, J. 1993 The equilibrium of a contact binary. *A&A* **271**, 209.
- [Hazelhurst (1996)] Hazelhurst, J. 1996 On a temperature-regulation mechanism for contact binaries. *A&A* **313**, 487.
- [Hazelhurst (1997)] Hazelhurst, J. 1997 Bernoulli's Equation and the Contact Binaries. *A&A* **326**, 155.
- [Hazelhurst (1999)] Hazelhurst, J. 1999 On the Flow Topology in Contact Binaries. *A&A* **341**, 567.
- [Hazelhurst, Hoppner and Refsdal (1982)] Hazelhurst, J., Hoppner, W., and Refsdal, S. 1982 On the Stability of Age-Zero Contact Binaries. II. *A&A* **109**, 117.
- [Hazelhurst and Refsdal (1980)] Hazelhurst, J. and Refsdal, S. 1980 On the Stability of Age-Zero Contact Binaries. I. *A&A* **84**, 200.
- [Herczeg (1993)] Herczeg, T.J. 1993 Observations and Period Studies of Two Neglected W UMa Systems: V401 Cygni and Y Sextantis. *PASP* **105**, 911.

- [Hilditch (1994)] Hilditch, R. 1994 Interacting Binary Stars. *The Observatory* 114, 212.
- [Hilditch, King and McFarlane (1989)] Hilditch, R.W.; King, D.J.; and McFarlane, T.M. 1989 Contact and Near-contact Binary Systems-X. The Contact System TV Muscae. *MNRAS* 237, 447.
- [Hill (1979)] Hill, G. 1979 Description of an Eclipsing Binary Light Curve Computer Code with Application to Y Sex and the W UMa Code of Rucinski. *PubDOA XV*, 297.
- [Hill (1993)] Hill, G. 1993 The Measurement of Radial Velocities Using Cross-Correlation Techniques as Applied to Binary Stars, in *New Frontiers in Binary Star Research*. ASP Conference Series, V 38. Leung, K.C. and Nha, I.S. (eds), 127.
- [Hill, Fisher and Holmgren (1989)] Hill, G.; Fisher, W.A.; and Holmgren, D. 1989 Studies of Late-type Binaries: The Physical Parameters of 44i Boo ABC. *A&A* 211, 81.
- [Hill and Hutchings (1970)] Hill, G. and Hutchings, J. 1970 The Synthesis of Close-Binary Light Curves. I. The Reflection Effect and Distortion in Algol. *ApJ* 162, 265.
- [Hoffmann (1978)] Hoffmann, M. 1978 The W UMa system TZ Boo. *A&AS* 33, 63.
- [Hoffmann (1982)] Hoffmann, M. 1982 GW Cephei, a W UMa type system. *Ap&SpSc* 83, 195.
- [Hrivnak (1982)] Hrivnak, B.J. 1982 A Photometric Study and Analysis of AW Ursae Majoris. *ApJ* 260, 744.
- [Hrivnak (1985)] Hrivnak, B.J. 1985 A Photometric Study and Analysis of XY Leonis. *ApJ* 290, 696.
- [Hrivnak (1988)] Hrivnak, B.J. 1988 Radial Velocity Studies and Absolute Parameters of Contact Binaries. I - AB Andromedae *ApJ* 335, 319.
- [Hrivnak (1989)] Hrivnak, B.J. 1989 Radial Velocity Studies and Absolute Parameters of Contact Binaries. II - OO Aquilae *Apj* 340, 458.
- [Hrivnak (1993)] Hrivnak, B.J. 1993 New Radial Velocity Curves of Six W UMa Binaries, in *New Frontiers in Binary Star Research*. ASP Conference Series, V 38. Leung, K.C. and Nha, I.S. (eds), 269.
- [Hrivnak and Milone (1989)] Hrivnak, B.J. and Milone, E.F. 1989 The Unusual High Mass Ratio Contact Binary VZ Psc. *AJ* 97, 532.
- [IAU Commission 42 (1991)] IAU com. 42 report for 1991, 483.
- [Iben and Livio (1993)] Iben, I. and Livio, M. 1993 Common Envelopes in Binary Star Evolution. *PASP* 105, 1373.

- [Jeong, *et al.* (1994)] Jeong, J.H., Kand, Y.W., Lee, W.B., and Sung, E.C. 1994 Analysis of the IUE satellite and the ground-based observations of SW Lacertae. *ApJ* **421**, 779.
- [Jianmin (1993)] Jianmin, W. 1993 The Interaction Between the Secondary and the Common Envelope in a Contact Binary. *Ap&SpSc* **209**, 273.
- [Jianmin (1994)] Jianmin, W. 1994 The Thermal Relaxation Oscillation States of Contact Binaries. *ApJ* **434**, 277.
- [Jianmin (1995)] Jianmin, W. 1995 Are Contact Binaries Undergoing Thermal Relaxation Oscillations with Contact Discontinuity? *AJ* **110**, 782.
- [Jurkevich (1970)] Jurkevich, I. 1970 Machine Solutions of Light Curves of Eclipsing Binary Systems, in *Vistas in Astronomy* V12, p 63.
- [Kahler (1995)] Kahler, H. 1995 Contact Binaries in Thermal Equilibrium. *A&A* **294**, 497.
- [Kahler (1997a)] Kahler, H. 1997 Evidence of Thermal Disequilibrium in Contact Binaries. *A&A* **318**, 171.
- [Kahler (1997b)] Kahler, H. 1997 The Energy Balance in Contact Binaries. *A&A* **320**, 787.
- [Kahler (1997c)] Kahler, H. 1997 On the Surface Condition for Stationary Contact Binaries. *A&A* **326**, 161.
- [Kallrath and Milone (1999)] Kallrath, J. and Milone, E. 1999 Eclipsing Binary Stars: Modeling and Analysis. Springer, New York.
- [Kaluzny and Krzeminski (1993)] Kaluzny, J. and Krzeminski, W. 1993 Contact Binaries and SX Phe Variables in the Globular Cluster NGC 4372. *MNRAS* **264**, 785.
- [Kaluzny and Shara (1987)] Kaluzny, J. and Shara, M.M. 1987 The Discovery of Six New Short-Period Variables in the Old Open Cluster NGC 188. *ApJ* **314**, 585.
- [Kang and Wilson (1989)] Kang, Y.W. and Wilson, R.E. 1989 A Least Squares Adjustment of Spot Parameters for three RS CVn Binaries. *AJ* **97**, 848.
- [Karimie (1983)] Karimie, M.T. 1983 Light Curve Variation and Period Changes of VW Cep. *Ap&SpSc* **93**, 53.
- [Kilmartin, Bradstreet and Koch (1987)] Kilmartin, P., Bradstreet, D., and Koch, R. 1987 V677 Centauri: Overcontact and Completely Eclipsing but A-type or W-type? *ApJ* **319**, 334.

- [Kim (1992)] Kim, C-H. 1992 Analysis of Period Changes of YY Eridani. In *Evolutionary Processes in Interacting Binary Stars*. Kondo, Y. et al. (eds), 383.
- [Kippenhahn and Weigert (1990)] Kippenhahn, R. and Weigert, A. 1990 *Stellar Structure and Evolution*. Springer. New York.
- [Kitamura (1990)] Kitamura, M. 1990 Effective Gravity-Darkening of Close Binary Systems, in *Active Close Binaries*. Ibanoglu, C (ed), 69.
- [Knipe (1965)] Knipe, G. 1965 The Eclipsing Binary RR Centauri. *ApJ* **142**, 1068.
- [Kopal (1959)] Kopal, Z. 1959 *Close Binary Systems* (New York, Wiley)
- [Kopal (1989)] Kopal, Z. 1989 *The Roche Problem* (Dordrecht, Kluwer)
- [Kopal (1990)] Kopal, Z. 1990 On Physical Causes of the Light Variations of Active Binary Systems and on Their Interpretation, in *Active Close Binaries*. Ibanoglu, C. (ed), 1.
- [Lafter and Grainger (1985)] Lafta, S. and Grainger, J.F. 1985 New Photoelectric Observations of Four W UMa Systems: OO Aql, V839 Oph, V566 Oph, and SW Lac. *Ap&SpSc* **114**, 23.
- [Lafta and Grainger (1986)] Lafta, S. and Grainger, J.F. 1986 A Photoelectric Study of the W UMa-system U Pegasi. *Ap&SpSc* **121**, 61.
- [Lai, Rasio and Shapiro (1993)] Lai, D., Rasio, F., and Shapiro, S. 1993 Hydrodynamic Instability and Coalescence of Close Binary Systems. *ApJ* **406**, 263.
- [Lapasset (1980)] Lapasset, E. 1980 Fundamental Photometric Data for Two Contact Binaries - MW Pavonis and TY Mensae. *AJ* **85**, 1098.
- [Lapasset and Claria (1986)] Lapasset, E. and Claria, J. 1986 Synthetic Light Curve Method Applied to the W UMa Systems SY Hor and VY Cet. *A&A* **161**, 264.
- [Lapasset and Funes (1985)] Lapasset, E., and Funes, J.G. 1985 The Peculiar Behaviour of the Photometric Variability of V508 Ophiuchi. *A&SpSc* **113**, 83.
- [Lapasset and Gomez (1990)] Lapasset, E. and Gomez, M. 1990 Simultaneous Analysis of Light and Radial Velocity Curves of the Peculiar Contact System V508 Oph. *A&A* **231**, 365.
- [Lapasset, Gomez and Farinas (1992)] Lapasset, E., Gomez, M., and Farinas, R. 1992 Test of the Optimization Techniques for the Photometric Analysis of Contact Binaries, in *Evolutionary Processes in Interacting Binary Stars*. Kondo, Y. et al. (eds), 387.
- [Lapasset, Gomez and Farinas (1996)] Lapasset, E., Gomez, M., and Farinas, R. 1996 Photometric Analyses of the Short-Period Contact Binaries HY Pav, AW Vir, and BP Vel. *PASP* **108**, 332.

- [Lapasset and Sistero (1984)] Lapasset, E. and Sistero, R.F. 1984 Differential Corrections Analysis of the UBV Photometry of UZ Octantis. *A&A* **130**, 97.
- [Lee (1989)] Lee, K.M. 1989 An Analysis of AM Leonis. Master's Thesis, Michigan State University.
- [Leung (1993)] Leung, K.C. 1993 A Method to decouple Light Curves, in *New Frontiers in Binary Star Research*. ASP Conference Series, V 38. Leung, K.C. and Nha, I.S. (eds), 154.
- [Leung and Schneider (1978)] Leung, K.C. and Schneider, D. 1978 Evolved Contact Systems of Spectral Type A: AU Puppis, V535 Arae, and V1073 Cygni. *ApJ* **222**, 917.
- [Leung, Zhai and Zhang (1985)] Leung, K.C., Zhai, D., and Zhang, Y. 1985 Two Very Similar Late-type Contact Systems: BX and BB Pegasi. *AJ* **90**, 515.
- [Linnell (1986)] Linnell, A.P. 1986 Light synthesis program for binary stars. II. Light curve and color curve effects in a contact system. *ApJ* **300**, 304.
- [Linnell (1991)] Linnell, A.P. 1991 A Light Synthesis Study of W Ursae Majoris. *ApJ* **374**, 307.
- [Lipari and Sistero (1984)] Lipari, S.L. and Sistero, R. 1984 V758 Centauri: UBV Photometry. *Ap&SpSc* **103**, 285.
- [Lipari and Sistero (1986)] Lipari, S.L. and Sistero, R. 1986 FT Lupi: UBV Photometry and synthetic solution. *MNRAS* **220**, 883.
- [Lipari and Sistero (1989)] Lipari, S.L. and Sistero, R. 1989 UBV Photometry of EZ Hya: The Beginning of Mass Transfer Detected? *AJ* **97**, 207.
- [Liu, *et al.* (1988)] Liu, Q., Yang, Y., Leung, K.C., Zhai, D., and Li, Y.F. 1988 Er Orionis: an Almost Contact W UMa System. *A&AS* **74**, 443.
- [Liu and Tan (1993)] Liu, X. and Tan, H. 1993 Photometry of Contact Binary System 471 Cas, in *New Frontiers in Binary Star Research*. ASP Conference Series, V 38. Leung, K.C. and Nha, I.S. (eds), 329.
- [Lu (1986)] Lu, W.X. 1986 The Spectroscopic Orbit of the W Ursae Majoris System V508 Ophiuchi. *PASP* **98**, 577.
- [Lu (1991)] Lu, W.X. 1991 Radial-velocity observations and absolute dimensions of eclipsing binaries: SS Ari. *AJ* **102**, 262.
- [Lu and Rucinski (1993)] Lu, W.X. and Rucinski, S. 1993 Spectral-line broadening functions of W UMa-type binaries. II. AH Vir. *AJ* **106**, 361

- [Lubow and Artymowicz (1992)] Lubow, S.H. and Artymowicz, P. 1992 Eccentricity Evolution of a Binary Embedded in a Disk, in *Binaries as Tracers of Stellar Formation*, 145.
- [Lucy (1968a)] Lucy, L.B. 1968 The Structure of Contact Binaries. *ApJ* **151**, 1123.
- [Lucy (1968b)] Lucy, L.B. 1968 The Light Curves of W Ursae Majoris Stars. *ApJ* **153**, 877.
- [Lucy and Wilson (1979)] Lucy, L.B. and Wilson R.E. 1979 Observational Tests of Theories of Contact Binaries. *ApJ* **231**, 502.
- [Maceroni (1994)] Maceroni, C. 1994 Star-spot Imaging: First Results for Contact Binaries *Mem.S.A.It.* **65**, 125.
- [Maceroni, Van Hamme and Van't Veer (1990)] Maceroni, C., Van Hamme, W., and Van't Veer, F. 1990 A spotted component in the very close late-type binary system VZ Piscium. *A&A* **234**, 177.
- [Maceroni and Van't Veer (1990)] Maceroni, C. and Van't Veer, F. 1990 Do Thermally Decoupled Late-Type Contact Binaries Really Exist?, in *Active Close Binaries*. Ibanoglu, C (ed), 309.
- [Maceroni and Van't Veer (1993)] Maceroni, C. and Van't Veer, F. 1993 The Uniqueness of Photometric Solutions for Spotted W UMa Binaries. *A&A* **277**, 515.
- [Maceroni and Van't Veer (1994)] Maceroni, C. and Van't Veer, F. 1994 Period variations of the late type contact binaries YY Eri and AE Phe: how to use light curves outside minimum. *A&A* **289**, 871.
- [Maceroni and Van't Veer (1996)] Maceroni, C. and Van't Veer, F. 1996 The Properties of W UMa Contact Binaries: New Results and Old Problems. *A&A* **311**, 523.
- [Maceroni, Milano and Russo (1983)] Maceroni, C., Milano, L., and Russo, G. 1983 Determination of Parameters of W UMa systems. IV - BV Dra, BW Dra, EM Lac, SW Lac. *A&AS* **51**, 435.
- [Mancuso, Milano and Russo (1978)] Mancuso, S., Milano, L., and Russo, G. 1978 A Detailed Photometric Study of the Eclipsing Binary AC Boo. *A&A* **63**, 193.
- [Markworth and Michaels (1982)] Markworth, N, and Michaels, E. 1982 The Eclipsing Binary UV Lyncis. *PASP* **94**, 350.
- [Martin and Davey (1995)] Martin, T. and Davey, S. 1995 Application of smoothed particle hydrodynamics to atmospheric motions in interacting binary systems. *MNRAS* **275**, 31.

- [Matraka (1987)] Matraka, B. 1987 Contact Binary Models with Dissipative Heating. *A&A* **171**, 95.
- [Mazeh and Goldberg (1992)] Mazeh, T. and Goldberg, D. 1992 A New Algorithm to Derive the Mass-Ratio Distribution of Spectroscopic Binaries, in *Binaries as Tracers of Stellar Formation* p 170.
- [Mazur, Kaluzny and Krzeminski (1993)] Mazur, B., Kaluzny, J., and Krzeminski, W. 1993 Photometric study of the intermediate-age open cluster Be 33. *MNRAS* **265**, 405.
- [McCartney (1997)] McCartney, S. 1997 A Statistical Study of the O'Connell Effect in W UMa Binaries, in *The Third Pacific Rim Conference on Recent Developments of Binary Star Research*. ASP Conference Series, V130. Leung, K.C (eds), 129.
- [McFarlane and Hilditch (1987)] McFarlane, T and Hilditch, R.W. 1987 Contact and near contact binary systems VII-EZ Hya, AD Phe, RS Col. *MNRAS* **227**, 381.
- [Merrill (1970)] Merrill, J.E. 1970 Rectification of Light Curves of W UMa-type Systems on the Russell Model, in *Vistas in Astronomy*, V12, p 43.
- [Milone (1968)] Milone, E.F. 1968 The O'Connell Effect in Some Eclipsing Variables, in *Non-Periodic Phenomena in Variable Stars* p 457.
- [Milone (1993)] Milone, E.F. 1993 Toward the Realization of Modeling Improvement Suggestions made at the Beijing Colloquium on Close Binary Stars, in *New Frontiers in Binary Star Research*. ASP Conference Series, V38. Leung, K.C. and Nha, I.S. (eds), 172.
- [Milone, et al. (1980)] Milone, E.F., Chia, T.T., Castle, K.G., Robb, R.M., and Merrill, J.E. 1980 RW Comae Berenices. I. Early photometry and UBV light curves.
- [Milone and Hrivnak (1984)] Milone, E.F. and Hrivnak, B.J. 1984 Observations of the O'Connell Effect System VY Crucis. *ApJSS* **56**, 295.
- [Milone, E.F., et al. (1995)] Milone, E.F., Stagg, C.R. Sugars, B.A. McVean, J.R., Schiller, S.J., Kallrath, J. and Bradstreet, D.H. Observations and Analysis of the Contact Binary H235 in the Open Cluster NGC 752. *AJ* **109**, 359.
- [Mochnacki (1981)] Mochnacki, S. 1981 Contact binary stars. *ApJ* **245**, 650.
- [Mochnacki (1985)] Mochnacki, S. 1985 Observational evidence for the evolution of contact binary stars, in *Interacting Binaries* p 51.
- [Mochnacki and Doughty (1972)] Mochnacki, S. and Doughty, N. 1972 Models for Five W UMa Systems. *MNRAS* **156**, 243.

- [Nelson and Davis (1972)] Nelson, B. and Davis, W. 1972 Eclipsing Binary Solutions by Sequential Optimization of the Parameters. *ApJ* **174**, 617.
- [Niarchos (1983)] Niarchos, P.G. 1983 Light Curves and Elements of AH Vir. *A&AS* **53**, 73.
- [Niarchos, Hoffman and Duerbeck (1992)] Niarchos, P.G., Hoffman, M., and Duerbeck, H.W. 1992 DF Hydrae: a W UMa system with spotted components. *A&A* **258**, 323.
- [Niarchos, Hoffman and Duerbeck (1994)] Niarchos, P.G., Hoffman, M., and Duerbeck, H.W. 1994 The Hot Contact Binary XZ Leonis. *A&A* **292**, 494.
- [Niarchos, Hoffman and Duerbeck (1996a)] Niarchos, P.G., Hoffman, M., and Duerbeck, H.W. 1994 RT Leonis Minoris: a spotted W Ursae Majoris system. *A&AS* **103**, 39.
- [Niarchos, Hoffman and Duerbeck (1996b)] Niarchos, P.G., Hoffman, M., and Duerbeck, H.W. 1996 TU Bootis: An Ambiguous W UMa System. *A&AS* **117**, 105.
- [Niarchos and Rovithis-Livaniou (1993)] Niarchos, P.G. and Rovithis-Livaniou, H. 1993 A Photometric Study of V566 Ophiuchi. *A&SpSc* **203**, 197.
- [O'Connell (1951)] O'Connell, D. 1951 *Riverview Publ.* **2**, 85.
- [Odell (1996)] Odell, A. 1996 W Corvi, a Contact Binary with a Large Temperature Difference. *MNRAS* **282**, 373.
- [Oh and Ahn (1993)] Oh, K.D. and Ahn, Y.S. 1993 EB-type Contact Binary DO Cas, in *New Frontiers in Binary Star Research*. ASP Conference Series, V38. Leung, K.C. and Nha, I.S. (eds), 337.
- [Piskunov and Rice (1993)] Piskunov, N.E. and Rice, J.B. 1993 Techniques for Surface Imaging of Stars. *PASP* **105**, 1415.
- [Proctor and Linnell (1972)] Proctor, D. and Linnell, A. 1972 Computer Solution of Eclipsing Binary Light Curves by the Method of Differential Corrections. *ApJS* **24**, 449.
- [Purgathofer (1964)] Purgathofer, A. 1964 Lichtelektrische Beobachtungen des Bedeckungsveränderlichen V 401 Cygni. *Z.f.Ap.* **59**, 29.
- [Rafert, Markworth and Michaels (1985)] Rafert, J.B., Markworth, N.L., and Michaels, E.J. 1985 Photoelectric Observations of CN Andromedae: An Unusual Overcontact Binary. *PASP* **97**, 310.
- [Rainger, Bell and Hilditch (1990)] Rainger, P.P., Bell, S.A., and Hilditch, R.W. 1990 The Binary System VW Bootis. *MNRAS* **246**, 47.

- [Rainger, Bell and Hilditch (1992)] Rainger, P.P., Bell, S.A. and Hilditch, R.W. 1992 The Spotted Contact Binary SS Arietis—Spectroscopy and Infrared Photometry, in *Evolutionary Processes in Interacting Binary Stars*. Kondo, Y. et al. (eds), 379.
- [Rainger, Hilditch and Bell (1990)] Rainger, P.P., Hilditch, R.W., and Bell, S.A. 1990 The Contact Binary System TY Bootis. *MNRAS* **246**, 42.
- [Rassio (1995)] Rassio, F. 1995 The Minimum Mass Ratio of W UMa Binaries. *ApJL* **444**, L41.
- [Rieuford (1992)] Rieuford, M. 1992 Ekman Circulation and the Synchronization of Binary Stars. *A&A* **259**, 581.
- [Rovithis, Niarchos and Rovithis-Livaniou (1988)] Rovithis, P., Niarchos, P.G., and Rovithis-Livaniou, H. 1988 Photoelectric Observations and Light Curve Analysis of V502 Ophiuchi. *A&AS* **74**, 265.
- [Rovithis and Rovithis-Livaniou (1984)] Rovithis, P. and Rovithis-Livaniou, H. 1984 Photoelectric Observations and Minima Times for RZ Comae Berenices. *A&AS* **58**, 679.
- [Rovithis and Rovithis-Livaniou (1989)] Rovithis, P. and Rovithis-Livaniou, H. 1989 The Peculiar Eclipsing Star BD+13°3496 (V508 Oph): New Observations and Light Curve Analysis. *Ap&SpSc* **151**, 115.
- [Rovithis and Rovithis-Livaniou (1990)] Rovithis, P. and Rovithis-Livaniou, H. 1990 New BV light curves of the eclipsing binary 44 ι Bootis. *A&AS* **86**, 523.
- [Rovithis-Livaniou and Rovithis (1981)] Rovithis-Livaniou, H. and Rovithis, P. 1981 The Eclipsing Binary AB Andromedae. *Ap&SpSc* **76**, 465.
- [Rovithis-Livaniou, Rovithis and Bitzaraki (1992)] Rovithis-Livaniou, H., Rovithis, P., and Bitzaraki, O. 1992 Evolutionary state of W UMa-type systems. *Ap&SpSc* **189**, 237.
- [Rucinski (1983)] Rucinski, S. 1983 Violet and ultraviolet continua of W UMa systems on the basis of uvby photometry observations. *A&A* **127**, 84.
- [Rucinski (1985)] Rucinski, S. 1985 Activity of contact binary systems, in *Interacting Binaries*. Eggleton, P.P. and Pringle, J.E. (eds), 13.
- [Rucinski (1992)] Rucinski, S. 1992 Can full convection explain the observed short period limit of W UMa type binaries? *AJ* **103**, 960.
- [Rucinski (1993)] Rucinski, S.M. 1993 A Simple Description of Light Curves of W UMa Systems. *PASP* **105**, 1433.

- [Rucinski (1994)] Rucinski, S. 1994 $M_V = M_V(\log P, \log T_e)$ Calibrations for W UMa Systems. *PASP* **106**, 462.
- [Rucinski (1995a)] Rucinski, S. 1995 Absolute-Magnitude Calibration for W UMa-type Systems. II. Influence of Metallicity. *PASP* **107**, 648.
- [Rucinski (1995b)] Rucinski, S. 1995 W UMa-type Systems discovered in the Central Baade's Window in the OGLE Experiment. *ApJL* **446**, L19.
- [Rucinski (1995c)] Rucinski, S. 1995 Radio Survey of W UMa type Systems. *AJ* **109**, 2690.
- [Rucinski and Kaluzny (1982)] Rucinski, S.M. and Kaluzny, J. 1982 BV Dra and BW Dra: Two Contact Systems in one Visual Binary. *Ap&SpSc* **88**, 433.
- [Rucinski, Lu and Shi (1993)] Rucinski, S., Lu, W.X., and Shi, J. 1993 Spectral Line Broadening Functions of W UMa-type Binaries. III. W UMa. *AJ* **106**, 1174.
- [Russell (1912a)] Russell, H. 1912 On the Determination of the Orbital Elements of Eclipsing Variable Stars. I. *ApJ* **35**, 315.
- [Russell (1912b)] Russell, H. 1912 On the Determination of the Orbital Elements of Eclipsing Variable Stars. II. *ApJ* **36**, 54.
- [Russell (1948)] Russell, H. 1948 Idealized Models and Rectified Light-Curves for Eclipsing Variables. *ApJ* **108**, 388.
- [Russo, *et al.* (1982)] Russo, G., Sallazzo, C., Maceroni, C., and Milano, L. 1982 Determination of Parameters of W UMa Systems. II: TW Cet, S Ant, U Peg, ER Ori. *A&AS* **47**, 211.
- [Samec (1989)] Samec, R.G. 1989 B and V light curves of the very short period binary VZ Piscium. *PASP* **101**, 661.
- [Samec (1990)] Samec, R.G. 1990 Photometric investigation of a very short period binary: is BX Pegasi undergoing continuous angular momentum losses? *AJ* **100**, 808.
- [Samec and Bookmeyer (1987a)] Samec, R.G. and Bookmeyer, B. 1987 B and V Light curves of TY Bootis. *PASP* **99**, 842.
- [Samec and Bookmeyer (1987b)] Samec, R.G. and Bookmeyer, B.B. 1987 BVRI light curves of the very short period binary AD Cancri. *PASP* **99**, 1298.
- [Samec, Carrigan and French (1996)] Samec, R.G., Carrigan, B., and French, J. 1996 CCD BVRI Photometry of the Short Period Solar Type Contact Binary V440 Cassiopeiae. *Observatory* **116**, 365.

- [Samec, Charlesworth and Dewitt (1991)] Samec, R.G., Charlesworth, S.D., and Dewitt, J.R. 1991 A Photometric Study of the Very Short Period Eclipsing Binary EH Hydrae. *AJ* **102**, 688.
- [Samec, *et al.* (1989)] Samec, R.G., Fuller, R.E., Bookmeyer, B.B., and Faulkner, D.R. 1989 RR Leporis: an Algol like system. *PASP* **101**, 180.
- [Samec, Gray and Carrigan (1995)] Samec, R.G., Gray, J.D., and Carrigan, B.J. 1995 Analysis of CCD photometry for the very short period eclipsing binary BM Ursae Majoris. *PASP* **107**, 136.
- [Samec, Gray and Carrigan (1996)] Samec, R.G., Gray, J., and Carrigan, B. 1996 A Photometric Study of the W-type W UMa Binary EK Comae Berenices. *Observatory* **116**, 75
- [Samec, *et al.* (1992)] Samec, R.G., Herr, S.A., Zetzl, J.T., and Kreidl, T.J. 1992 CCD photometry and preliminary analysis of V865 Cygni. *PASP* **104**, 29.
- [Samec and Hube (1991)] Samec, R.G. and Hube, D. 1991 BX Pegasi. II. Spectroscopic Observations and Simultaneous Synthetic Photometric-Spectroscopic Solution. *AJ* **102**, 1171.
- [Samec, Pauley and Carrigan (1997)] Samec, R.G., Pauley, B.R., and Carrigan, B.J. 1997 U,B,V Light Curves of the Short-Period Solar-Type Eclipsing Binary, V417 Aquilae. *AJ* **113**, 401.
- [Samec and Su (1993)] Samec, R.G. and Su, W. 1993 V803 Aquilae: A Newborn W UMa Siamese Twin? *PASP* **105**, 1441.
- [Samec, *et al.* (1993)] Samec, R.G., Su, W., Terrell, D., and Hube, D.P. 1993 Photometric Investigation of a Very Short Period W UMa-type Binary: Does CE Leonis have a Large Superluminous Area? *AJ* **106**, 318.
- [Samec and Terrell (1995)] Samec, R.G. and Terrell, D. 1995 YZ Phoenicis: photometric study of a W UMa binary near the short period limit. *PASP* **107**, 424.
- [Schaub (1990)] Schaub, D. 1990 Photoelectric Photometry of TZ Bootis. *IBVS* **3524**.
- [Schieven, *et al.* (1983)] Schieven, G, Morton, J.C., McLean, B.J., and Hughes, V.A. 1983 Photometric Observations of AC Boo. *A&AS* **52**, 463.
- [Schmidt and Herczeg (1959)] Schmidt, H. and Herczeg, T. 1959 Untersuchungen an W UMa-Sternen. IV: AK Herculis. *Zs.f.Ap.* **47**, 106.
- [Sezer (1985)] Sezer, C. 1985 Photometry and Analysis of the Star HD 199497. *Ap&SpSc* **115**, 309.

- [Sezer (1993)] Sezer, C. 1993 A Photometric Study of the Eclipsing Binary V1073 Cygni. *Ap&SpSc* **208**, 15.
- [Shaolan (1993)] Shaolan, B. 1993 The Angular Momentum Loss of Low-Mass Close Binary Systems. *A&SpSc* **206**, 179.
- [Shu and Lubow (1981)] Shu, F. and Lubow, S.H. 1981 Mass, Angular Momentum and Energy Transfer in Close Binary Stars. *Ann Rev A&A* **19**, 277.
- [Sinjab, Robertson and Smith (1990)] Sinjab, I., Robertson, J., and Smith, R. 1990 The dissipation factor in contact binaries revisited. *MNRAS* **244**, 619.
- [Smith and Smith (1981)] Smith, R.C. and Smith, D.H. 1981 Tidally Driven Circulation in Close and Contact Binary Systems. *MNRAS* **194**, 583.
- [Spinrad (1959)] Spinrad, H. 1959 Photoelectric Observations of the Eclipsing System V401 Cygni. *PASP* **71**, 53.
- [Tassoul (1992)] Tassoul, J. 1992 On the interior structure of contact binaries and the light curve paradox. *ApJ* **389**, 375.
- [Terrell, Gunn and Kaiser (1994)] Terrell, D., Gunn, J.B., and Kaiser, D.H. 1994 New Light Curves and Analysis of the Short Period Algol XZ CMi. *PASP* **106**, 149.
- [Terrell, Williams and Kaiser (1995)] Terrell, D., Williams, D.B., and Kaiser, D.H. 1995 V1061 Tauri: analysis of a newly discovered eclipsing binary. *PASP* **107**, 653.
- [Trimble (1985)] Trimble, V. 1985 Interacting Binaries, Summing Up, in *Interacting Binaries* Eggleton P.P. and Pringle, (eds) 393.
- [Twigg (1979)] Twigg, L.W. 1979 Analysis of W Ursae Majoris Systems. I - The A-type Systems. *MNRAS* **189**, 907.
- [Van Hamme (1982a)] Van Hamme, W. 1982 On the evolutionary state of the W Ursae Majoris contact binaries. *A&A* **105**, 389.
- [Van Hamme (1982b)] Van Hamme, W. 1982 Estimated absolute dimensions and the inferred lifetime and angular momentum of W Ursae Majoris contact binaries. *A&A* **116**, 27.
- [Van Hamme (1993)] Van Hamme, W. 1993 New Limb-Darkening Coefficients for Modeling Binary Star Light Curves. *AJ* **106**, 2096.
- [Vandenbergh (1985)] Vandenbergh, S. 1985 The Luminosity Function of Globular Clusters. *ApJ* **297**, 361.
- [Van't Veer (1993)] Van't Veer, F. 1993 How to Study the Approach of Late-type Very Close Binary Components? in *New Frontiers in Binary Star Research*. ASP Conference Series, V38. Leung, K.C. and Nha, I.S. (eds), 229.

- [Van't Veer and Maceroni (1990)] Van 'T Veer, F. and Maceroni, C. 1990 The Evolution of the Period and Synchronization for Close G-Type MS Binaries, in *Active Close Binaries* p 321.
- [Vilhu (1992)] Vilhu, O. 1992 W UMa Binaries, in *Evolutionary Processes in Interacting Binary Stars*, Kondo, Y. et al. (eds), p 61.
- [Vinko, Hegedus and Hendry (1996)] Vinko, J., Hegedus, T., and Hendry, P. 1996 UZ Leo and CV Cyg, two evolved contact binaries. *MNRAS* **280**, 489.
- [Walker (1993)] Walker, R.L. 1993 Third Light in the Solution of an Eclipsing Binary Light Curve: V505 Sagittarii. *AJ* **106**, 2051.
- [Walker (1996)] Walker, R.L. 1996 GZ Andromeda, The More the Merrier. *AAS Meeting* **188**, 6011.
- [Walker and Chambliss (1985)] Walker, R.L. and Chambliss, C.R. 1985 A W UMa variable in the visual binary system ADS 9019: a UBV photoelectric investigation. *AJ* **90**, 346.
- [Walter, Niarchos and Duerbeck (1989)] Walter, K., Niarchos, P., and Duerbeck, H. 1989 Photometric Data and Analysis of the Light Curve of the W UMa Variable ST Ind. *Ap&SpSc* **161**, 1.
- [Webbink (1977)] Webbink, R.F. 1977 The Evolution of Low-Mass Close Binary Systems. V. Transport Processes in the Envelopes of Contact Components. *ApJ* **215**, 851.
- [Williamon, Collins and Chen (1978)] Williamon, R.M., Collins, T.F., and Chen, K.Y. 1978 The eclipsing variable AQ Tucanae. *A&AS* **34**, 207.
- [Wilson (1979)] Wilson, R.E. 1979 Eccentric Orbit Generalization and Simultaneous Solution of Binary Star Light and Velocity Curves. *ApJ* **234**, 1054.
- [Wilson (1990)] Wilson, R.E. 1990 Accuracy and Efficiency in the Binary Star Reflection Effect. *ApJ* **356**, 613.
- [Wilson (1993)] Wilson, R.E. 1993 Computation Methods and Organization for Close Binary Observables, in *New Frontiers in Binary Star Research*. ASP Conference Series, V38. Leung, K.C. and Nha, I.S. (eds), 91.
- [Wilson (1994)] Wilson, R.E. 1994 Binary-Star Light-Curve Models. *PASP* **106**, 921.
- [Wilson and Biermann (1976)] Wilson, R.E. and Biermann, P. 1976 TX Cancri-Which Component is Hotter? *A&A* **48**, 349.
- [Wilson and Woodward (1995)] Wilson, R.E. and Woodward, E.J. 1995 UBV Light Curves of V356 Sagittarii. *PASP* **107**, 132.

- [Wood (1971)] Wood, D. 1971 An Analytic Model of Eclipsing Binary Systems. *AJ* **76**, 701.
- [Yan and Mateo (1994)] Yan, L. and Mateo, M. 1994 Primordial Main Sequence Binary Stars in the Globular Cluster M71. *AJ* **108**, 1810.
- [Zahn (1992)] Zahn, J-P. 1992 Present State of the Tidal Theory, in *Binaries as Tracers of Stellar Formation* p 253.
- [Zhang, et.al. (1993)] Zhang, R.X., Zhang, J.T., Lee, Q.S., and Zhai, D.S. 1993 The Photoelectric Investigations of AP Aurigae, in *New Frontiers in Binary Star Research*. ASP Conference Series, V38. Leung, K.C. and Nha, I.S. (eds), 322.
- [Zhou and Leung (1990)] Zhou, D.Z. and Leung, K.C. 1990 An Explanation of Light-Curve Asymmetries in Contact Binaries by means of the Coriolis Effect. *ApJ* **355**, 271.
- [Zhou and Leung (1993)] Zhou, D.Q. and Leung, K.C. 1993 A Numerical Model for Two-dimensional Circulation in Contact Binary Systems, in *New Frontiers in Binary Star Research*. ASP Conference Series, V38. Leung, K.C. and Nha, I.S. (eds), 206.
- [Zhou and Leung (1997a)] Zhou, D.Q. and Leung, K.C. 1997 Temperature Inhomogeneity on the Surfaces of Close Binary Systems Due to Irradiation, in *The Third Pacific Rim Conference on Recent Developments of Binary Star Research*. ASP Conference Series, V130. Leung, K.C (eds), 69.
- [Zhou and Leung (1997b)] Zhou, D.Q. and Leung, K.C. 1997 A 2-D Numerical Simulation of the Circulation in the Envelope of a Contact Binary System, an Update, in *The Third Pacific Rim Conference on Recent Developments of Binary Star Research*. ASP Conference Series, V130. Leung, K.C (eds), 95.
- [Zhou (1988)] Zhou, H.N. 1988 The Photometric Solution of CC Com by use of the Wilson and Devinney Code. *Ap&SpSc* **141**, 199.

Appendix A

W Ursae Majoris Data Table

A.1 The Database

This is the collation of the observational data for W UMa's, as well as the model values (primarily from WD method) for the systems. The notes section describes which modeling method was used to determine the physical parameters. A column by column description of the table parameters follows the table.

W Ursae Majoris Data Table, Part I

	MV	Period (days)	B-V	Mass Ratio		$(\frac{L_1}{L_1+L_2})_V$	Incl.(°)	$T_1(^{\circ}K)$	$T_2(^{\circ}K)$	Ω_{cont}	$f(\%)$	WD Mean				Type
				q_{sp}	q_{ph}							r_1	r_2	ρ_1	ρ_2	
AB And	27	0.332	0.90	0.491	0.491		86.8	5450	5821	2.814	15	0.451	0.327	1.25	1.61	W
CN And	65	0.463	0.56		0.450		70.3	6200	4680	2.662	43	0.478	0.340	0.56	0.70	A
GZ And	-	0.305	0.75													
S Ant	74	0.648			0.871		68.8	7800	7340	3.503	7	0.396	0.371	0.39	0.41	A
OO Aql	68	0.507	0.61	0.843	0.835		90.0	5700	5635	3.350	27	0.416	0.386	0.56	0.58	A
V417 Aql	-	0.370	0.62		0.368	0.676	84.5	6030	6256	2.570	19	0.480	0.307	0.91	1.28	W
V803 Aql	5	0.263	1.07		1.000	0.503	82.9	4594	4600	3.702	8	0.385	0.385	2.39	2.39	W
V535 Ara	73	0.629	0.24	0.300	0.361		82.1	8750	8572	2.591	3	0.473	0.287	0.33	0.54	A
SS Ari	44	0.406	0.62	0.295	0.302		75.3	5745	5950	2.446	13	0.496	0.279			W
44i Boo	7	0.268	0.85	0.498	0.501		70.9	5553	5800	2.905	-9	0.417	0.315	2.41	2.80	W
AC Boo	-	0.352	0.50		0.295		83.3	5520	5530	2.422	18					W
CK Boo	-	0.355														
TU Boo	-	0.324			0.498	0.648	88.1	5800	5805	2.777	32	0.463	0.343	1.18	1.45	A
TY Boo	19	0.317	0.76	0.466	0.467		77.5	5469	5834	2.783	10	0.454	0.322	1.37	1.79	W
TZ Boo	-	0.297			0.220											A/W
VW Boo	-	0.342		0.428	0.428	0.764	75.6	5700	5190			0.470	0.322			A
XY Boo	53	0.371	0.49	0.160	0.182		69.0	7200	7102	2.182	5	0.559	0.254	0.66	1.29	A
AO Cam	25	0.330			0.769		75.0	5520	5826	3.359	1	0.400	0.358	1.53	1.64	W
CW Cas	20	0.319			0.543		73.4	5086	5440	2.922	11	0.439	0.332	1.42	1.78	W
V440 Cas	-	0.326	0.83		0.375	0.635	76.7	5006	5347	2.598	12	0.471	0.304	1.20	1.70	W
V523 Cas	2	0.237	0.87	0.420	0.571		83.7	4207	4407	2.966	13	0.437	0.340	2.56	3.11	W
RR Cen	72	0.606	0.36	0.210	0.180		78.7	7250	7188	2.142	35	0.555	0.247	0.25	0.52	A
V677 Cen	24	0.325			0.142		87.1	5745	5841	2.050	34	0.563	0.240	0.88	1.61	W
V752 Cen	39	0.370		0.311	0.300		83.2	6210	6234	2.455	6	0.494	0.275	0.88	1.53	W
V757 Cen	31	0.343	0.65	0.684	0.671		69.3	5927	6000	3.138	14	0.421	0.348	0.88	1.53	W
V758 Cen	-	0.581	0.10		0.270			11800	8180	2.327	42			1.29	1.53	A
EP Cep	-	0.290	0.90		0.233		74.9	5100	4774	2.312	0	0.504	0.261	1.42	2.38	A
EQ Cep	-	0.307	0.90	0.450	0.463	0.618	85.0	5150	5376	2.774	11	0.456	0.323	1.44	1.88	W
ER Cep	13	0.286	0.82	0.560	0.549	0.537	78.1	5061	5330	2.888	1	0.429	0.319	1.89	2.52	W
ES Cep	-	0.342	0.88		0.782	0.621	71.0	5500	5203	3.387	0	0.401	0.358	1.40	1.54	A
GW Cep	21	0.319			0.370		83.9	5800	6113	2.591	11	0.474	0.302	1.27	1.82	W
VW Cep	-	0.278	0.86	0.410	0.370		66.0	5040	5200	2.594	10	0.483	0.190	1.58	9.61	W
TW Cet	18	0.312	0.69	0.530	0.581		83.2	5460	5600	3.018	3	0.426	0.227	1.59	6.09	W

W Ursae Majoris Data Table, Part I (continued)

	MV	Period (days)	B-V	Mass Ratio		$(\frac{L_1}{L_1+L_2})_V$	Incl.(°)	$T_1(^{\circ}K)$	$T_2(^{\circ}K)$	Ω_{cont}	f(%)	WD Mean		ρ_1	ρ_2	Type
				q_{sp}	q_{ph}							r_1	r_2			
VY Cet	30	0.341	0.69		0.665	0.540	78.4	5393	5610	3.181	0	0.411	0.339	1.40	1.66	W
AD Cnc	10	0.283			0.625		64.9	4825	5164	3.058	14	0.430	0.348	1.82	2.15	W
AH Cnc	34	0.360	0.53	0.537	0.610		62.9	6416	6500	2.936	41	0.453	0.369	0.97	1.10	W
TX Cnc	42	0.383	0.61	0.530	0.596		62.4	6338	6400	3.028	8	0.428	0.333	1.03	1.30	W
RS Col	75	0.672			0.500		68.7	5950	5789	2.804	24	0.457	0.336	0.29	0.37	A
CC Com	1	0.221	1.24	0.470	0.518		87.9	4302	4500	2.849	20	0.449	0.328	2.81	3.73	W
EK Com	-	0.267	0.83		0.304	0.683	88.5	5000	5310	2.447	15	0.494	0.289	1.68	2.52	W
RW Com	-	0.237	0.84													
RZ Com	29	0.339	0.57	0.430	0.436		86.0	5500	5564	2.732	7	0.457	0.306	1.20	1.74	W
ϵ CrA	70	0.591	0.39		0.112		72.3	7100	6639	1.974	30	0.595	0.213	0.23	0.56	A
FS CrA	6	0.264	1.13		0.758		86.5	4567	4700	3.280	15	0.415	0.366	2.15	2.38	W
VY Cru	-															
W Crv	57	0.388	0.71		0.817		86.0	5600	4937	3.285	35	0.421	0.382	0.92	1.01	A
DK Cyg	66	0.471	0.37		0.271		80.3	7351	7200	2.308	55	0.529	0.292	0.45	0.73	A
V401 Cyg	-	0.583	0.36		0.275	0.742	80.0	7300	7160	2.333	45	0.521	0.299	0.31	0.45	A
V508 Cyg	-	0.780			0.839	0.530	76.3	5565	5600	3.225	55	0.448	0.418	0.19	0.19	W
V865 Cyg	-	0.365	0.69		0.446	0.668	84.2	5650	5537	2.724	18	0.462	0.321	0.98	1.28	A
V1073 Cyg	-	0.786	0.42		0.320	0.752	69.4	6856	6740		-8	0.457	0.271			A
LS Del	37	0.364			0.562		48.5	5704	5780	2.973	6	0.429	0.328	1.15	1.45	W
BV Dra	33	0.350	0.54	0.402	0.411		76.3	6245	6345	2.673	11	0.472	0.318	1.04	1.40	W
BW Dra	14	0.292	0.63	0.280	0.280		74.4	5980	6164	2.404	10	0.499	0.281	1.39	2.18	W
YY Eri	23	0.322	0.66	0.400	0.439		82.2	5389	5585	2.730	10	0.458	0.315	1.32	1.78	W
H235	-	0.412	0.45		0.202	0.814	58.6	6500	6421	2.207	21	0.532	0.262	0.61	1.04	A
AK Her	61	0.422	0.53		0.233		80.8	6400	6033	2.298	10	0.519	0.257	0.61	1.18	A
SY Hor	17	0.312	0.83		0.667	0.502	82.4	4934	5240	3.165	5	0.417	0.367	1.60	1.57	W
DF Hya	26	0.331	0.60		0.400	0.660	82.5	5676	5980	2.622	23	0.474	0.316	1.16	1.56	W
EH Hya	-	0.297	0.79		0.314	0.692	81.9	5300	5536	2.474	12	0.492	0.282	1.38	2.08	W
EZ Hya	-	0.450	0.65	0.25												W
FG Hya	50	0.328	0.61		0.142		85.2	5900	5816	2.010	78	0.592	0.247	0.74	1.48	A
ST Ind	-	0.402	0.50		0.240	0.805	76.6					0.573	0.254			A
EM Lac	43	0.389	0.68		0.629		74.4	5450	5500	3.014	28	0.441	0.360	0.89	1.03	W
SW Lac	22	0.321	0.75	0.797	0.812		80.6	5468	5630	3.282	34	0.426	0.389	1.31	1.39	W
AM Leo	38	0.366	0.53	0.450	0.426		87.0	6200	6380	2.692	15	0.464	0.362	0.99	0.89	W

W Ursae Majoris Data Table, Part I (continued)

	MV	Period (days)	B-V	Mass Ratio		$(\frac{L_1}{L_1+L_2})_V$	Incl.(°)	$T_1(^{\circ}K)$	$T_2(^{\circ}K)$	Ω_{cont}	f(%)	WD Mean		ρ_1	ρ_2	Type
				q_{sp}	q_{ph}							r_1	r_2			
CE Leo	16	0.303	0.98		0.505		84.6	4850	5111	2.876	3	0.441	0.321	1.59	2.08	W
XY Leo	11	0.284	0.98	0.500	0.500		65.8	4575	4850	2.858	6	0.444	0.323	1.78	2.31	W
XZ Leo	67	0.488			0.726	0.658	73.3	7850	7147	3.281	2	0.407	0.351	0.64	0.72	A
RT LMi	41	0.375			0.385	0.672	84.0	5855	6000	2.586	26	0.479	0.314	0.88	1.20	W
FT Lup	-	0.470	0.42	0.430	0.465	0.962	90.0	6700	3916	2.807	-	0.447	0.300	0.65	1.00	A
UV Lyn	59	0.415			0.526	0.542	67.7	6709	6290	2.882	14	0.444	0.326	0.82	1.09	A
TY Men	64	0.462			0.215		79.5	8164	7183	2.256	10	0.561	0.256	0.41	0.93	A
TV Mus	63	0.446	0.83	0.119	0.150		78.9	5980	6088	2.019	87	0.587	0.265	0.41	0.67	A
UZ Oct	78	1.149	0.54		0.278	0.760	78.6	6605	6577	2.372	26	0.506	0.287	0.09	0.13	A
V502 Oph	47	0.453	0.66	0.370	0.377		71.3	5968	6200	2.575	24	0.479	0.300	0.61	0.93	W
V508 Oph	51	0.345	0.73	0.520	0.530	0.704	86.1	6000	5830	2.902	10	0.441	0.341	1.21	1.38	A
V566 Oph	58	0.410	0.44	0.240	0.239		79.8	6700	6618	2.265	41	0.534	0.271	0.60	1.09	A
V839 Oph	-	0.409			0.588	0.613	79.8	5620	5796			0.411	0.314			W
ER Ori	46	0.423	0.54	0.613	0.610		80.5	5770	5800	3.082	0	0.419	0.334	0.89	1.07	W
FZ Ori	-															
BF Pav	-	0.302	0.85		0.714	0.555	84.8	5330	5430	3.227	10	0.414	0.355	1.70	1.93	W
HY Pav	-	0.352	0.84		0.470	0.599	80.5	4739	5000	2.795	8	0.448	0.320	1.15	1.49	W
MW Pav	76	0.795			0.182		85.1	7620	7570	2.129	50	0.551	0.267	0.15	0.24	A
BB Peg	35	0.362			0.402		79.9	5883	6200	2.591	37	0.482	0.312	0.92	1.36	W
BX Peg	9	0.280			0.371	0.663	87.8	5700	6070	2.586	16	0.477	0.305	1.58	2.19	W
U Peg	40	0.375	0.62	0.315	0.331		76.0	5515	5800	2.515	9	0.488	0.297	0.87	1.27	W
AD Phe	54	0.380	0.59		0.940		73.6	5850	5815	3.574	15	0.396	0.386	1.08	1.10	A
AE Phe	36	0.362	0.64	0.461	0.400		88.0	6000	6145	2.637	17	0.471	0.312	0.98	1.35	W
YZ Phe	-															
RW PsA	52	0.360	0.75		0.813		77.4	5600	5325	3.407	7	0.398	0.360	1.27	1.40	A
VZ Psc	49	0.261	1.20	0.920	0.920		49.6	4500	4352	3.583	7	0.391	0.376	2.41	2.50	A
TY Pup	77	0.819			0.326		67.8	7800	7658	2.396	63	0.517	0.313	0.15	0.23	A
FG Sct	8	0.271	1.07		0.786		89.9	4662	4800	3.357	8	0.406	0.359	2.15	2.44	W
AU Ser	56	0.387	0.87	0.710	0.800		80.2	5100	4780	3.385	7	0.405	0.366	1.05	1.14	A
Y Sex	-	0.420														
RZ Tau	60	0.416	0.59	0.540	0.372		82.9	7200	7146	2.495	55	0.500	0.331	0.64	0.82	A
AQ Tuc	71	0.595	0.41	0.354	0.270		80.2	6900	7113	2.324	44	0.518	0.296	0.30	0.44	A
AA UMa	48	0.468	0.60	0.564	0.551		80.3	5932	6030	2.924	15	0.441	0.347	0.65	0.73	W

W Ursae Majoris Data Table, Part I (*continued*)

	MV	Period (days)	B-V	Mass Ratio		$(\frac{L_1}{L_1+L_2})_V$	Incl.(°)	$T_1(^{\circ}K)$	$T_2(^{\circ}K)$	Ω_{cont}	f(%)	WD Mean		ρ_1	ρ_2	Type
				q_{sp}	q_{ph}							r_1	r_2			
AW UMa	62	0.439	0.36	0.070	0.072		79.1	7175	6875	1.832	78	0.559	0.185	0.52	1.04	A
BM UMa	-	0.271			0.540	0.529	89.0	4600	4982	2.897	17	0.444	0.331	1.85	2.28	W
TY UMa	32	0.355	0.68		0.400		83.3	5849	5550	2.648	12	0.468	0.307	1.04	1.48	W
W UMa	28	0.334	0.66	0.488	0.470		82.9	5800	6194	2.727	32	0.467	0.337	1.13	1.41	W
BP Vel	-	0.265	0.91		0.533	0.561	82.1	4717	5000	2.894	14	0.444	0.334	2.00	2.51	W
BU Vel	69	0.516	0.29		0.251		84.9	7500	7448	2.259	61	0.510	0.289	0.43	0.59	A
AG Vir	-	0.643	0.30		0.325	0.687	83.3	7240	6645	2.403	1	0.448	0.268	0.38	0.58	A
AH Vir	45	0.408	0.78	0.420	0.342		86.5	5400	5783	2.507	24	0.489	0.304	0.72	1.03	W
AW Vir	-	0.353	0.69		0.675	0.584	83.0	6000	5980	3.207	11	0.417	0.354	1.25	1.38	A
BI Vul	4	0.252	1.00		0.692		78.8	4549	4600	3.114	29	0.434	0.370	2.15	2.40	W

W Ursae Majoris Data Table, Part II

	LCA	$\frac{\Delta T}{T_1}$ $\times 10^5$	$\frac{\Delta T}{T_2}$ $\times 10^5$	m_1 (M_\odot)	m_2 (M_\odot)	R_1 (R_\odot)	R_2 (R_\odot)	L_1 (L_\odot)	L_2 (L_\odot)	OER_U	OER_B	OER_V	Δm_U	Δm_B	Δm_V	Ref
AB And		-6807	-6373	1.04	0.51	1.05	0.76	0.87	0.60		0.886			-0.055		1
CN And	0.02310	24516	32479	1.25	0.56	1.47	1.04	2.85	0.47		1.067	1.063		0.026	0.036	2
GZ And																3
S Ant		5897	6267	1.94	0.76	2.07	1.36	14.15	4.86							4
OO Aql	0.05243	1140	1154	1.19	1.00	1.44	1.34	1.97	1.62		1.077	1.121		0.013	0.022	5
V417 Aql	0.01069	-3748	-3613	1.13	0.42	1.22	0.61	1.72	0.48	0.994	1.000	0.999	0.003	0.004	0.010	6
V803 Aql	0.04355	-131	-130	0.79	0.79	0.77	0.77	0.24	0.24		1.018	1.006		0.033	0.004	7
V535 Ara		2034	2077	2.18	0.79	2.10	1.27	23.17	7.86	0.960			-0.019			4
SS Ari	0.03160	-3568	-3445	1.16	0.35	1.31	0.74	1.68	0.61		0.957	0.948		-0.006	-0.007	8
44i Boo		-4448	-4291	0.98	0.49	0.83	0.63	0.59	0.40		1.018			0.008		4
AC Boo	0.02427	-181	-189								0.977					9
CK Boo																10
TU Boo	0.03804	-86	-86	0.97	0.48	1.05	0.78	1.12	0.62		1.060			0.020		11
TY Boo	0.02138	-6674	-6256	1.03	0.48	1.02	0.72	0.83	0.54		0.983					12
TZ Boo										0.937	0.959	0.963	-0.04	-0.02	-0.02	13
VW Boo		8947	9827	0.98	0.42	1.08	0.74	1.12	0.35		0.996			-0.002		60
XY Boo		1361	1380	1.49	0.27	1.47	0.67	5.17	1.01		0.968	0.970		-0.008	-0.012	4
AO Cam		-5543	-5252	1.03	0.79	0.98	0.88	0.80	0.80							14
CW Cas		-6960	-6507	0.99	0.54	0.99	0.75	0.59	0.44		0.991			-0.004		15
V440 Cas	0.01803	-6812	-6377	0.95	0.36	1.05	0.68	0.53	0.33		0.950			-0.025	-0.019	16
V523 Cas		-4754	-4538	0.79	0.45	0.75	0.58	0.16	0.12		1.020					4
RR Cen		855	863	1.80	0.32	2.15	0.96	11.44	2.19		1.003			0.002		4
V677 Cen		-1671	-1644	1.06	0.15	1.19	0.51	1.39	0.27	0.967	0.983	0.985	-0.011	-0.008	-0.007	17
V752 Cen		-386	-385	1.20	0.36	1.24	0.69	2.06	0.65							4
V757 Cen	0.01562	-1232	-1217	1.07	0.72	1.05	0.87	1.23	0.88	0.946	0.966	0.958				4
V758 Cen	0.02632										1.102	1.072	1.063			18
EP Cep	0.01947	6392	6829	1.12	0.27	1.18	0.35	1.31	0.38		1.038					19
EQ Cep	0.04488	-4388	-4204	1.04	0.48	1.09	0.61	1.22	0.60		1.052					19
ER Cep		-5315	-5047	0.95	0.52	1.05	0.67	1.12	0.56							19
ES Cep		5400	5708	1.01	0.79	1.01	0.92	1.04	0.82							19
GW Cep	0.04706	-5397	-5120	1.06	0.39	1.05	0.67	1.12	0.56		0.922					20
VW Cep	0.02751	-3174	-3078	0.81	0.33	1.05	0.41	0.84	0.37	0.973	0.989					21
TW Cet		-2564	-2500	1.01	0.58	0.96	0.74	0.74	0.48							22

W Ursae Majoris Data Table, Part II (continued)

	LCA	$\frac{\Delta T}{T_1}$ $\times 10^5$	$\frac{\Delta T}{T_2}$ $\times 10^6$	m_1 (M_\odot)	m_2 (M_\odot)	R_1 (R_\odot)	R_2 (R_\odot)	L_1 (L_\odot)	L_2 (L_\odot)	OER_U	OER_B	OER_V	Δm_U	Δm_B	Δm_V	Ref
VY Cet	0.02233	-4024	-3868	1.02	0.68	1.01	0.83	0.77	0.61	1.035	1.035	1.035				23
AD Cnc		-7026	-6565	0.93	0.58	0.89	0.72	0.39	0.33		1.025	1.029		0.012	0.014	24
AH Cnc		-1309	-1292	1.34	0.82	1.25	1.02	2.36	1.65							4
TX Cnc		-978	-969	1.37	0.82	1.23	0.96	2.20	1.38							25
RS Col		2756	2781	1.46	0.73	1.92	1.41	4.13	2.00		1.027	1.021		0.013	0.010	26
CC Com	0.03675	-4603	-4400	0.79	0.41	0.73	0.54	0.17	0.11		0.961					4
EK Com	0.05802	-6200	-5838	0.95	0.29	0.94	0.55	0.43	0.28		0.872			-0.086		27
RW Com																28
RZ Com		-1164	-1150	1.03	0.45	1.06	0.71	0.93	0.43		1.006			0.003		4
ϵ CrA		6493	6944	1.76	0.20	2.20	0.79	11.07	1.08							61
FS CrA		-2912	-2830	0.86	0.65	0.82	0.73	0.26	0.23							59
VY Cru	0.09140										1.536	1.374				29
W Crv		11839	13429	1.04	0.85	1.16	1.06	1.19	0.59							30
DK Cyg		2054	2097	1.68	0.45	1.73	0.96	7.86	2.20							61
V401 Cyg	0.08520	1918	1955	1.64	0.45	1.71	0.96	7.49	2.15		1.076	1.044				31
V508 Cyg		-629	-625	1.02	0.86	1.08	0.98	1.11	0.61							32
V865 Cyg	2000	2041	1.08	0.48	1.17	0.61	1.25	0.49								33
VI073 Cyg		1692	1721	1.60	0.51	2.12	1.27	2.17	0.71		1.015	1.011		0.007	0.002	34
LS Del		-1332	-1315	1.06	0.60	1.09	0.83	1.12	0.69		1.103	1.085		0.050	0.030	35
BV Dra	0.01170	-1601	-1576	1.20	0.49	1.17	0.79	1.88	0.91	1.022	1.024	1.009				4
BW Dra	0.01967	-3077	-2985	1.05	0.29	1.02	0.57	1.19	0.43	1.003	0.999	1.011				4
YY Eri	0.01491	-3637	-3509	1.01	0.44	1.02	0.70	0.79	0.43		1.018	1.026				4
H235		1215	1230	1.18	0.24	1.39	0.68	3.09	0.70		0.976	0.983		-0.006	-0.003	62
AK Her	0.02157	5734	6083	1.31	0.30	1.44	0.71	3.11	0.60		1.075					4
SY Hor	0.02522	-6202	-5840	0.97	0.64	0.95	0.83	0.47	0.47	0.947	0.982	0.976				23
DF Hya	0.03072	-5356	-5084	1.06	0.42	1.09	0.72	1.10	0.60		1.054	1.038		0.035	0.022	36
EH Hya	-4453	-4263	0.99	0.31	1.00	0.35	1.08	0.33			1.010	1.013		0.005	0.011	63
EZ Hya	0.04344									1.176	1.159	1.132	0.040	0.040	0.040	37
FG Hya		1424	1444	1.08	0.15	1.27	0.53	1.75	0.29							61
ST Ind											1.038	1.023		0.018	0.008	64
EM Lac		-917	-909	1.06	0.67	1.19	0.97	1.12	0.77							65
SW Lac	0.08069	-2963	-2877	1.02	0.83	1.03	0.94	0.85	0.80		0.923					38
AM Leo	0.02090	-2903	-2821	1.25	0.53	1.21	0.94	1.94	1.32	0.922	0.939	0.915				39

W Ursae Majoris Data Table, Part II (continued)

	LCA	$\frac{\Delta T}{T_1}$ $\times 10^5$	$\frac{\Delta T}{T_2}$ $\times 10^5$	m_1 (M_\odot)	m_2 (M_\odot)	R_1 (R_\odot)	R_2 (R_\odot)	L_1 (L_\odot)	L_2 (L_\odot)	OER_U	OER_B	OER_V	Δm_U	Δm_B	Δm_V	Ref
CE Leo	0.05036	-5381	-5107	0.94	0.47	0.94	0.68	0.44	0.29		1.118					40
XY Leo		-6011	-5670	0.89	0.44	0.89	0.65	0.31	0.21		0.950					42
XZ Leo	0.05077	8955	9836	1.65	1.20	1.50	1.30	7.70	3.94		0.901	0.973		-0.050		43
RT LMi	0.02452	-2477	-2417	1.16	0.45	1.23	0.80	1.59	0.75		1.003	0.976	0.015	0.020	0.020	44
FT Lup	0.02781	4155	7110	1.43	0.61	1.43	0.94	4.22	0.17		1.042					45
UV Lyn		6245	6661	1.34	0.71	1.32	0.97	3.16	1.32	1.116	0.994	1.015	0.040	-0.003	0.007	46
TY Men		12016	13657	1.86	0.40	1.85	0.84	13.60	1.70							66
TV Mus		-1806	-1774	1.32	0.20	1.66	0.75	3.14	0.69		0.997	0.992		0.008	0.010	47
UZ Oct	0.01404	424	426	2.05	0.56	3.22	1.82	17.64	5.58	1.044	1.036	1.028				48
V502 Oph		-3887	-3742	1.26	0.48	1.43	0.90	2.33	1.06		0.884	0.875		-0.057	-0.060	4
V508 Oph	0.00802	2833	2916	1.08	0.57	1.08	0.83	1.35	0.72		1.001	0.977				4
V566 Oph	0.04154	1224	1239	1.41	0.34	1.49	0.76	4.02	0.99		0.993	0.982				4
V839 Oph	0.02904	-3132	-3037	1.08	0.64	1.14	0.91	1.28	0.88		1.040	1.027				5
ER Ori	0.04107	-520	-517	1.14	0.69	1.22	0.97	1.47	0.95	1.014	1.006	1.013				4
FZ Ori	0.01563									0.923	0.993	0.973				49
BF Pav	0.05388	-1876	-1842	0.83	0.60	0.88	0.76	0.58	0.46		1.011					50
HY Pav	0.02125	-5507	-5220	0.88	0.41	0.88	0.42	0.38	0.18		0.977	0.962	-0.055	-0.010	-0.022	51
MW Pav		656	661	2.13	0.39	2.70	1.31	22.10	5.05							52
BB Peg	0.03195	-5388	-5113	1.16	0.47	1.21	0.78	1.58	0.81		1.091	1.079				52
BX Peg	0.01779	-6491	-6096	1.03	0.38	0.96	0.62	0.88	0.46		1.004	0.992				52
U Peg	0.05081	-5168	-4914	1.06	0.35	1.20	0.73	1.19	0.54		1.013	1.030				4
AD Phe		598	602	1.05	0.98	1.11	1.08	1.28	1.19		0.875	0.917		-0.060	-0.040	26
AE Phe	0.02148	-2417	-2360	1.17	0.47	1.19	0.79	1.63	0.79	1.099	1.068	1.055				4
YZ Phe	0.07204										0.834			-0.086		67
RW PsA		4911	5164	1.02	0.83	1.04	0.94	0.96	0.64							68
VZ Psc		3289	3401	0.79	0.72	0.77	0.74	0.22	0.18		0.966	0.978		-0.021	-0.010	53
TY Pup	0.00985	1821	1854	2.22	0.72	2.73	1.65	24.68	8.41		1.020	1.012				4
FG Sct	0.04661	-2960	-2875	0.87	0.68	0.83	0.73	0.29	0.25		0.982					59
AU Ser		6275	6695	0.98	0.78	1.09	0.99	0.72	0.46							69
Y Sex																54
RZ Tau		750	756	1.57	0.58	1.51	1.00	5.51	2.34							4
AQ Tuc		-3087	-2995	1.71	0.46	2.00	1.14	8.10	2.99							4
AA UMa		-1652	-1625	1.26	0.69	1.40	1.10	2.17	1.43							14

W Ursae Majoris Data Table, Part II (*continued*)

	LCA	$\frac{\Delta T}{T_1}$ $\times 10^5$	$\frac{\Delta T}{T_2}$ $\times 10^5$	m_1 (M_\odot)	m_2 (M_\odot)	R_1 (R_\odot)	R_2 (R_\odot)	L_1 (L_\odot)	L_2 (L_\odot)	OER_U	OER_B	OER_V	Δm_U	Δm_B	Δm_V	Ref
AW UMa		4181	4364	1.52	0.11	1.60	0.53	6.06	0.56		0.985			-0.007		55
BM UMa	0.01516	-8304	-7668	0.86	0.46	0.87	0.59	0.42	0.22		0.983			-0.008		56
TY UMa		5112	5387	1.06	0.43	1.13	0.72	1.33	0.45		0.868	0.874		-0.060	-0.053	57
W UMa		-6793	-6361	1.08	0.51	1.10	0.79	1.23	0.83							4
BP Vel	0.06692	-6000	-5660	0.90	0.48	0.99	0.62	0.84	0.65		0.912	0.915	-0.041	-0.063	-0.055	51
BU Vel		693	698	1.75	0.44	1.79	1.02	9.11	2.85							61
AG Vir		8218	8954	1.61	0.51	2.07	1.27	11.48	3.47		0.971	0.973		0.002	0.002	58
AH Vir		-7093	-6623	1.18	0.41	1.32	0.82	1.33	0.67		1.010	1.014		0.005	0.007	4
AW Vir	0.01802	333	334	1.09	0.74	1.32	0.98	1.87	1.33		0.993	1.009	0.010	0.001	0.005	51
BI Vul	0.04661	-1121	-1109	0.86	0.59	0.82	0.70	0.26	0.20		0.883					59

A.2 Column Descriptions

Part I:

1. Designation. The name of the system.
2. MV Number. The number assigned by Maceroni and Van't Veer (1996)
3. Period. The orbital period in days.
4. B-V. The observed (unreddened) B-V color.
5. q_{sp} . The spectroscopically measured mass ratio.
6. q_{ph} . The photometrically (usually via WD) determined mass ratio.
7. $\frac{L_1}{L_1+L_2}V$. The luminosity fraction of the primary in the V filter.
8. Incl. The orbital inclination, in degrees. 90.0° implies an edge on system.
9. T_1 . The photospheric temperature of the primary.
10. T_2 . The photospheric temperature of the secondary.
11. Ω_{cont} . The Roche Equipotential of the contact surface.
12. f . The percent fillout of contact for the system.
13. r_1 . The backside (farthest from the contact point) radius of the primary.
14. r_2 . The backside (farthest from the contact point) radius of the secondary.
15. ρ_1 . The density of the primary, using Mochnakci's (1981) method.
16. ρ_2 . The density of the secondary, using Mochnakci's (1981) method.
17. Type. The W UMa class, based on the Binnendijk (1970) method.

Part II:

1. Designation. The name of the system.
2. LCA. The LCA value of the system.
3. $\frac{\Delta T}{T_1}$. The temperature variation, scaled with primary temperature.
4. $\frac{\Delta T}{T_2}$. The temperature variation, scaled with secondary temperature.
5. m_1 . The primary mass, as determined by the Maceroni and Van't Veer (1996) method.
6. m_2 . The secondary mass, as determined by the Maceroni and Van't Veer (1996) method.
7. R_1 . The primary radius, as determined by the Maceroni and Van't Veer (1996) method.
8. R_2 . The secondary radius, as determined by the Maceroni and Van't Veer (1996) method.
9. L_1 . The primary luminosity, as determined by the Maceroni and Van't Veer (1996) method.

10. L_2 . The secondary luminosity, as determined by the Maceroni and Van't Veer (1996) method.
11. OER_U . The OER for the U filter.
12. OER_B . The OER for the B filter.
13. OER_V . The OER for the V filter.
14. Δm_U . The classic measurement of the O'Connell Effect for the U filter.
15. Δm_B . The classic measurement of the O'Connell Effect for the B filter.
16. Δm_V . The classic measurement of the O'Connell Effect for the V filter.
17. Ref. The primary reference for this paper, usually the source photometry or the published model.

A.3 Table References

List of references for W Ursae Majoris Data Table (Part II, Column 17):

1. Hrivnak (1988)
2. Rafert, Markworth and Michaels (1985)
3. Walker (1996)
4. Batten, Fletcher and McCarthy (1989)
5. Hrivnak and Milone (1989)
6. Samce, Pauley and Carrigan (1997)
7. Samec and Su (1993)
8. Lu (1991)
9. Mancuso, Milano and Russo (1978)
10. Aslan and Derman (1986)
11. Niarchos, Hoffman and Duerbeck (1996b)
12. Samec and Bookmeyer (1987a)
13. Hoffmann (1978)
14. Barone, *et al.* (1993)
15. Burchi, Milano and Russo (1977)
16. Samec, Carrigan and French (1996)
17. Kilmartin, Bradstreet and Koch (1987)
18. Lipari and Sistero (1984)
19. Branly, *et al.* (1996)
20. Hoffmann (1982)
21. Karimie (1983)
22. Russo, *et al.* (1982)
23. Lapasset and Claria (1986)
24. Samec and Bookmeyer (1987b)
25. Wilson and Biermann (1976)
26. McFarlane and Hilditch (1987)
27. Samec, Gray and Carrigan (1996)
28. Milone, *et al.* (1980)
29. Milone and Hrivnak (1984)
30. Odell (1996)

31. Purgathofer (1964)
32. Goderya, Leung and Schmidt (1995)
33. Samec, *et al.* (1992)
34. Sezer (1993)
35. Demircan, Selam and Derman (1991)
36. Niarchos, Hoffman and Duerbeck (1992)
37. Lipari and Sistero (1989)
38. Lafter and Grainger (1985)
39. Lee (1989)
40. Samec, *et al.* (1993)
41. Vinko, Hegedus and Hendry (1996)
42. Hrivnak (1985)
43. Niarchos, Hoffman and Duerbeck (1994)
44. Niarchos, Hoffman and Duerbeck (1996a)
45. Lipari and Sistero (1986)
46. Markworth and Michaels (1982)
47. Hilditch, King and McFarlane (1989)
48. Lapasset and Sistero (1984)
49. Al-Away (1993)
50. Gonzales, *et al.* (1996)
51. Lapasset, Gomez and Farinas (1996)
52. Leung, Zhai and Zhang (1985)
53. Samec (1989)
54. Hill (1979)
55. Hrivnak (1982)
56. Samec, Gray and Carrigan (1995)
57. Broglia and Conconi (1983)
58. Bell, Rainger and Hilditch (1990)
59. Bradstreet (1985)
60. Awadalla and Yamasaki (1984)
61. Twigg (1979)
62. Milone, E.F., *et al.* (1995)
63. Samec, Charlesworth and Dewitt (1991)

64. Walter, Niarchos and Duerbeck (1989)
65. Maceroni, Milano and Russo (1983)
66. Lapasset (1980)
67. Samec and Terrell (1995)
68. Lucy and Wilson (1979)
69. Binnendijk (1972)

Appendix B

V401 Cygni: A Wilson-Devinney Model

V401 Cygni is a neglected W UMa type binary. The only known comprehensive photoelectric photometry was completed over 35 years ago (Purgathofer (1964)) and still no published model exists. Using the Wilson-Devinney approach, V401 Cyg was modeled to fit Purgathofer's B and V observations simultaneously. Due to a pronounced O'Connell effect, there is evidence for spot activity. Two solutions (one with a hot spot and one with a cold spot) are presented.

B.1 Basic Data

Purgathofer summarizes the early observational history of V401 Cygni. It was first classified as a short periodic variable of RR Lyr type. In 1947, Lurye announced that V401 Cyg is of W UMa type. Purgathofer used his observations of minimum with the previously published minima to obtain the following epoch:

$$\text{Min I} = J.D.2434215.693 + 0.58271901E.$$

A review (Herczeg (1993)) of the available work shows a slow secular period increase, but that information does not affect this analysis, since Purgathofer's observations are all within one observing season.

Spectroscopic information on V401 Cygni is unfortunately sparse, thus the spectral types usually quoted were presumably obtained from the color of the system. Measured values for $B - V$ range from +0.27 (Spinrad (1959)) to +0.36 (Purgathofer 1964)), corresponding approximately to a spectral type of A9-F0. These $B - V$ values have, however, not been dereddened. V401 Cygni is at $b = +5^\circ$, so considerable reddening is possible. Using Purgathofer's measurement of $U - B = +0.10$ and dereddening by using the $U - B$ vs $B - V$ diagram indicates a spectral type of late A. Accordingly, an assumed value of $T_{Hot} = 7300\text{K}$ has been used.

B.2 Preliminary Photometric Solution

The preliminary photometric solution was done with the 1993 version of the Wilson-Devinney code (Wilson and Devinney (1971), Wilson (1994)). The light curve constructed from Purgathofer's data indicates an A Type W UMa system, following the definition of Binnendijk (1970). The (B-V) value is also consistent with A type, as plotted on the color-period diagram (see e.g. Mochnacki 1985). At first a solution without spots was attempted, which resulted in a fairly flat Σ (sum of the residuals) vs q (mass ratio) diagram (see Figure B.1), with a shallow minimum around $q = 0.25$.

However, a pronounced O'Connell effect indicates that star spots would probably yield a better solution. Two methods were tried: (1) placing a superluminous spot visible around 0.25 phase, and (2) placing an underluminous spot visible around 0.75 phase. In both cases, the spot was placed on the secondary (less massive and cooler) star. Samec *et al.* (1993) get a solution for the W-type system CE Leonis which discusses the

Σ vs q

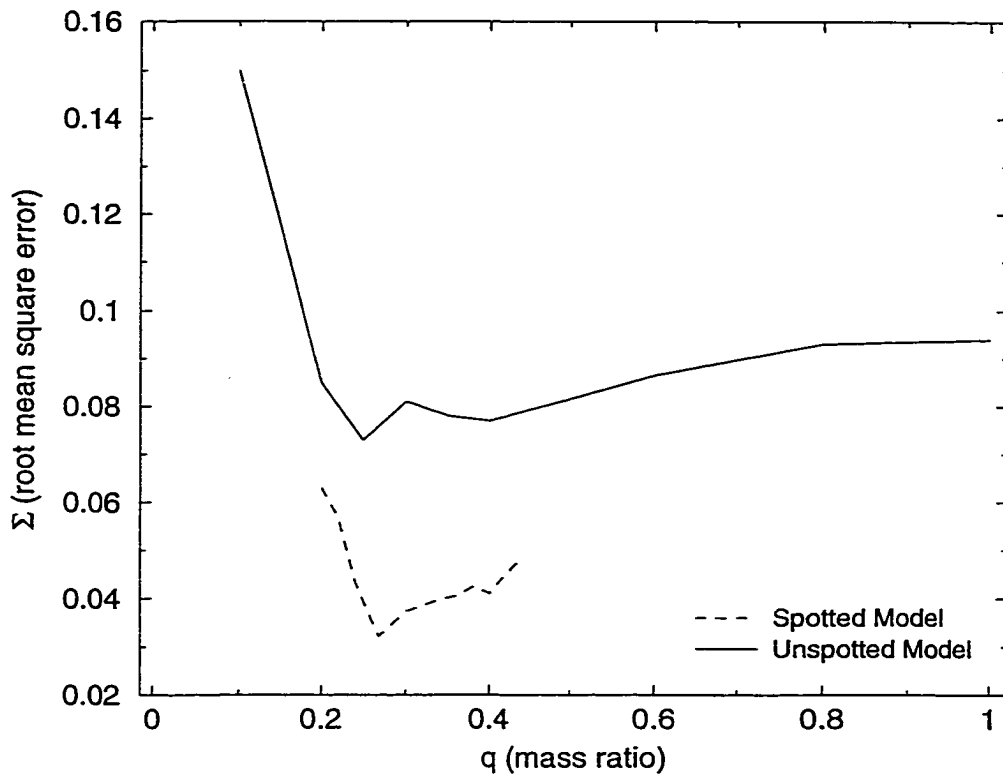


Figure B.1: A plot showing the error in the best fit solution for the range of q 's. Both the unspotted and spotted solutions are shown. The spotted model plotted is for the hot spot fit. The curve for the solution with cool spot(s) is nearly identical.

possibility of a superluminous spot; they also reviewed W UMa systems with published hot spots. Moreover, they recommend that all older light curve analysis be rechecked with the WD code for the possibility of a hot spot solution.

In Table B.1, the final parameters for V401 Cygni with hot spot and cold spot models are shown. The fit of the models to the light curve are shown in Figures B.2 and B.3.

In both cases the results are consistent with standard A type systems. Of the 30 A types included in a recent study (Maceroni and van't Veer 1996), only two have calculated solutions where $T_2 > T_1$: TV Mus and AQ Tuc. With these possible exceptions, A types have the more massive primary as the physically larger and hotter component. This is also true for V401 Cygni.

B.3 Spot Model Solution

In the following we outline our procedure of solutions with spots. As mentioned above, in both cases the spots were on the cooler component.

Case (1):

At first the solution ignored the region around phase 0.25 by dropping these points to a statistical weight of zero, and a preliminary fit was obtained for i , T_2 , $\Omega_{contact}$, q , and L_1 . An estimate of the center of the spot was obtained by examining where the center of the excess occurred in the original light curve. This enabled us to obtain a first guess for the longitude of the spot. Then the ignored data points around 0.25 phase were re-entered into the data set and the spot temperature factor and spot radius were allowed to adjust as free parameters. The spot longitude was also allowed to adjust.

The latitude was kept fixed, and assumed to be centered on the equator (a value of 90° in the Wilson-Devinney code). In the absence of doppler imaging, this has been

V401 Cygni Hot Spot Light Curve

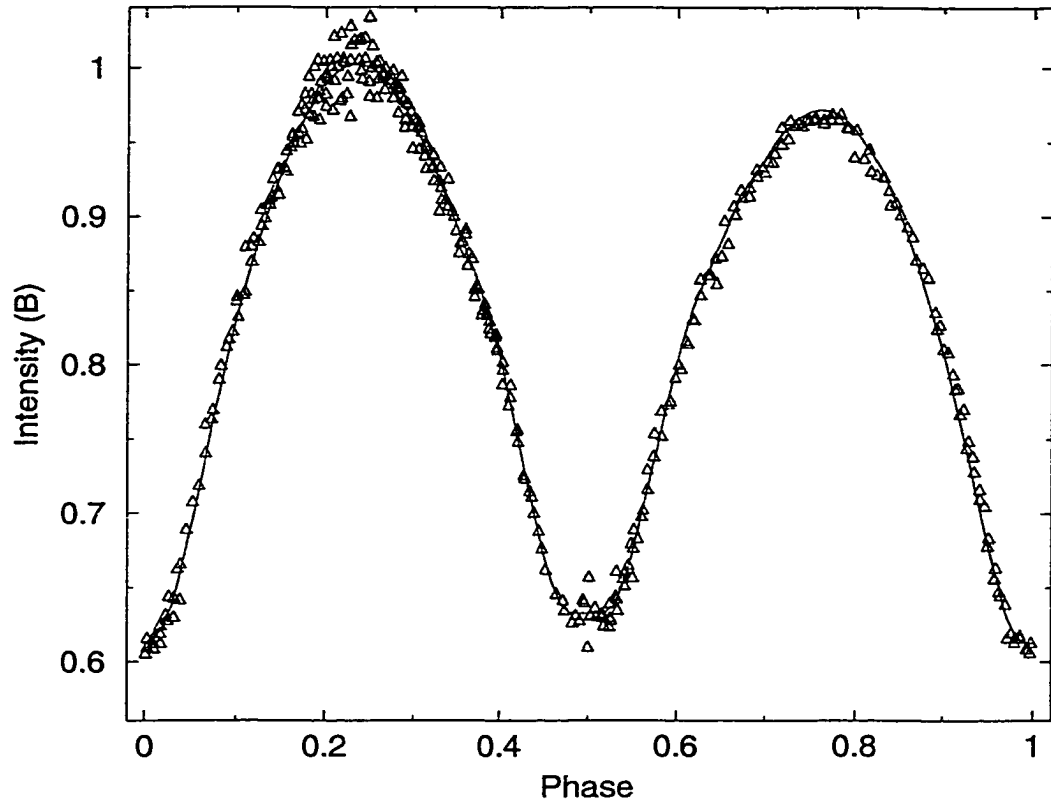


Figure B.2: Light curve fit for the hot spot solution for the B-filter.

V401 Cygni Cool Spot Light Curve

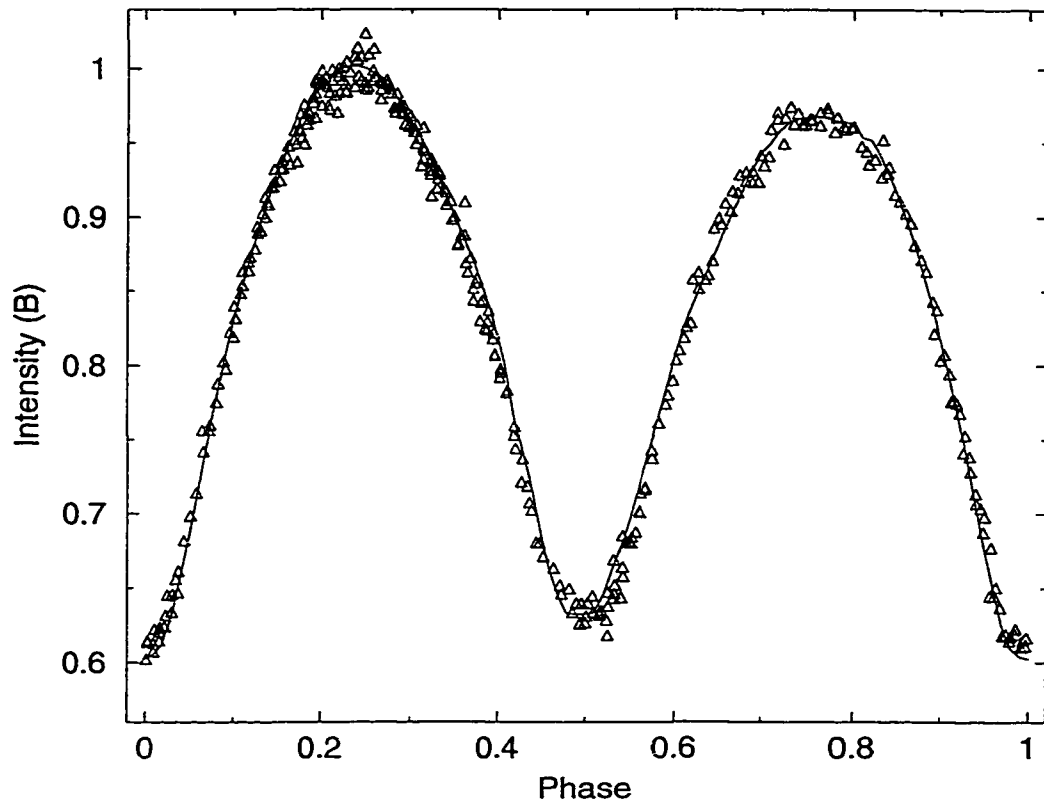


Figure B.3: Light curve fit for the cool spot solution for the B-filter.

the standard method for most solutions in the literature (see e.g. Samec *et al.* (1993)). The method of subset solutions was followed, as outlined in the WD manual (Wilson (1994)), with the multiple subsets of: {spot longitude}, {spot size}, {temperature factor}, $\{i, T_2\}$, and $\{\Omega, q\}$. Each was adjusted separately until the parameters converged. The final solution is shown in Table B.1.

A major drawback of spot modeling is the high inverse correlation between spot size and temperature factor. Maceroni and Van't Veer (1993) discuss the uniqueness problem when using spots on W UMa systems. They issue a strong warning: "From our work it has become clear that with the present photometric precision it is impossible to determine reliable (bright or dark) spot parameters". Hence the solution for V401 Cygni presented here should be considered preliminary. As recommended by Maceroni and van't Veer, spectroscopic imaging should also be included *with* the photometric data to describe the spot parameters.

Case (2):

The possibility of a cold spot solution was also checked. As with the hot spot solution, part of the data was at first ignored to obtain a preliminary fit. This time, the flux region ignored was around 0.75 phase. The spot was moved 180° in longitude and then allowed to readjust. On the first Differential Corrections (DC) run, the temperature factor adjusted to < 1 . Yet, obtaining a stable solution proved difficult. The same method of subsets was used, however the spot longitude kept oscillating wildly in longitude and the spot size kept expanding up to around 120° in longitude extent, most of the size of the star. A quick run in LC revealed that the first guess for the cool spot fit reasonably well from around phase 0.5 to 0.75, but poorly from phase 0.75 to 1.0. LC indicated a light deficit still in this phase region. Since the first part of the curve, from phase 0.0 to 0.5, was being used as the preliminary fit, this usually indicates perhaps a need for a second cool spot that would be visible on the secondary in the phase 0.75 to

1.0 region. With this in mind, a spot was placed again at the equator. This spot was kept fixed and not adjusted. Then, returning to DC resulted in solution convergence, with the final parameters shown in Table B.2.

B.4 Discussion

The two solutions have similar Σwr^2 , but the hot spot solution was obtained with only one spot. Perhaps the two spot solution needed for the cool spot case is more indicative of a *cool band* near the equator (see e.g. Rucinski (1985)). Based on the period-spectral type diagram (Leung and Schneider (1978)), V401 Cygni should be an evolved contact system. The fillout factor of around 40% is high, but not anomalous, when compared with the latest statistics for A type W UMa's (Maceroni and van't Veer (1996)).

The photometric data upon which this analysis is based is over 35 years old, thus new photometry should be obtained to calculate a more accurate model. Obtaining a spectra in order to better determine T_1 is also a necessity. Doppler imaging would resolve the difficulty with determining whether the primary, secondary or both components have spots.

Table B.1		
	Hot Spot Solution	Cold Spot Solution
q	$0.2687 \pm .0029$	$0.2815 \pm .0009$
$L_1/(L_1 + L_2)(4700 \text{ \AA})$	$0.7664 \pm .0154$	$0.7399 \pm .0054$
$L_1/(L_1 + L_2)(5500 \text{ \AA})$	$0.7652 \pm .0133$	$0.7416 \pm .0062$
i	$80.24 \pm .25$	$80.33 \pm .08$
$\Omega_{contact}$	$2.3187 \pm .0057$	$2.3607 \pm .0026$
f	$45 \pm 4\%$	$37 \pm 2\%$
$g_1 = g_2^*$	0.32	0.32
$x_1 = x_2^{**}$	0.54	0.54
$A_1 = A_2^{***}$	0.50	0.50
$r_1(pole)$	$0.4816 \pm .0006$	$0.4747 \pm .0006$
$r_1(side)$	$0.5246 \pm .0008$	$0.5154 \pm .0008$
$r_1(back)$	$0.5552 \pm .0010$	$0.5450 \pm .0009$
$r_2(pole)$	$0.2719 \pm .0019$	$0.2716 \pm .0020$
$r_2(side)$	$0.2859 \pm .0024$	$0.2850 \pm .0025$
$r_2(back)$	$0.3378 \pm .0056$	$0.3319 \pm .0053$
T_1^+	$7300K$	$7300K$
T_2	$7197 \pm 32K$	$7190 \pm 40K$
Σwr^2 (rms error)	0.0003276	0.0003298

*: Assumed (Lucy (1967))
 **: Assumed (Van Hamme (1993))
 ***: Assumed (Rucinski (1973))
 +: Assumed from (B-V)

Table B.1: The hot spot and cold spot solutions for V401 Cygni using the WD method on the data of Purgathofer (1964).

Table B.2		
	Hot Spot Solution	Cold Spot Solution
Latitude Spot 1	90°*	90°*
Longitude Spot 1	146° ± 5°	348° ± 2°
Spot Radius Spot 1	60° ± 3°	61° ± 2°
Temp. Factor Spot 1	1.050 ± 0.005	0.920 ± 0.001
Latitude Spot 2	—	90°*
Longitude Spot 2	—	225°*
Spot Radius Spot 2	—	30°*
Temp. Factor Spot 2	—	0.960*

*: Assumed

Table B.2: The final values for the spot(s) for each model.